

EXPLORING THE RELATIONSHIPS BETWEEN LIVER FAT, GUT MICROBIOTA,
SEROTONIN, AND BROWN ADIPOSE TISSUE IN HUMANS

EXPLORING THE RELATIONSHIPS BETWEEN LIVER FAT, GUT MICROBIOTA,
SEROTONIN, AND BROWN ADIPOSE TISSUE IN HUMANS

BY: BASMA AHMED, BM BCH, MSC

A Thesis Submitted to the School of Graduate Studies in Partial Fulfillment of the Requirements
for the Degree Doctor of Philosophy

McMaster University © Copyright by Basma Ahmed, July 2021

Ph.D. Thesis – Basma Ahmed – McMaster University – Health Sciences

McMaster University DOCTOR OF PHILOSOPHY (2021) Hamilton, Ontario (Department of Biochemistry and Biomedical Sciences)

TITLE: EXPLORING THE RELATIONSHIPS BETWEEN LIVER FAT, GUT MICROBIOTA, SEROTONIN, AND BROWN ADIPOSE TISSUE IN HUMANS

AUTHOR: Basma Ahmed, BM BCh, MSc

SUPERVISOR: Professor Gregory R. Steinberg, PhD

NUMBER OF PAGES: xv, 184

LAY ABSTRACT

Obesity is a risk factor for the accumulation of extra liver fat, a problem known as non-alcoholic fatty liver disease (NAFLD). Brown adipose tissue (BAT) is a kind of body fat that rather than storing calories like white fat burns calories when switched on by cold. Studies in adults have shown that people with obesity and type 2 diabetes have less active BAT suggesting switching it on may be helpful to promote weight loss and lower glucose. However, whether this relationship exists in children is not known. In rodents, increased BAT activity has also been linked to reductions in NAFLD, effects that might involve a hormone called serotonin, or changes in the gut microbiome but whether this is important in children and adults is also not understood. In this thesis, we utilized magnetic resonance imaging (MRI) to examine BAT activity after whole-body cold exposure in adults (3 hours) and children (1 hour). In 60 adults (aged 18-57 years), we report that higher cold-stimulated BAT activity is linked to NAFLD, but gut microbiota does not seem to play a role in this relationship. In 26 boys (aged 8-10 years), BAT is less responsive to cold in boys with overweight/obesity compared to boys with normal weight. Additionally, serotonin is lower in boys with overweight/obesity compared to boys with normal weight. These findings suggest that increasing BAT activity in adults and children could potentially be a new avenue for the treatment of NAFLD and obesity.

ABSTRACT

Obesity is a growing problem that impacts both adults and children. Obesity is linked to the development of unfavorable health outcomes like excess fat accumulation in the liver, a problem known as non-alcoholic fatty liver disease (NAFLD). Brown adipose tissue (BAT), a thermogenic body fat that can be turned on by cold, produces heat by consuming circulating lipids and glucose in a futile cycle. Less active cold-stimulated BAT is linked to obesity and type 2 diabetes in adults but whether this relationship exists in children is unknown. In rodents, increases in BAT activity are associated with reductions in NAFLD, effects that may be mediated through changes in the gut microbiome and reductions in peripheral serotonin. Whether the gut microbiome and serotonin play a role in regulating BAT activity in adults and children is not known. In this thesis, we have utilized magnetic resonance imaging (MRI) proton density fat fraction (PDFF) to assess BAT in the supraclavicular (SCV) region after three hours and one hour of whole-body cold exposure in adults and children, respectively. In 60 adults (aged 18-57 years), we examined whether there is a relationship between cold-stimulated BAT activity and liver fat (assessed via MRI) and whether gut microbiota plays a role in connecting these two tissues. In children, we investigated, BAT activity after whole-body cold exposure in 26 boys (aged 8-10 years). We also explored if BAT activity was different between boys with and without overweight/obesity. Finally, in young boys, we measured the levels of serotonin in platelet-poor plasma and its metabolic end product 5-hydroxyindole acetic acid (5-HIAA) in the urine. We explored if these measures of circulating serotonin were related to cold-stimulated BAT activity and if they were different between boys with and without overweight/obesity. The findings from this research indicate that higher cold-stimulated BAT activity is associated with lower liver fat in adults, but that this relationship is unlikely mediated through changes in the gut microbiota. Additionally, boys with

overweight/obesity have lower cold-stimulated BAT activity and lower 5-HIAA in their urine compared to those with normal weight. Moreover, circulatory serotonin is negatively related to total adiposity. However, circulating serotonin is not related to cold-stimulated BAT activity in this cohort. These findings are important as they indicate for the first time that increasing BAT activity in adults and children could potentially be a new avenue for the treatment of NAFLD and obesity.

ACKNOWLEDGEMENTS

I would have never been able to reach the point of completing this work without the continuous support of great people that I knew through the Ph.D. journey. Four months after I started the Ph.D. program, I become a single mom for three young children. I had no family around except my mom who was a visitor in Canada, and I was in Hamilton, a new city with no friends. Over the past five years, I struggled in almost all aspects of my new life, but I was determined not to quit the Ph.D. program and I did not!

This is an opportunity to thank my supervisor, Dr. Steinberg, for his support during this journey. I recall the conversations we had about my situation at every step through the Ph.D. and the support he always offered. I appreciate that he believed in me and pushed me to get out of my comfort zone in research. I also thank him for always being available to talk knowing how busy he is. Dr. Steinberg, thank you for all the valuable directions especially around the comprehensive exam and writing the thesis during the COVID-19 pandemic. I will always recall that I have never left one of our meetings without a very clear plan on my next steps and answers to all my questions.

Thanks to my supervisory committee Dr. Katherine Morrison and Dr. Johnathan Schertzer for the great support, conversation, and feedback about the research projects. Dr. Morrison, thanks for offering me the opportunity to work under your wing and with your amazing research team. Thanks for the support during the hard times, the directions to navigated clinical research, and the continuous interaction during the pandemic. Dr. Schertzer, I appreciate the support you and your team, especially Dr. Nicole Barra, offered on the germ-free mice experiments. I have learned from you to think about the applicability and practicality in my research projects and how to translate preclinical science.

Thanks to the former GETBAT team members especially future physicians, Nina Varah and Stephan Oreskovich. Nina, thanks for your help in the pediatric project, it was fun working with you, chasing free food, and having you as a friend. Stephan, you are the definition of a dedicated, smart, and hard-working doctor.

Thanks to the former and current Morrison's research team members. You have been a family and a home. Elizabeth Gunn, thanks for all the support you have offered whenever I needed it, and especially during the pandemic, you have made this transition the easiest possible. Vivian William, I have always enjoyed our life and motherly talks, thanks for being an amazing friend. Dr. Patrick McPhee, I am glad I had the opportunity to know you as a very kind person, as a knowledgeable researcher, especially in statistical analysis, and as a very good friend.

Efrah Yousuf, you are one of the best, if not the best gains I had during the Ph.D. Journey. You have consistently reminded me that there is a light at the end of the dark tunnel and that I am capable. You gave me the best 40th birthday gift ever. I learned a lot from you about gut microbiota. Frank Ong, no words can explain how much I appreciate having you as a colleague and a close friend. You have patiently taught me a lot at the start of the Ph.D. especially the MRI analysis, I enjoyed our coffee walks, talks, and dessert outings. You have been always such a good listener. Jennifer Li, thank you for being always there for me, you are a very thoughtful and kind person and my "to go person" when I look for sincere advice.

Thanks to current and previous members of Steinberg's research team. Dr. Emily day, mentioning your name puts a smile on my kids' faces. Thanks for being so kind and ready to help even from Ireland! Thanks to Dr. Julian Yabut for his help with the serotonin analysis and to Eric Desjardin for his continuous help and support.

Dr. Hifaa Alfaraidi, thanks for being a very kind and lovely friend through this journey. Thanks to the members of the MRI research unit especially Norm Konyer, Dr. Michael Noseworthy, and all the great technicians, especially Judy. Thanks to Jake Szamosi, Saad Syed, and Dr. Michael Surette and for their help in the microbiota analysis.

Thanks to my siblings for the continuous support and for being always so proud of me. Mom, I am who I am today because of your continuous reminders that I am capable and strong. Your trust has never shaken that I will do what I set my mind for. You are the reason for my strength and happiness. Thanks for all the sacrifices you made for me and my kids. Dad, I inherited your resilience. You taught me to fly if I have wings, and to make ones if I need to. I love you and I miss you! I am so proud of you, and I hope I can make you proud too.

To my children, Asal, Anas, and Adam, we made it! Thanks for being such a blessing in my life. Asal, you are a beautiful reliable young lady. You teach me how to be strong. Anas, you make my days with your kind words and comments. Adam, you wipe my tears with your hugs. Finally, the Ph.D. journey has been such a tough ride, but I owe it keeping me busy and distracted from all the sad moments I faced in my personal life.

TABLE OF CONTENTS

LAY ABSTRACT	iii
ABSTRACT.....	iv
ACKNOWLEDGEMENTS.....	vi
TABLE OF CONTENTS.....	ix
LIST OF ABBREVIATIONS.....	xi
DECLARATION OF ACADEMIC ACHIEVEMENTS.....	xiv
CHAPTER ONE	1
INTRODUCTION	2
1.1 OBESITY.....	2
1.2 PATHOPHYSIOLOGY OF OBESITY	3
1.3 HEALTH CONSEQUENCES OF OVERWEIGHT AND OBESITY	3
1.4 NON-ALCOHOLIC FATTY LIVER DISEASE.....	4
1.4.1 ADIPOSE TISSUES.....	4
1.4.2 DYSFUNCTIONAL WHITE ADIPOSE TISSUE IS ALSO DIRECTLY LINKED TO THE DEVELOPMENT OF NAFLD.....	5
1.4.3 GUT MICROBIOME AND NAFLD	6
1.4.4 IMAGING OF NAFLD	7
1.4.5 TREATMENT OF NAFLD.....	8
1.5 BROWN ADIPOSE TISSUE	9
1.5.1 BAT MORPHOLOGY, LOCATION, AND PREVALENCE	10
1.5.2 UTILIZATION OF COOLING PROTOCOLS TO STIMULATE BAT.....	11
1.5.3 IMAGING MODALITIES TO MEASURE BAT	14
1.5.3.1 PET-CT.....	14
1.5.3.2 MAGNETIC RESONANCE IMAGING (MRI).....	16
1.5.3.3 ¹⁸ F-FDG PET/MR.....	19
1.6 FACTORS RELATED TO BAT ACTIVITY.	26
1.6.1 ADIPOSITY	26
1.6.2 GLUCOSE HOMEOSTASIS	27
1.6.3 OUTDOOR TEMPERATURE.....	27
1.6.4 SEX.....	28
1.7 BAT AND NAFLD.....	28
1.7.1 THE MECHANISMS LINKING BAT AND NAFLD.....	30
1.7.1.1 GUT MICROBIOME	30
1.7.1.2 SEROTONIN.....	31

1.7.1.3 FUNCTIONS OF PERIPHERAL SEROTONIN	32
1.8 BAT IN CHILDREN	33
1.9 STUDY OBJECTIVES AND HYPOTHESIS.....	36
CHAPTER TWO	38
LOWER BROWN ADIPOSE TISSUE ACTIVITY IS ASSOCIATED WITH NON-ALCOHOLIC FATTY LIVER DISEASE (NAFLD) BUT NOT CHANGES IN THE GUT MICROBIOTA.	39
2.1 PREFACE AND SIGNIFICANCE TO THE THESIS	39
2.2 AUTHOR CONTRIBUTION	40
CHAPTER THREE	100
IMPAIRED COLD STIMULATED SUPRACLAVICULAR BROWN ADIPOSE TISSUE ACTIVITY IN YOUNG BOYS WITH OBESITY	101
3.1 PREFACE AND SIGNIFICANCE TO THE THESIS	101
3.2 AUTHOR CONTRIBUTION	101
CHAPTER FOUR.....	135
BOYS WITH OBESITY HAVE LOW CONCENTRATIONS OF 5-HYDROXYINDOLE ACETIC ACID (5-HIAA) IN THE URINE.....	136
4.1 PREFACE AND SIGNIFICANCE TO THE THESIS	136
4.2 AUTHOR CONTRIBUTION	136
CHAPTER FIVE	150
DISCUSSION.....	151
5.1 EXPLORING THE ASSOCIATION BETWEEN COLD-STIMULATED BAT ACTIVITY AND NAFLD	151
5.1.1 LIMITATIONS AND FUTURE DIRECTIONS	153
5.2 EXPLORING COLD-STIMULATED BAT ACTIVITY IN YOUNG BOYS	154
5.2.1 LIMITATIONS AND FUTURE DIRECTIONS	156
5.3 EXPLORING THE RELATIONSHIP BETWEEN BAT ACTIVITY AND CIRCULATING SEROTONIN IN CHILDREN.....	157
5.3.1 LIMITATIONS AND FUTURE DIRECTIONS	159
5.4 OVERALL LIMITATIONS	159
5.5 CONCLUSION.....	160
REFERENCES	162

LIST OF ABBREVIATIONS

¹⁸ F-FDG	¹⁸ F-fluorodeoxyglucose
¹⁸ F-FTHA	¹⁸ F-Fluoro-6-thia-heptadecanoic acid
¹ H MRS	Proton magnetic resonance spectroscopy
5-HIAA	5-hydroxyindole acetic acid
5-HIAL	5-hydroxyindole acetaldehyde
5-HT	5-hydroxytryptamine
5-HTOL	5-hydroxytryptophol
AAD	Aromatic amino acid decarboxylase
ALT	Alanine transaminase
AST	Aspartate transaminase
AUCs	Areas under the receiver operating characteristic curve
BAT	Brown adipose tissue
BBB	Blood-brain barrier
BMI	Body mass index
CAP	Controlled attenuation parameter
CCL2	CC chemokine ligand-2
CU	Contrast ultrasound
EMG	Electromyography
FGF21	Fibroblast growth factor-21
FF	Fat fraction
FFAs	Free fatty acids
GDS	Gut derived serotonin
HDL	High-density lipoprotein
HOMA-IR	Homeostasis model assessment of insulin resistance
IL-6	Interleukin-6
IRT	Infrared thermography

ISMIRM	International Society for Magnetic Resonance in Medicine
LDL	Low-density lipoprotein
MAOs	Mono Amino Oxidases
MRI	Magnetic Resonance Imaging
NAFLD	Non-alcoholic fatty liver disease
NASH	Non-Alcoholic Steatohepatitis
NEFA	Non-esterified fatty acid
NRG4	Neuregulin 4
NIRS	Near-infrared spectroscopy
PDFF	Proton density fat fraction
PET-CT	Computed tomography
PPAR γ	Peroxisome proliferator-activated receptor- γ
PPP	Platelet-poor plasma
QUICKI	Quantitative insulin sensitivity check index
ROI	Region of interest
SAT	Subcutaneous adipose tissue
SCV	Supraclavicular
SERT	Serotonin transporters
SUVs	Standard uptake values
TGs	Triglycerides
TNF- α	Tumor necrosis factor- α
Tph1	Tryptophan hydroxylase enzyme 1
Tph2	Tryptophan hydroxylase enzyme 2
Trp	Tryptophan
T2D	Type 2 diabetes
UCP-1	Uncoupling protein 1
US	Ultrasonography
VAT	Visceral adipose tissue

VLDL	Very-low-density lipoprotein
WAT	White adipose tissue
WHO	World Health Organization
β 3-AR	Beta-3 adrenergic receptor

DECLARATION OF ACADEMIC ACHIEVEMENTS

This thesis is presented in a sandwich format. Included herein is a general introduction containing a peer-reviewed review article, three manuscripts (two research articles and one short communication report), and a discussion. The candidate is the first co-author for the review article (excerpt was added to the introduction) and the first manuscript (chapter two). The candidate is the first author for the other two manuscripts (chapters three and four). The candidate is also listed as a third author on a peer-reviewed article that was done as a sub-study related to her projects.

THESIS PUBLICATIONS

1- Recent advances in the detection of brown adipose tissue in adult humans: a review

Frank J. Ong*, Basma A. Ahmed*, Stephan M. Oreskovich, Denis P. Blondin, Tahniyah Haq, Norman B. Konyer, Michael D. Noseworthy, Francois Haman, Andre C. Carpentier, Katherine M. Morrison*, and Gregory R. Steinberg* (2018). *Clinical Science* 132 (10): 1039–1054.

* These authors contributed equally to the work.

2- Lower brown adipose tissue activity is associated with non-alcoholic fatty liver disease (NAFLD) but not changes in the gut microbiota.

Basma A. Ahmed*, Frank J. Ong*, Nicole G. Barra, Denis P. Blondin, Elizabeth Gunn, Stephan M. Oreskovich, Jake C. Szamosi, Saad A. Syed, Emily K. Hutchings, Norman B. Konyer, Nina P. Singh, Julian M. Yabut, Eric M. Desjardins, Fernando F. Anhô, Kevin P. Foley, Alison C. Holloway, Michael D. Noseworthy, Francois Haman, Andre C. Carpentier, Michael G. Surette, Jonathan D. Schertzer, Zubin Punthakee, Gregory R. Steinberg*, Katherine M. Morrison*. *Cell Reports Medicine*, <https://doi.org/10.1016/j.xcrm.2021.100397>

* These authors contributed equally to the work.

3- Impaired cold stimulated supraclavicular brown adipose tissue activity in young boys with obesity.

Basma A. Ahmed, Nina Varah, Frank J. Ong, Denis P. Blondin, Elizabeth Gunn, Norman B. Konyer, Nina P. Singh, Michael D. Noseworthy, Francois Haman, Andre C. Carpentier, Zubin Punthakee, Gregory R. Steinberg*, Katherine M. Morrison*.

* These authors contributed equally to the work.

Prepared for publication.

4- Boys with obesity have low concentrations of 5-hydroxyindole acetic acid (5-HIAA) in the urine.

Basma A. Ahmed, Nina Varah, Frank J. Ong, Denis P. Blondin, Julian M. Yabut, Elizabeth Gunn, Norman B. Konyer, Nina P. Singh, Michael D. Noseworthy, Francois Haman, Andre C. Carpentier, Zubin Punthakee, Gregory R. Steinberg*, Katherine M. Morrison*.

* These authors contributed equally to the work.

Prepared for publication as a short report.

OTHER PUBLICATIONS

MRI Reveals Human Brown Adipose Tissue Is Rapidly Activated in Response to Cold.

Stephan M. Oreskovich, Frank J. Ong, Basma A. Ahmed, Norman B. Konyer, Denis P. Blondin, Elizabeth Gunn, Nina P. Singh, Michael D. Noseworthy, Francois Haman, Andre C. Carpentier, Zubin Punthakee, Gregory R. Steinberg * and Katherine M. Morrison* (2019). *Journal of the Endocrine Society* 3(12): 2374-2384

* These authors contributed equally to the work.

<https://doi.org/10.1210/js.2019-00309> PMID: 31745532

CHAPTER ONE

INTRODUCTION

1.1 OBESITY

Obesity is a growing health problem worldwide, not only in adults but also in children. According to the 2014 World Health Organization (WHO) report of non-communicable diseases, the prevalence of obesity has almost doubled between 1980 and 2014¹. Obesity among Canadians has also dramatically increased over the past 30 years and has been deemed to constitute an “epidemic.” WHO defines and classifies obesity using the body mass index (BMI) which is calculated by dividing the body weight in kilograms by the square of the height in meters (kg/m^2). Using calculated BMI, WHO defines overweight in adults as a $\text{BMI} \geq 25$ - $29.9 \text{ kg}/\text{m}^2$ and obesity as a $\text{BMI} \geq 30$ - $34.9 \text{ kg}/\text{m}^2$, and severe obesity as a $\text{BMI} \geq 35 \text{ kg}/\text{m}^2$. In the period between 1985 and 2015/2016, the prevalence of calculated obesity among Canadian adults increased by 300%².

Based on the WHO standards, obesity among children can be defined according to the BMI Z-score where children with BMI Z-score ≥ 1 (+1 standard deviation of the mean) are considered overweight and those with Z-score ≥ 2 (+2 standard deviations of the mean) are considered to suffer from obesity³. In 2016, WHO estimated more than 340 million children and adolescents (5-19 years old) suffer from overweight or obesity globally⁴. Based on a study that investigated the prevalence of obesity between Canadian children (6-17 years old) from 2004 to 2014; 1 out of every 7 children and youth were found to suffer from obesity however the overall rates of excess body weight appeared to be stable over that period⁵. The world obesity federation predicts that Canada will be one of the countries to have more than 1 million school-age children and youth suffering from obesity by 2030⁶.

1.2 PATHOPHYSIOLOGY OF OBESITY

Obesity generally results from a disturbance in energy balance i.e., the imbalance between energy intake and energy expenditure. Many factors contribute to enhanced caloric intake such as increased availabilities of the ready-made, high caloric, more sweetened, and palatable foods that are being presented in large portions⁷. Additionally, there is a continuous lifestyle change towards a more sedentary life which contributes to lower energy expenditure. So, there is a clear role of the modern obesogenic environment in the development of obesity.

1.3 HEALTH CONSEQUENCES OF OVERWEIGHT AND OBESITY

The link between obesity and clinical comorbidities is well established. For example, obesity is commonly associated with dyslipidemia which includes abnormalities in the plasma lipid profile characterized by low levels of high-density lipoprotein low levels (HDL) cholesterol and elevated levels of triglycerides (TGs), low-density lipoprotein (LDL) cholesterol, very-low-density lipoprotein (VLDL) cholesterol, and Apolipoprotein B⁸. Subsequently, obesity has been reported as an independent predictor of cardiovascular diseases⁹. Additionally, higher BMI is strongly related to the earlier age of first non-ST-segment elevation myocardial infarction¹⁰. Obesity is also considered a risk factor for total and ischemic cerebrovascular strokes in both men¹¹ and women¹² with every one unit increase in BMI associated with around a 5% increase in risk¹³.

Obesity is also a major risk factor for obstructive sleep apnea, asthma¹⁴, osteoarthritis, and some cancers i.e., breast, colon, esophageal cancers, and leukemia¹⁵. This is in addition to the psychosocial implications of obesity like anxiety, depression, and low self-Esteem¹⁶.

Moreover, obesity is strongly related to the development of type 2 diabetes (T2D). More than 90% of people with T2D have obesity¹⁷. A meta-analysis on 18 prospective studies showed that

overweight individuals had 3 times higher risk of diabetes compared to those with normal weight and those with obesity had 7 times higher risk of diabetes compared to those with normal weight¹⁸.

1.4 NON-ALCOHOLIC FATTY LIVER DISEASE

Non-alcoholic fatty liver disease (NAFLD) is one of the major comorbidities of obesity in both adults and children^{19,20}. NAFLD is also an important risk factor for T2D as it promotes insulin resistance. NAFLD can be identified as the fat accumulation in more than 5% of the hepatocytes with the absence of other risk factors such as infection or autoimmune diseases²¹. The severity of NAFLD ranges from simple steatosis (fat accumulation without inflammation) to Non-alcoholic steatohepatitis (NASH) characterized by the presence of inflammation “ballooning” on histological examination²¹.

NASH can progress into liver cirrhosis and in some cases, fibrosis and hepatocellular carcinoma²². Globally, the prevalence of NAFLD was estimated to be 25.2% based on studies from 1989-2015¹⁹. The highest prevalence was estimated in the Middle East and South America and the lowest was in Africa¹⁹. In Canada, it was estimated that the number of adults with NAFLD would increase by 20% between 2019 and 2030, causing a growing burden on the health care system²³.

1.4.1 ADIPOSE TISSUES

Historically, two types of adipose tissues were described: white adipose tissue (WAT) and brown adipose tissue (BAT). Both tissues are visibly distinct by their colors²⁴. Beige or brite fat is a third and recently described type of adipose tissue²⁴. White adipocytes are characterized by the large, single lipid droplet that pushes all other organelles to the periphery of the cell contrary to brown adipocytes that contain multiple lipid droplets as will be explained later in more details. Beige adipocytes share the specifications of white and brown adipocytes. They develop in

subcutaneous WAT either from preadipocytes or from white adipocytes in response to specific stimuli like after cold exposure in rodents²⁴.

WAT is the main energy reservoir during energy surplus. White adipocytes take up dietary fatty acids and respond to insulin stimulation to enhance glucose uptake and storage in the form of TGs²⁴. Insulin also inhibits the breakdown/ lipolysis of TGs. During obesity, expansion of the white adipocytes occurs to accommodate storage for the excess TGs. This leads to insulin resistance in the adipocytes leading to increased lipolysis that can elevate free fatty acids (FFAs) and cause insulin resistance in other tissues including the liver and skeletal muscle while also promoting pancreatic beta-cell failure²⁵. Elevations in FFAs can also trigger a state of low-grade inflammation in WAT and other tissues²⁶ further promoting insulin resistance.

1.4.2 DYSFUNCTIONAL WHITE ADIPOSE TISSUE IS ALSO DIRECTLY LINKED TO THE DEVELOPMENT OF NAFLD.

During obesity, an excess flux of FFAs to the liver occurs due to WAT insulin resistance and increased lipolysis. It was estimated that WAT lipolysis accounts for 60% of the FFAs flux to the liver in NAFLD patients followed by de novo lipogenesis (25%) and lastly 15% from the diet²⁷. Additionally, the decreased liver secretion of VLDL-TGs also contributes to hepatocyte fat accumulation. Liver steatosis also promotes immune cell infiltration and activation ultimately triggering inflammation and histological changes i.e., ballooning of the hepatocytes.

Pre-clinical and clinical studies have reported that inflammation in the subcutaneous and visceral adipose tissues, SAT and VAT respectively, contribute to NAFLD development and progression²⁸. A positive association was found between NAFLD status and both SAT and VAT areas in 3197 adults²⁹. Additionally, SAT and VAT from patients with NAFLD and NASH had increased expression of inflammatory genes and the increased expression of these genes was directly related

to the disease progression³⁰. The mechanisms that initiate adipose tissue inflammation are not fully clear yet, however, it is proposed that the hypoxia and death of the rapidly expanding adipocytes play a role³¹. Adipocytes produce inflammatory cytokines and chemokines i.e., tumor necrosis factor- α (TNF- α), interleukin-6 (IL-6), and CC chemokine ligand-2 (CCL2) which can promote both adipose tissue and hepatic insulin resistance³¹.

1.4.3 GUT MICROBIOME AND NAFLD

Like the development of obesity, NAFLD development and progression include an interplay between several factors. The model of “multiple parallel hits” was proposed in 2010³² which hypothesized that the integration of dietary factors, inflammation in multiple tissues including the intestine as well as alterations in the gut microbiota promotes the development of NAFLD/NASH development²⁸.

Changes in the characteristics of gut microbiota have been reported in association with NAFLD spectrum^{33,34}, its progression, severity, and complications^{35–38}. While NAFLD is highly prevalent among adults with obesity and T2D¹⁹, studies reported that the altered gut microbiome composition associated with NAFLD was independent of BMI and insulin resistance³⁹. Moreover, gut dysbiosis, which is the disruption of normal intestinal bacterial homeostasis, was found in lean NAFLD patients³⁶. The reported state of dysbiosis associated with NAFLD included not only a reduction in the diversity of the bacterial community but also changes in the composition at different levels; phyla, families, genera, and species, as well as an alteration in the microbial functions^{35,40,41}. For example, Holey et al reported an association between phenylacetic acid, a product of bacterial metabolism for aromatic amino acid, and hepatic steatosis⁴¹.

Several mechanisms have been proposed to explain the association between the gut microbiome and NAFLD. For example, studies have shown that children with NAFLD had increased intestinal

permeability compared to controls and a positive association was found between the increased intestinal permeability and the steatosis severity⁴². Similarly, in human adults, NAFLD was associated with increased intestinal permeability^{43,44} and increased circulating levels of bacterial endotoxin that was also directly related to the degree of liver damage as well as increased ethanol production that could promote hepatic damage⁴⁴. Other suggested mechanisms that explain the association between the gut microbiome and NAFLD include disturbances of the choline and bile acids metabolism and increased energy harvesting from the diet⁴⁵. However, it is still not clear if gut microbiome alterations cause NAFLD or if NAFLD causes alteration of the gut microbiome.

1.4.4 IMAGING OF NAFLD

Liver biopsy is the gold standard method for NAFLD quantification, NASH diagnosis, and fibrosis staging⁴⁶. However, liver biopsy is an invasive procedure with significant risks, that are difficult to justify in healthy adults or children²⁰. Liver biopsy is also prone to sampling error and high intra- and inter-reader variability due to the unevenness in the distribution of liver lesions in NASH⁴⁷. Thus, there are continuous efforts to find non-invasive and more accurate diagnostic tools.

Ultrasonography (US) is a widely used clinical imaging method for the diagnosis of NAFLD due to its safety and low cost. However, it has been reported that US can not detect steatosis that extends less than 33% of the hepatocytes⁴⁸, and recently the reported lower limit of US detection of NAFLD was 10% of the hepatocytes⁴⁹. Additionally, US has low accuracy in the diagnosis of NAFLD in patients with morbid obesity⁵⁰. Another way to assess liver steatosis using US is the controlled attenuation parameter (CAP) that can be found in FibroScan (transient elastography technique to measure liver fibrosis). In 440 biopsies proven NAFLD patients, CAP had areas under the receiver operating characteristic curve (AUCs) of 0.79 (95% CI 0.74–0.84), 0.84 (95% CI

0.80–0.88), and 0.84 (95% CI 0.80–0.88) for the diagnosis of steatosis >10%, steatosis >33%, and steatosis >66% of the hepatocytes, respectively. However, one of the drawbacks of CAP was its failure in measuring steatosis in 7.7% of the cases and this was influenced by higher BMI⁵¹.

Alternatively, Magnetic Resonance Imaging (MRI), has been shown to accurately estimate fat in the entire liver^{52,53}. MRI detects liver fat through chemical shift-based water and fat separation to calculate proton density fat fraction (PDFF) which is the ratio between MR proton signal of tissue fat to the sum of MR proton signals of fat and water ($PDFF \% = \frac{FAT}{FAT+Water} * 100\%$). Importantly, MRI assessment of liver fat correlates well with the tissue histology in adults⁵³ as well as in children and adolescents⁵⁴. Additionally, MRI-PDFF showed more accuracy than CAP in the diagnosis of steatosis in 142 NAFLD patients; AUCs were 0.96 (95% CI 0.92–1.00) vs 0.88 (95% CI 0.80–0.95; $p = 0.048$) respectively for the diagnosis of grade ≥ 1 steatosis; and 0.90 (95% CI 0.82–0.97) vs 0.73 (95% CI 0.64–0.81; $p < 0.001$) for the diagnosis of grade ≥ 2 steatosis and 0.79 (95% CI 0.65–0.94) vs 0.70 (95% CI 0.58–0.83; $p = 0.015$) for the diagnosis of grade ≥ 3 steatosis⁵⁵. Thus, MRI is a promising and accurate way to quantify hepatic steatosis however it is not widely used in clinical practice due to the high cost and availability issues.

1.4.5 TREATMENT OF NAFLD

Lifestyle modification, including reductions in food intake and increased physical activity, along with bariatric surgery is currently the keystone for reducing hepatic steatosis⁵⁶ and other histological features of NASH⁵⁷. As it is challenging to sustain weight loss with lifestyle modifications and bariatric surgery has serious complications, many pharmacological interventions have been developed. However, and despite the extensive efforts, pharmacological agents targeting lipid metabolism or fibrosis in the liver have been largely ineffective at reducing liver fibrosis in large-scale clinical trials^{21,58}, and as such, no therapies have yet to be approved

leading to the concept that a combination strategy will likely be needed²¹. One potential mechanism for combining with other strategies for treating NASH involves the activation of BAT.

1.5 BROWN ADIPOSE TISSUE

The following section of the introduction about BAT anatomy, morphology, activation, and imaging modalities is an excerpt from the below review article for which the candidate is the first co-author.

Recent advances in the detection of brown adipose tissue in adult humans: a review.⁵⁹

Frank J. Ong*, Basma A. Ahmed*, Stephan M. Oreskovich, Denis P. Blondin, Tahniyah Haq, Norman B. Konyer, Michael D. Noseworthy, Francois Haman, Andre C. Carpentier, Katherine M. Morrison*, and Gregory R. Steinberg*(2018). *Clinical Science* 132(10): 1039–1054.

* These authors contributed equally to the work.

<https://doi.org/10.1042/CS20170276> PMID: 29802209

Author contribution: F.J.O., and B.A.A., contributed equally to the conceptualization, writing, and revision of this manuscript with S.M.O., K.M.M., and G.R.S. F.J.O. was the main contributor to Table 1 and B.A.A. was the main contributor to Table 2. D.P.B., T.H., N.B.K., M.D.N., F.H., A.C.C. edited the manuscript, provided comments, and additional references.

- Since the re-discovery and definitive identification of functional brown adipose tissue (BAT) in adult humans, there has been a renewed interest in exploring the potential importance of this tissue in the context of metabolic health^{60–63}. BAT is a uniquely equipped thermogenic organ with an abundance of uncoupling protein 1 (UCP-1)-containing mitochondria⁶⁴. UCP-1 is a protein that uncouples mitochondrial oxidative phosphorylation resulting in a futile cycle that bypasses ATP production causing elevated metabolic activity that generates heat⁶⁵. Over the last several years, studies in humans have shown that cold-induced BAT activation is important for non-shivering thermogenesis and can contribute to whole-body glucose and non-esterified fatty acid (NEFA)

clearance, although the extent of this contribution may be relatively small compared with skeletal muscle⁶⁶⁻⁶⁸. Given this inherent capacity to utilize substrates in a futile cycle, the activation of BAT may have important implications in the treatment of metabolic disorders such as obesity, type 2 diabetes, and non-alcoholic fatty liver disease (NAFLD). In order to evaluate BAT's therapeutic potential, standardized and reproducible non-invasive methodologies for the assessment of BAT volume and metabolic activity in humans are needed. The purpose of this review article is to discuss the strengths, weaknesses, and opportunities of different exposure protocols and imaging methodologies including: (i) static and dynamic positron emission tomography and computed tomography (PET-CT) imaging using ¹⁸F-fluorodeoxyglucose (¹⁸F-FDG) (a glucose analog that is not metabolized beyond glucose-6-phosphorylation) and alternative tracers such as ¹¹C-acetate, ¹⁸F-Fluoro-6-thia-heptadecanoic acid (¹⁸F-FTHA), ¹⁵O-H₂O and ¹⁵O-O₂; (ii) magnetic resonance imaging (MRI); (iii) local skin temperature measurements; (iv) contrast ultrasound (CU); and (v) near-infrared spectroscopy (NIRS) in order to guide the evaluation of BAT volume and activity in humans.

1.5.1 BAT MORPHOLOGY, LOCATION, AND PREVALENCE

Multiple methodologies have been utilized to assess BAT volume and activity. These techniques aim to differentiate BAT from surrounding tissues based on its physical and metabolic properties. Brown adipocytes are polygonal cells with a central nucleus and multiple, small vacuoles that store triglycerides⁶⁹. These cells contain an abundance of large, spherical iron-rich mitochondria with lamellar cristae⁶⁹. BAT is highly vascularized and densely innervated by terminal fibers of the sympathetic nervous system⁶⁹. In contrast, white adipose tissue (WAT) houses fat cells with a unilocular lipid droplet, a displaced peripheral nucleus, and limited cytoplasm⁷⁰. Another key feature of BAT is the high expression of UCP-1, which can be enhanced by adrenergic stimulation

and peroxisome proliferator-activated receptor- γ (PPAR γ) agonists⁶⁵. Cells with thermogenic potential and morphologic features similar to brown adipocytes have been identified within WAT depots⁷⁰. Termed as ‘beige’, ‘brite’, ‘induced BAT’, ‘recruitable BAT’, and/or ‘white adipose BAT’, these cells express UCP-1 in response to adrenergic stimuli and function similar to classic brown adipocytes. It has been suggested that this cell type characterizes most of the human BAT⁷⁰.

Although the presence of BAT in humans has been confirmed across the age spectrum⁷¹, its metabolic activity has not been directly compared in different age groups. However, it has been suggested that BAT prevalence, volume, and activity follow an age-related decline in adults^{72,73}. In infants, BAT constitutes 1–5% of their body weight and is largely found in the interscapular region⁷⁴. In adults, BAT is located mainly in the supraclavicular (SCV) and cervical regions, as well as in the paravertebral, mediastinal, and perirenal areas⁷⁵. Based on a systematic review of studies examining cold-induced ¹⁸F-FDG uptake (a modality for estimating BAT volume and activity), the volume of BAT in adult humans is estimated to range from 4 to >1500 ml in those with detectable ¹⁸F-FDG uptake⁷⁶. This wide variability is believed to be the result of inherent biological variation between individuals but is also likely to be influenced by technical differences in study protocols including varying stimuli to increase BAT activity (i.e., type and duration of cold exposure) and methodologies for detecting BAT. These will be discussed in detail in the following sections of this review.

1.5.2 UTILIZATION OF COOLING PROTOCOLS TO STIMULATE BAT.

The prevalence of spontaneously detectable BAT (i.e., measurement of ¹⁸F-FDG uptake at ambient temperature) in adult humans ranges from 6.8 to 8.5% in retrospective studies^{75,77}. When subjects are exposed to cold, the prevalence of BAT is between 20 and 100%⁷⁶. This wide disparity between subjects may be a function of the somewhat subjective measures of

what constitutes active BAT using the different imaging methodologies (which will be discussed in detail below) that may artificially preclude individuals who are likely to have some active BAT when exposed to cold. And although the metabolic activity of BAT can also be increased using high doses of sympathomimetics (i.e. ephedrine)^{78,79} or β adrenergic agonists^{80,81}, these effects are often relatively modest when compared with cold exposure and can increase the risk of adverse events in study participants due to increased heart rate and blood pressure. Thus, cold exposure has been primarily used to activate BAT in humans, however variability in exposure protocols, is a significant barrier to comparing findings between studies^{76,82,83}.

Protocols for BAT stimulation vary^{84–86}, in part, related to the chosen imaging modality. For instance, infrared thermography (IRT) can detect a significant increase in SCV skin temperature minutes after a hand is immersed in ice water⁸⁴, whereas static ¹⁸F-FDG PET-CT requires at least 60 min of cold after the radiotracer is injected in order to visualize the uptake of the tracer into BAT⁸³. Furthermore, the published protocols also vary by the extent of body surface area to be exposed, with lower temperatures (as low as 5°C) generally used for small surface areas (i.e., hands and feet), and temperatures in the 16–18°C range being used for near whole-body exposures. As outlined in Supplementary Table S1, the most commonly employed protocols include a whole-body cold exposure using a temperature-controlled room^{61,80,94–103,86,104,87–93}, water-perfused suits which cover most of the body^{66,67,113–115,105–112}, water-perfused vest or blanket which cover a specific region of the^{68,78,123–132,81,133–140,116–122}, or exposure of the extremities (i.e. hands and/or feet)^{60,63,146–152,73,84,85,141–145}. It is important to note that the metabolic response, including BAT stimulation, elicited by the latter approach might be confounded by the stimulation of

nociceptors in the skin and as such, liquid-perfused garments are often regarded as the most robust method^{77,83}. In addition to differences in the method of cold exposure detailed above, there is also controversy in whether the best approach to measure BAT activity involves the use of a ‘standardized’ or ‘individualized’ cold-exposure protocol. A standardized cold-exposure protocol as the name implies involves exposing all subjects to the exact same temperature and duration of cold exposure. Under a standardized protocol, there can be wide variances between subjects with respect to the degree of BAT activation and shivering at any set temperature that is dependent on multiple factors including but not limited to cold acclimation status and morphological differences such as the surface-to-volume ratio, skeletal muscles¹⁵³, insulative capacity of subcutaneous fat¹⁵⁴, and vasoactive response¹⁵⁵. In order to take into account these variations between subjects to maximize BAT activation, ‘individualized’ cooling protocols have been developed, wherein subjects are cooled at a temperature slightly above shivering⁸². However, in order to standardize such a procedure between subjects and across laboratories, it is important that concurrent objective (i.e. electromyography; EMG) and subjective (i.e. participant and observer-indicated) assessments of shivering, and real-time monitoring of core and mean skin temperature values are assessed⁷⁶. It is important to note that even with these measurements, the interpretation of individualized cooling protocols is limited by the inherent shortcomings of surface EMG, as this modality is unable to detect deep muscle shivering and therefore underestimates the contributions of skeletal muscle to cold-induced thermogenesis^{66,107}. Therefore, in order to calculate absolute cold exposure levels, regardless of whether a standardized or individualized cooling protocol is used, it is important that cold-induced measures of whole-body heat production (e.g. indirect calorimetry and/or monitoring of the inlet and outlet

temperature of a liquid-perfused garment), along with changes in mean skin temperature, and shivering be made concurrent with BAT measurements⁷⁶. That way, the reliability and efficacy of the cooling protocol, as well as BAT's relevance in the realm of whole-body systemic thermogenesis (i.e., shivering thermogenesis), can be reproduced by different laboratories in all subjects.

1.5.3 IMAGING MODALITIES TO MEASURE BAT.

1.5.3.1 PET-CT

The use of PET-CT with ¹⁸F-FDG has been instrumental in the identification of BAT in humans, as biopsies and subsequent histological analysis of ¹⁸F-FDG-containing tissues were shown to contain the morphological characteristics of BAT^{60,62,75,77,156,157}. Thus, the combination of CT radio-density (in Hounsfield units) and static PET imaging of ¹⁸F-FDG uptake (in standard uptake values-SUVs) has been widely used for anatomical localization of BAT¹⁵⁸ and tissue-specific estimations of glucose metabolism⁷⁶. A detailed review and consensus on standardized guidelines for static ¹⁸F-FDG PET-CT imaging has recently been developed by Chen et al.⁸³ and therefore will only be briefly discussed.

¹⁸F-FDG uptake is typically reported in the literature as SUV_{max} or SUV_{mean} , which estimates ¹⁸F-FDG biodistribution in a specified region of interest (ROI) in relation to the injected radiotracer dose and distribution volume in a subject (i.e. body weight, body surface area or lean body mass)^{77,104,159,160}. Though this approach has clinical applicability due to its more straightforward data acquisition and analysis procedure compared to dynamic PET imaging, results from static PET scans vary tremendously across studies^{76,160,161}. One of the reasons for these differences may be related to the method used to determine the ROI. Specifically, Leitner et al.¹⁰⁴ have found that

use of the most common method for ROI selection, 2D-coronal, results in overestimation of BAT volume by $63 \pm 16\%$ compared to 3D-axial, which more accurately estimates BAT volume.

In addition to systematic errors, underreporting of methodological parameters (e.g. SUV thresholds, radiotracer dose, and time between injection and scan), may also contribute to heterogeneity in results^{76,83,160–162}. While these shortcomings can be minimized by using standardized criteria for image acquisition and defining the presence of BAT with static ¹⁸F-FDG PET acquisitions as recently described⁸³, other concerns related to this methodology may still persist. For example, static ¹⁸F-FDG measurements rely on one time frame to represent overall tracer metabolism despite a known variation in tissue glucose responsiveness^{76,161,162}. As such, this approach is highly influenced by inter/intrasubject dissimilarities in plasma glucose concentrations and clearance, including the potential contribution of recruited skeletal muscle during shivering^{160–162}. And although implementation of a simplified kinetic model can, to an extent, correct for the aforementioned variables during a static PET scan procedure, it cannot fully account for these inherent limitations.

Many of the limitations associated with ¹⁸F-FDG static imaging can be largely eliminated through the use of dynamic acquisition coupled with kinetic modelling approaches^{159,161}. Dynamic scanning allows for the development of a time-activity curve of the rate of ¹⁸F-FDG metabolism in BAT^{76,83,159,163} with estimates of plasma glucose levels, vascular transport, cellular metabolism, and blood activity concentration (via invasive arterial blood sampling or image-derived measurements of arterial input function¹⁶³). Although dynamic PET imaging using ¹⁸F-FDG is inherently complex in nature and requires subjects to remain completely still throughout prolonged scanning periods, this modality has proven effective in measuring cold-stimulated BAT activity in adult populations^{60,66,145,152,164,165,67,68,108,111,112,126,136,138}. Given these findings, it is now important

that a consensus on standardized guidelines for dynamic scanning is developed for this technology, much like what was recently proposed by Chen et al.⁸³ for static acquisitions.

Despite the invaluable contributions that ¹⁸F-FDG PET-CT imaging has had on our understanding of human BAT, this modality has notable limitations. The most potentially significant is the assumption that glucose uptake reflects BAT activity. As recent studies indicate that fatty acids from intracellular triglyceride lipolysis, not glucose, are the primary substrate for activated BAT^{113,166}. Therefore it has been suggested that utilizing other tracers such as ¹¹C-acetate, ¹⁵O-O₂ or assessing perfusion using ¹⁵O-H₂O may more accurately reflect BAT metabolic activity^{66,67,165,167,68,98,105,107,108,113,152,164}. A challenge with these tracers is their rapid clearance from tissues and relatively short half-life that is only overcome with technically challenging PET dynamic acquisitions¹⁶⁸. Therefore, recent studies¹⁶⁹ have utilized ¹⁸F-FTHA, to estimate NEFA uptake by BAT. This tracer has a relatively long radioactive half-life (~ 110 minutes), accumulates into intracellular metabolic pathways as ¹⁸FDG does, and therefore can be used in both static and dynamic imaging modes¹⁶⁸. Ultimately, the combination of several different radiotracers with dynamic imaging may increase the precision of PET-CT for assessing global BAT metabolic activity.

1.5.3.2 Magnetic Resonance Imaging (MRI)

Despite the many strengths of PET-CT for measuring BAT activity, a major limitation to the use of this technique is the significant exposure to ionizing radiation which precludes the frequent use of this modality in healthy adults and children¹⁷⁰. In order to avoid this exposure to radiation, recent studies have utilized alternative methodologies to measure BAT, including MRI. This technology to measure BAT is based on the differing physical properties of BAT and surrounding tissues including WAT and muscle. Although multiple MR strategies have been reported in the literature,

pulse sequences based on the water-fat separation technique are most widely used to measure BAT. Proton-density fat fraction (PDFF) values¹⁷¹⁻¹⁷³ are recommended by the International Society for Magnetic Resonance in Medicine (ISMRM) as the standardized imaging biomarker of tissue fat content because of proven accuracy, precision, robustness, and reproducibility¹⁷⁴. Several papers have reported significantly different PDFF values between BAT and WAT depots^{101,136,175,176} (see **Table 1**). PDFF may also be used to measure BAT metabolic activity as BAT uses endogenous derived fatty acids when activated resulting in a decreased triglyceride content (i.e. lower PDFF value) upon BAT activation^{66,177}. Although this decline in PDFF may be confounded by the increase in blood perfusion that occurs during BAT activation^{98,152,177}, a recent study showed that these effects can be eliminated after a brief exposure to warm temperatures¹⁰². Further, it has been suggested that MRI could be used to measure BAT metabolic activity independent of cold exposure as lower PDFF values are generally reflective of a browner phenotype¹⁷⁸. This notion has recently been extended by Holstila et al.¹³⁶ where a strong correlation between pre-cold PDFF and ¹⁸F-FDG uptake was reported.

Importantly, like ¹⁸F-FDG PET-CT, the use of water-fat imaging of BAT has been validated with histology and immunohistochemistry in infants post-mortem^{173,179} and in adult humans¹⁸⁰. This approach has also been shown to have good reliability and agreement in both infant¹⁸¹ and adult populations¹⁷⁵. To date, however, researchers are challenged by the wide and overlapping range of PDFF values in BAT and WAT tissues in both children^{171,172,176,182} and adults^{101,102,183,109,119,131,136,138,171,175,176} (see **Table 1**). The PDFF range in the SCV area of children (n=33; 32 to 94)¹⁷⁶, adults (n=16; 56.0 to 87.0)¹¹⁹ and elderly (n=11; 84 to 94)¹⁷⁶ is broad. The large variability in PDFF may be explained by the difference in BAT metabolic activity often associated with variations in age and adiposity⁷³. Structurally, the fat in the SCV region in adult humans is not exclusively BAT, but is rather a mix

of brown, beige and white adipocytes¹⁸⁴. As such, while measurement of PDFF is a promising method for characterizing BAT, given variations across the population, there is unlikely to be a clearly defined PDFF range to dichotomize between BAT and WAT and metabolically active and inactive BAT.

One potential MRI methodology to further differentiate BAT and WAT involves the measurement of T2* relaxation (T2*). T2* is defined as the decay of the MR signal in the transverse plane of an inhomogeneous magnetic field¹⁸⁵, resulting in a faster T2* relaxation, and hence, a smaller T2* value¹⁸⁵. In BAT, the high abundance of iron-rich mitochondria contributes to a faster de-phasing of transverse magnetization resulting in lower T2* values compared to WAT^{185,186}. T2* relaxation can be used to measure BAT metabolic activity based on the magnetic properties of hemoglobin, which can exist in either a diamagnetic (oxyhemoglobin) or paramagnetic (deoxyhemoglobin) state¹⁸⁵. Since oxygen consumption, and therefore deoxyhemoglobin abundance, is increased in regions with BAT activation, there is a resultant decrease in T2* values¹⁸⁵. Additionally, an assumption can be made that the change in T2* signal after an acute cold exposure is primarily due to the ratio of oxyhemoglobin and deoxyhemoglobin as the number of mitochondria is not expected to change. Thus, T2* signalling may provide a complementary measurement of BAT volume and activity. With recent advances in MR technology, PDFF and T2* can be acquired simultaneously, making possible the use of a combination of these measures to differentiate BAT and WAT. A specific T2* threshold to define the presence of BAT has yet to be established, although in reviewing other published studies, it was noted that there is less overlap in T2* values between BAT and WAT when compared to PDFF (see **Table 1**). This may suggest that the use of a composite of T2* and PDFF may be more sensitive MR signal in discriminating different types of adipose tissues than either measure on its own.

Due to the wide applicability of MR technology, several other approaches are currently being developed for the purpose of BAT detection. One of these techniques is diffusion-weighted imaging, which is a widely-used MR imaging technique that measures microscopic water mobility (i.e. diffusion)¹⁸⁷. Since brown adipocytes have more intracellular space than white adipocytes, this translates to greater tissue water mobility and a faster decay of the diffusion-weighted imaging signal. For example, Deng et al.¹⁸² found that the SCV region of children with obesity not only had higher PDFF and T2* values than a comparable region in normal weight controls, but also had consistently lower diffusion coefficients¹⁸². Although diffusion-weighted imaging has yet to be used in studies investigating cold-activated BAT, water diffusion is expected to be elevated during non-shivering thermogenesis due to an increase in intracellular space resulting from cold-induced BAT vasodilation suggesting this may be a further measure to assess BAT metabolic activity.

1.5.3.3 ¹⁸F-FDG PET/MR

To mitigate radiation exposure from CT and to enhance soft tissue contrast, several research groups have investigated combining ¹⁸F-FDG PET with MRI for studying BAT^{136,176,188–191}. This has largely been investigated in the context of validating the use of MRI in the identification of BAT with or without cold stimulation, and to offer an additional mean by which BAT can be discriminated from WAT (i.e. overlaying areas of high ¹⁸F-FDG uptake with MR-derived anatomical maps of the human SCV region)^{119,176}. However, rather surprisingly, the results of these studies have revealed significant inconsistencies between BAT-specific MR parameters (i.e. PDFF and T2*) and ¹⁸F-FDG uptake by BAT^{119,151,176}. One potential explanation for these findings is that BAT utilizes high amounts of intracellular triglyceride for oxidation and may have a reduced reliance on glucose uptake or vice versa. An important limitation in the use of PET/MR is the reliance on estimates for given tissues to correct for PET attenuation artifacts as it cannot be

directly determined unlike with CT. Future studies investigating this relationship with alternative PET tracers will be important for further understanding whether this methodology may be important for assessing BAT metabolism.

Table 1. Select MRI studies that used FF% and/or T2* to measure BAT characteristics and activity.

Reference	Population	BAT	WAT	Notes
Holstila et al. (2017) ¹³⁶ 3T; PDFF	Adults N: 13 (7M:6F) Age: 32.7 (9.9); 19 to 55 BMI: 24.4 (3.1); 20.3 to 31.5	Location: SCV	Location: not provided	<ul style="list-style-type: none"> • BAT FF% and T2* did not significantly change after cooling • FF% and T2* were significantly different between BAT and WAT
		FF% Pre-Cold: 82.3 (3.8); ≈ 75.5 to 87 Post-Cold: 81.9 (4.0); ≈ 73 to 86.5 T2* Pre-Cold: 14.8 (1.8); ≈ 12.0 to 19.5 Post-Cold: 15.3 (1.1); ≈ 13.5 to 17.0	FF% Pre-Cold: 89.1 (3.2); ≈ 83 to 93.5 Post-Cold: 90.0 (2.9); ≈ 86 to 94 T2* Pre-Cold: 20.4 (1.4); ≈ 18.0 to 22.5 Post-Cold: 20.7 (2.0); ≈ 18.0 to 25.0	
Koskensalo et al. (2017) ¹³⁸ 3T; PDFF	Adults N: 10 (6M:4F) Age: 33.1 (7.4); 25 to 45 BMI: 24.3 (2.2)	Location: left SCV via ¹ H-MRS * 1 voxel = 1.75mm x 2mm x 1.5mm	Location: upper posterior thoracic	<ul style="list-style-type: none"> • BAT FF% significantly decreased after cooling • FF% tended to be different between BAT and WAT
		FF% Pre-Cold: 80.9 (5.9); ≈ 69 to 87 Post-Cold: 76.0 (5.6); ≈ 67 to 86	FF% Pre-Cold: 88.3 (4.8) Post-Cold: 83.9 (6.6) * no range provided	
Franssens et al. (2016) ¹⁸³ 1.5T; PDFF	Adults N: 50 (39M: 11F) Age: 61.4 (7.6) BMI: 26.2 (3.6)	Location: SCV	Location: posterior to trapezius	<ul style="list-style-type: none"> • FF% was significantly different between BAT and WAT
		FF% Ambient (no cold): 82.6 [78.8 to 84.3]	FF% Ambient (no cold): 90.2 [87.3 to 91.9]	
	Adults	Location: SCV	NOT ANALYZED	

<p>McCallister et al. (2016)¹¹⁹ 3T; SFF</p>	<p>N: 16 (9M:7F) Age: 20 to 53 BMI: 19.3 to 36.6</p>	<p>FF% Range: 56.0 to 87.0 FF% Threshold: 40 to 100 * No summarized data provided for post-cold scans</p>		
<p>Stahl et al. (2016)¹³¹ 3T; SFF</p>	<p>Adults N: 10 (5M:5F) Age: 27 (2); 23 to 30 BMI: 23 (2); 19.6 to 26.8</p>	<p>Location: small ROI at left and right interscapular * Mean ROI (SD) = 1.31 mL (1.43 mL)</p>	<p>Location: posterior to trapezius</p>	<p>• BAT FF% significantly decreased after cooling</p>
		<p>FF% Ambient: 71 (2); ≈ 67 to 74 Pre-Cold: 71 (3); ≈ 65 to 73 Post-Cold: 66 (5); ≈ 59 to 71 Post-Warm: 68 (5); ≈ 56 to 72</p>	<p>FF% Ambient: 76 (8) * Values were only provided for ambient, and no range was provided</p>	
<p>Gifford et al. (2016)¹⁰¹ 3T; PDFF</p>	<p>Adults N: 17 (6M:11F)</p>	<p>Location: SCV Subject-specific binary mask</p>	<p>Location: umbilicus level</p>	

	Age: 25.1 (2.9); 21.6 to 34.5 BMI: 23.9 (2.9); 20.2 to 31.5	FF% Pre-Cold: 62.4 (6.8); 51.6 to 78.7 Post-Cold: 60.2 (7.6); ≈ 47 to 77 R2* Pre-Cold: ≈ 110 [≈ 101 to 118] Post-Cold: ≈ 113 [≈ 108 to 127]	FF% Pre-Cold: ≈ 94 [≈ 92 to 94.5] Post-Cold: ≈ 93.5 [≈ 92.5 to 94.5] R2* Pre-Cold: ≈ 50 [≈ 44 to 55] Post-Cold: ≈ 48 [≈ 45 to 53]	<ul style="list-style-type: none"> • FF% significantly decreased after cold exposure while R2* did not • FF% and R2* were significantly different between BAT and WAT
Franssens et al. (2015) ¹⁷⁵ 1.5T; PDFF	Adults N: 25 (19M:6F) Age: 61.4 (6.8) BMI: 25.8 (2.9); 20.6 to 32.8	Location: SCV	Location: posterior to trapezius	
		FF% Ambient (no cold): 82.5 [78.6 to 84.0]	FF% Ambient (no cold): 89.7 [87.2 to 91.5]	
Franz et al. (2015) ¹⁷⁶ 3T; SFF	Children N: 33 (24M:9F) Age: 14.7 (7.4 to 21.4) BMI: not provided	Location: SCV Subject-specific binary mask	Location: gluteal	• FF% was significantly different between BAT and WAT
		FF% Ambient (no cold): 73 (10); 32 to 94	FF% Ambient (no cold): 91 (4); 81 to 97	
	Elderly N: 11 (7M:4F) Age: 79.9 (76.3 to 88.6) BMI: not provided	Location: SCV	Location: gluteal	• FF% was not significantly different between BAT and WAT
		FF% Ambient (no cold): 90 (2); 84 to 94	FF% Ambient (no cold): 93 (3); 86 to 97	
Deng et al. (2015) ¹⁸² 3T; PDFF	Children (normal weight) N: 13 (8M:5F) Age: 11.4 (2.4) BMI: 51 st (31)	FF% Ambient (no cold): 77.2 (6.4) T2* Ambient (no cold): 12.5 (4.0)	NOT ANALYZED	

	Children (obese) N: 15 (10M:5F) Age: 12.5 (1.5) BMI: 98 th (1.3)	FF% Ambient (no cold): 84.3 (6.5) T2* Ambient (no cold): 15.6 (4.9)	NOT ANALYZED	
Lundström et al. (2015) ¹⁰² 1.5T; PDFF	Adults N: 9 (5M:4F) Age: 30 (5); 22 to 37 BMI: 23.2 (2.5); 18.1 to 25.7	Location: SCV FF% Pre-Cold: 82.8 (5); 72.4 to 88.7 Post-Cold: 80.9 (6.1); 67.3 to 87.6 Post-Warm: 80.9 (6.5); 66.3 to 86.9 R2* Pre-Cold: 21.0 (1.8); 19.1 to 25.2 Post-Cold: 21.6 (2.1); 19.3 to 26.3 Post-Warm: 21.1 (2.1); 19.4 to 25.9	Location: posterior to trapezius FF% Pre-Cold: 85.2 (5.1); 77.0 to 91.8 Post-Cold: 85.5 (4.8); 77.2 to 92.2 Post-Warm: 84.7 (4.7); 76.4 to 91.0 R2* Pre-Cold: 19.6 (2.8); 15.7 to 23.6 Post-Cold: 20.0 (2.7); 16.4 to 23.7 Post-Warm: 20.1 (3.0); 16.6 to 25.0)	<ul style="list-style-type: none"> • FF% significantly decreased after cold exposure while R2* tended to increase. • FF% and R2* were not significantly different between BAT and WAT
Hu et al. (2012) ¹⁷² 3T; PDFF	Children N: 39 (31M:8F) Age: 13.4 (2.8); 9.2 to 19.0 BMI: 74.7 th (31.0); 4.0 to 99.7 * Data on infants were not included in this table	Location: SCV FF% Ambient (no cold): 72.5 (12.1); 44.5 to 89.9 T2* Ambient (no cold): 18.0 (3.6); 11.9 to 25.5	Location: adjacent to SCV FF% Ambient (no cold): 86.2 (6.5); 70.7 to 94.2 T2* Ambient (no cold): 27.2 (6.8); 15.0 to 44.4	

Hu et al. (2012) ¹⁷¹ 3T; PDFF	Adults N: 5 (2M:3F) Age: 18 to 49 BMI: not provided * Data on infants and post-mortem individuals were not included in this table	Location: SCV	Location: adjacent to SCV	
		FF% Ambient (no cold): 52.0 to 93.9 T2* Ambient (no cold): 12.5 to 33.4	FF% Ambient (no cold): 82.8 to 95.4 T2* Ambient (no cold): 28.8 to 40.1	

END OF THE EXCERPT.

1.6 FACTORS RELATED TO BAT ACTIVITY.

1.6.1 ADIPOSITY

Cumulative evidence suggests that higher BAT activity is associated with lower adiposity in humans. Using ^{18}F -FDG PET-CT scans, BAT at ambient temperature^{62,72,192}, and in response to cold stimulation^{61,63,142,143}, was negatively related to measures of total adiposity. Participants with detectable BAT at ambient temperature had less SAT and VAT than those without detectable BAT^{193,194}. BAT activity in response to cold stimulation and insulin was lower in individuals with obesity¹⁴⁵. Similar findings were obtained from the MRI studies of BAT with and without cold stimulation. Lower SCV PDFF (browner phenotype) at ambient temperature was related to lower anthropometric obesity measures^{172,183,195,196} and lower VAT^{195,196} in both adults and children. Obesity in adults and children was associated with a higher SCV FF than those without obesity, before^{123,182} and after cold exposure¹²³. The relationship of BAT and adiposity starts early in life since higher SCV FF (whiter phenotype) was related to higher weight gain in infants between birth and 6 months of age¹⁹⁷.

Several research groups have investigated the impact of weight loss on the recruitment of BAT activity in subjects with obesity. For example, weight reduction after bariatric surgery in subjects with morbid obesity was accompanied by the detection of cold stimulated BAT measured, via ^{18}F -FDG PET-CT, that did not exist before the operation¹³⁴. Similar results were obtained in obese non-diabetic participants 8 months after Roux-in-Y gastric bypass and the detection of BAT after the surgery was accompanied by increased expression of beige/brown adipose tissue markers i.e., UCP1⁹³. However, weight reduction did not induce BAT activity in obese diabetic patients as it did in obese non-diabetic ones¹⁹⁸. Taken together, BAT activity is linked to lower total and visceral

adiposity, and it increases with weight loss but whether this is a consequence, or a cause of the weight loss is not clear.

1.6.2 GLUCOSE HOMEOSTASIS

As mentioned earlier, BAT can take up blood glucose upon stimulation, so it was proposed that BAT plays a role in regulating glucose homeostasis. For example, in an ^{18}F -FDG PET-CT study conducted at ambient temperature in 5070 participants, BAT glucose uptake is an independent negative predictor of T2D¹⁹⁹. In one study, patients with T2D also had impaired BAT glucose uptake in response to cold stimulation⁶⁷. In contrast, in other studies both acute and chronic cold exposure is associated with increased BAT glucose uptake and improvements in whole-body insulin sensitivity^{108,115,138} in patients with obesity and T2D. BAT can also be activated using high doses of Mirabegron, a β_3 -AR agonist and this is associated with improved insulin sensitivity in women²⁰⁰. While these data are interesting and suggesting a role for BAT in regulating glucose homeostasis, it was also reported that after acute cold stimulation, BAT contributes < 0.1% to whole-body glucose turnover^{66,67,113}. This limited role of BAT in glucose turnover is probably attributed to the small size of BAT compared to the skeletal muscles and the liver²⁰¹. So, even though activation of BAT results in increases in glucose uptake, whether its activation is vital for controlling whole-body glucose homeostasis is still unclear.

1.6.3 OUTDOOR TEMPERATURE

The detection of BAT via ^{18}F -FDG PET-CT at ambient temperature was found to be negatively related to outdoor temperature in human adults^{62,75,77} however, other research groups did not find a similar association in children²⁰² or adults¹⁹³. These studies assessed BAT retrospectively without offering an acclimation period before BAT imaging. Cold-induced thermogenesis, when assessed via indirect calorimetry, was found to be inversely related to 7-days outdoor temperature before

cold exposure²⁰³. However, it was also reported that offering an acclimation period at 32°C or room temperature on the day of BAT imaging hinders the impact of outdoor temperature on BAT measures¹²¹ and as such, no association between cold-stimulated BAT and outdoor temperature was found in this study¹²¹. The lack of association between outdoor temperature and pharmacologically stimulated BAT was also reported²⁰⁰.

1.6.4 SEX

Retrospective ¹⁸F-FDG PET-CT reports showed a higher prevalence of BAT at ambient temperature in women than in men^{62,72,75,193,204}. However, no sex-related differences in cold-stimulated BAT were reported in prospective studies^{78,112,205}. Similarly, contradicting findings were reported about BAT and sex in children. For example, the detection of BAT via ¹⁸F-FDG PET-CT at ambient temperature was not different between girls and boys^{202,206,207}. However, more SCV BAT volume with a stronger association with lower adiposity was noticed in preschool girls compared to boys¹⁹⁶. The change in SCV temperature, using IRT, after 5 minutes of hand cold exposure was higher in prepubertal girls than in boys²⁰⁸. A noticeable difference between the retrospective and the prospective studies that investigated sex differences in BAT is the sample size i.e., retrospective studies investigated thousands of scans. Further prospective studies to include larger cohorts are needed to better understand if there are sex differences in cold-stimulated BAT activity.

1.7 BAT AND NAFLD

As mentioned earlier, BAT can utilize substrates in a futile cycle, thus in pre-clinical animal models, it has been investigated for its role in NAFLD. Several preclinical studies showed that increased BAT activity is related to lower hepatic fat accumulation. For example, in a mouse model with hyperphagia, the defect in adaptive thermogenesis contributed to obesity, glucose intolerance,

and NASH in addition to increased caloric intake²⁰⁹. In another study that used the previously mentioned mouse model with established NASH, Beta-3 adrenergic receptor (β 3-AR) agonist coupled with caloric restriction restored BAT function, reduced hepatic fat and hepatic inflammation²¹⁰. Similarly, mice with genetic deletion of tryptophan hydroxylase enzyme 1 (Tph1), a key enzyme in the synthesis of peripheral serotonin hormone, were more sensitive to β 3-AR-induced activation of BAT and were resistant to diet-induced obesity and accumulated less liver fat despite high-fat diet²¹¹. These data suggest that, at least in rodents, the activation of BAT may be beneficial for reducing NAFLD.

In humans, retrospective studies using ¹⁸F-FDG PET-CT showed that BAT-positive participants had lower hepatic fat content^{193,194}. Similarly, another retrospective study showed that participants with non-detectable BAT had a higher odds ratio for NAFLD diagnosis by CT (characterized by a lower ratio of the liver: spleen attenuation)²¹². Likewise, another retrospective ¹⁸F-FDG PET-CT study showed a lower prevalence of NAFLD and lower levels of liver enzymes, alanine transaminase (ALT), and aspartate transaminase (AST), in participants with detectable BAT compared to those without BAT²¹³. In a prospective study that used MRI-PDFF for evaluation of BAT without cold stimulation in 61 adults, higher SCV BAT PDFF%, reflecting whiter phenotype of BAT¹⁷⁸, was directly related to liver PDFF%¹⁹⁵. Collectively, there is cumulative evidence that the presence of BAT is related to lower hepatic fat content. However, all the previously mentioned human studies relied on investigating BAT at ambient temperature. The relationship between cold-stimulated BAT and liver fat is yet to be explored.

1.7.1 THE MECHANISMS LINKING BAT AND NAFLD

The mechanisms linking the presence of BAT and lower hepatic fat in humans are not known. At room temperature, human BAT has a higher capacity to uptake FFAs than WAT and the BAT uptake capacity for FFAs is doubled with cold exposure⁶⁶⁻⁶⁸. Although the clearance capacity of BAT for FFAs accounts for <0.1% of whole-body fatty acid turnover, it can be still significant over a prolonged time to reduce the load of FFAs toward different organs like the liver²⁰¹. Since the role of BAT in human metabolism is not fully understood²¹⁴, investigating BAT in humans, as well as its different regulators, is important.

1.7.1.1 GUT MICROBIOME

As mentioned earlier, gut microbiota plays an important role in the development and progression of NAFLD. Preclinical studies have shown that the gut microbiota also impacts BAT activity and browning of WAT. For example, gut microbiota was found to negatively regulate WAT browning in rodents as depletion of gut microbiota via antibiotics or in germ-free mice was found to be associated with the recruitment of beige adipocytes into WAT depots²¹⁵. Changes in the composition of gut microbiota after cycles of intermittent fasting in mice also led to WAT browning and further improvement of obesity, hepatic steatosis, and insulin resistance²¹⁶. Additionally, acute (one day) and chronic (four weeks) cold exposure in mice led to compositional changes in the gut microbiota and enhanced the interscapular UCP1 expression and BAT thermogenesis²¹⁷. Cold exposure was associated with changes in the metabolism of bile acids via induced hepatic enzymes responsible for the conversion of endogenous and dietary cholesterol into bile acids^{217,218}. On the other hand, cold exposed mice had increased production of bacterially derived compounds such as butyrate that can augment BAT function²¹⁹. Taken together, these data suggest that in rodents the gut microbiota plays an important role in BAT-liver crosstalk.

1.7.1.2 SEROTONIN

Another potential mechanism linking BAT and NAFLD is serotonin. Serotonin or 5-hydroxytryptamine (5-HT), is a monoamine hormone formed from the essential amino acid tryptophan (Trp). The first and the rate-limiting step in the synthesis of 5-HT is regulated by the Tph enzyme to form 5 hydroxy Trp. Aromatic amino acid decarboxylase (AAD) regulates the second step in the synthesis pathway. AAD is widely distributed in the central and peripheral nervous systems and peripheral body tissues²²⁰. Serotonin exists in the body as two separate systems: peripheral serotonin and central serotonin. Serotonin can not cross the blood-brain barrier (BBB) and thus peripheral and central serotonin function in two distinct ways. The Tph enzyme has two different isoforms encoded by two different genes: Tph1 and Tph2²²¹. Tph1 exists in the peripheral tissues such as the Enterochromaffin (EC) cells of the gut, adipocytes, pancreatic B cells, and osteocytes. EC cells produce more than 90% of total body serotonin. Gut-derived serotonin (GDS) plays a very important role in controlling intestinal secretion and motility²²¹ and it can be absorbed into the general circulation. Very small amounts of serotonin are formed by the pancreas, adipocytes, and mammary gland²²². Tph1 activity in the EC cells in different regions of the gut is regulated by carbohydrates availability^{223,224}, CD4+T cells, and IL-13. Importantly, short-chain fatty acids produced by the gut microbiota increase the expression of colonic Tph1²²⁵, and this is important for the glucose-lowering effects of serotonin²²⁶. However, whether serotonin plays a role in linking higher BAT activity with lower hepatic fat in humans is yet to be explored.

A challenge with measuring serotonin in humans is that platelets uptake and store more than 90% of the circulating serotonin via the serotonin transporters (SERT) to be stored into dense granules and released for blood coagulation²²⁷. A small part of the serotonin (around 2%) exists free in the circulation and acts directly on target cells and can be measured in the platelet-poor plasma (PPP)

portion of the blood²²⁸. Non-platelet serotonin is typically metabolized to 5-hydroxyindole acetaldehyde (5-HIAL) by oxidative deamination through the action of the Mono Amino Oxidases (MAOs) that are present in the mitochondria of many cells. This is considered the main catabolic pathway of serotonin and occurs mostly in the liver and the lung²²⁹. MAO has two isoforms: MAO-A and MAO-B. MAO-A has a high affinity to serotonin. Around 99% of the 5-HIAL is further oxidized into 5-hydroxyindole acetic acid (5-HIAA) and only 1% can be reduced into 5-hydroxytryptophol (5-HTOL) by the action of aldehyde dehydrogenase. 5-HIAA is then excreted in the urine.

Measurement of urinary metabolites of serotonin is widely used in clinical practice. For example, detecting the levels of 5-HIAA is used to monitor the progression and treatment of carcinoid tumors; a tumor of the EC cells which is the primary site of Trp conversion into serotonin²³⁰. Patients with carcinoid tumors will show increased urinary excretion of 5-HIAA due to increased production of serotonin²³⁰. Alcohol consumption leads to an increased synthesis of 5-HTOL and a concomitant decrease in the synthesis of 5-HIAA, resulting in an increased 5-HTOL/5-HIAA ratio, which is a sensitive marker for the detection of recent alcohol intake²³¹.

1.7.1.3 FUNCTIONS OF PERIPHERAL SEROTONIN

Central 5-HT plays an important role as a neurotransmitter in controlling mood-anxiety, cognition, nociception, impulsivity, aggressiveness, libido, feeding behavior, and body temperature²³².

Peripherally, produced 5-HT also has a wide range of physiological functions in the body including the suppression of β -adrenergic stimulated energy expenditure in BAT²¹¹. Consistent with these observations in mice, in humans, elevated levels of peripheral serotonin are also observed in obesity and diabetes. For example, adults with obesity had two folds higher levels of PPP-serotonin than the controls and these levels were directly related to BMI and hemoglobin A1c

(HbA1c)²³³. Twenty-four hours urinary excretion of 5-HIAA was higher in diabetic adults than in normal controls²³⁴. In the previous study, urinary 5-HIAA was also directly related to fasting plasma glucose and HbA1c²³⁴. Adults with metabolic syndrome were reported to have higher plasma 5-HIAA than controls²³⁵. In individuals with metabolic syndrome, plasma 5-HIAA was also directly related to waist circumference, plasma TGs, and homeostasis model assessment of insulin resistance (HOMA-IR)²³⁶. Taken together, these data suggest that human obesity is associated with higher levels of circulating serotonin.

However, contradicting data has been also reported in human adults as serum and whole blood serotonin levels were found to be inversely related to BMI and total body fat^{237,238}. Additionally, plasma levels of serotonin decreased after ten weeks of lifestyle intervention for weight loss in 44 children and adolescents with overweight and obesity²³⁹. In the previous report, plasma serotonin was directly related to glucose levels and inversely related to BMI²³⁹. Moreover, adolescents with diabetes and obesity had lower urinary 5-HIAA compared to non-diabetic controls²⁴⁰. Thus, further studies are needed to explore these relationships and to navigate the reasons for the contradicting data.

1.8 BAT IN CHILDREN

As mentioned earlier, there is still a gap in the literature comparing BAT activity in different age groups, especially in children and adolescents. To date, no studies have been done to investigate whole-body cold-stimulated BAT activity in a pediatric population. ¹⁸F-FDG PET-CT was used to investigate BAT in children at ambient temperature mostly through retrospective studies^{72,176,248,206,241–247}. Due to the risk of ionizing radiation, ¹⁸F-FDG PET-CT scans were mostly done in children as a part of medical investigations for cancer screening and/or diagnosis. These studies revealed that BAT has similar anatomical distribution in children to adults but it is more detectable in children

, at ambient temperature, than it is in adults, with one out of every two children having it compared to one out of every 20 adults^{202,207,247}, and that BAT detection and volume increased during puberty^{202,247,249,250}. Additionally, ¹⁸F-FDG PET-CT reports showed that children with detectable BAT have considerably more muscle volume than those without²⁰⁷ and had lower BMI²⁰². The presence of BAT is also negatively correlated to cancer status in children with lymphoma²⁴². Therefore, even though ¹⁸F-FDG PET-CT studies provide valuable initial knowledge about BAT in children, there is still a need to explore other imaging modalities that are suitable to investigate cold-stimulated BAT in healthy children.

One of these non-invasive imaging modalities that have been used in children is the assessment of skin temperature using IRT. In several studies, IRT has been used to examine BAT activity in healthy pediatric populations after cold-stimulation protocols that were mostly brief and covered only a small portion of the body^{84,146,208,251,252} (i.e. during hand or foot immersion in cold water around 20 °C for 5 minutes). These studies have reported that children who had a lower increase in skin temperature after cold stimulation, reflecting lower BAT activity, had a higher BMI⁸⁴ and higher liver fat²⁰⁸. Although IRT is a non-invasive, safe, portable, low-cost, and rapid imaging modality that can be used repeatedly on the same individual, this method has significant challenges. Blood flow increases to the SCV region upon cold exposure¹²⁹ due to the proximity to large blood vessels in the neck. The generated heat from local blood flow may influence the change in SCV temperature independently of BAT activation²⁵³ however BAT surrounding tissues were found to have little impact on BAT temperature¹³⁶. Additionally, the variability in the thickness of the subcutaneous fat overlying BAT in the SCV region cannot be accounted for. Therefore, those with higher SCV subcutaneous fat thickness may have less change in skin temperature resulting in underestimation of BAT activity²⁵⁴.

Another concern is that even though cold exposure for 5 minutes was sufficient to show changes in the SCV skin temperature via IRT in children, this protocol might be too brief to reflect the maximal activity of BAT. Our team has previously reported that 10 minutes of whole-body cold exposure are needed to induce detectable BAT activity via MRI in young adults and this response plateaued after 35 minutes of cold exposure²⁵⁵. Thus, evaluation of BAT activity in children after prolonged cold exposure is needed. Due to the shortcomings of IRT, exploring cold-stimulated BAT activity in children using a different imaging modality is warranted.

As mentioned earlier, MRI measures BAT depending on its morphological and histological characteristics without the need for radiotracer uptake. MRI avoids the ionizing radiation of PET-CT and thus it can be used safely⁵⁹. MRI also avoids the influence of superficial subcutaneous fat. To date, MRI has been used to examine BAT in children without cold stimulation. MRI studies showed that lower FF at ambient temperature in the SCV region of infants predicted less gain in body fat during the first 6 months of life¹⁹⁷. The presence of BAT at ambient temperature in preschool children was associated with lower BMI, lower hepatic fat, and abdominal obesity¹⁹⁶. Further, in 7-year-old children, the higher SCV FF (whiter phenotype of BAT) was directly related to BMI and waist circumference²⁵⁶. Children with overweight/obesity had higher SCV FF^{172,182} and lower SCV perfusion¹⁸² compared to those with normal weight. Adolescents with obesity had a lower volume ratio between SCV BAT/WAT compared to normal weight controls²⁵⁷. Moreover, adolescents with higher SCV FF at ambient temperature had higher 2-hour glucose levels independent of age, sex, and adiposity²⁵⁸. Taken together, cumulative evidence indicates that BAT is related to obesity in children however the evaluation of cold-stimulated BAT activity in children using MRI is yet to be explored.

1.9 STUDY OBJECTIVES AND HYPOTHESIS

The general objective of this dissertation is to investigate BAT activity using MRI after a standardized whole-body cold exposure protocol in both adults and children and to explore the relationship of cold-stimulated BAT to metabolic health parameters including total and visceral adiposity, hepatic fat, glycemia, and plasma lipids.

In chapter two, using MRI, we explored BAT activity in 60 adults after three hours of whole-body standardized cold exposure protocol. MRI measures PDFF of the tissues¹⁹⁷. Reduction in PDFF was reported in the SCV region in response to cold stimulation which suggests an increase in intracellular TGs utilization^{131,255}. Therefore, the main aim of the study was to investigate if cold-stimulated BAT activity (represented as cold-induced percent decline in SCV PDFF) is related to hepatic fat content in adults. We explored if the gut microbiota could be an intermediary factor in linking BAT activity and hepatic fat and we further transplanted germ-free mice with human stools to examine the transferability of BAT activity through the microbiota. We also examined the relationships of cold-stimulated BAT to metabolic health parameters. The study hypotheses are 1. Individuals with higher BAT activity will have lower hepatic fat after controlling for confounders i.e., factors impacting or related to either BAT activity or hepatic fat; and 2. Individuals with higher BAT activity and lower hepatic fat will share transmissible gut microbiota characteristics that explain the link between the two tissues; and 3. Higher BAT activity will be related to lower adiposity and better glycemic control.

In chapter three, we explored BAT activity in 26 boys (8-10 years old) after one hour of a whole-body standardized cold exposure protocol. The main aim of that study is to evaluate cold-stimulated BAT activity with MRI (represented as cold-induced percent decline in SCV PDFF) in young children. We also investigated if cold-stimulated BAT activity is different between children

with and without overweight/obesity. We further explored the relationship of cold-stimulated BAT activity to metabolic health parameters. The hypotheses of this study are 1. Like in adults, cold exposure will result in a reduction of SCV PDFF in young children but not in subcutaneous fat depots i.e., abdominal fat. 2. Children with overweight/obesity will have lower cold-stimulated BAT activity compared to those with normal BMI; and 3. Higher BAT activity will be related to lower adiposity, lower hepatic fat, lower glycemia, higher insulin sensitivity, and better plasma lipid profile.

Chapter four is a sub-study from the above-mentioned pediatric cohort where we explored if measures of circulating free serotonin i.e., PPP-serotonin and urinary 5-HIAA in children are related to cold-stimulated BAT activity. We also explored if these measures are different between boys with and without overweight/obesity and if they are related to total and visceral adiposity. The hypotheses of this study are 1. Higher levels of circulating serotonin will be inversely related to cold-stimulated BAT activity and directly related to adiposity measures; and 2. Children with overweight/obesity will have higher levels of circulating serotonin compared to controls.

The findings of these studies will fill important knowledge gaps about the relationship of cold-stimulated BAT and hepatic fat as well as cold-stimulated BAT in children. Through these projects, we also explored if factors that are known to regulate BAT activity in rodents; like the gut microbiota and serotonin play a similar role in humans.

CHAPTER TWO

Lower brown adipose tissue activity is associated with non-alcoholic fatty liver disease (NAFLD) but not changes in the gut microbiota.

Basma A. Ahmed*, Frank J. Ong*, Nicole G. Barra, Denis P. Blondin, Elizabeth Gunn, Stephan M. Oreskovich, Jake C. Szamosi, Saad A. Syed, Emily K. Hutchings, Norman B. Konyer, Nina P. Singh, Julian M. Yabut, Eric M. Desjardins, Fernando F. Anhô, Kevin P. Foley, Alison C. Holloway, Michael D. Noseworthy, Francois Haman, Andre C. Carpentier, Michael G. Surette, Jonathan D. Schertzer, Zubin Punthakee, Gregory R. Steinberg*, Katherine M. Morrison*.

*These authors contributed equally to this work.

Published. Cell Reports Medicine (September 2021)

<https://doi.org/10.1016/j.xcrm.2021.100397>

2.1 Preface and Significance to the Thesis

In rodents, reductions in the thermogenic function of BAT are related to increased hepatic fat^{209–211}, an effect that may potentially be mediated via the gut microbiota²¹⁶, but this relationship has not been explored in humans. In this chapter, we show that cold-stimulated BAT activity (assessed via MRI), is negatively related to liver fat in 60 adults, independent of age, biological sex, and adiposity. However, fecal microbiota characteristics are not related to BAT activity and are not different between participants with high and low BAT activity. Moreover, fecal microbiota characteristics from these participants are not transmissible through fecal transplant to mice. Finally, BAT activity is negatively related to glycemia, total and visceral adiposity. These findings show that higher BAT activity is related to lower hepatic fat however gut microbiota is not likely to mediate this relationship. These findings are important as they show that enhancing BAT activity could potentially be a therapeutic target for NAFLD in adults.

2.2 Author contribution

B.A.A. and F.J.O. made comparable contributions toward this manuscript as detailed below and were the primary contributors to Figures 1 and 2 and Tables 1 and 2. B.A.A. was the main contributor to Figure 3. N.G.B. was the main contributor to Figures 4 and the writing about the animal experiments with J.D.S. B.A.A. and F.J.O. wrote the human part of the manuscript with G.R.S. and K.M.M.

F.J.O., B.A.A., G.R.S., and K.M.M. conceptualized the study. F.J.O., B.A.A., N.G.B., D.P.B., N.B.K., N.P.S., M.D.N., F.H., A.C.C., Z.P., S.A.S., J.M.Y., E.M.D., K.P.F., F.F.A., J.D.S., G.R.S., and K.M.M developed the methodology. F.J.O., B.A.A., N.G.B., E.G., J.C.S ran the formal Analysis. F.J.O., B.A.A., S.M.O., D.P.B., E.G., and E.K.H. ran the experiments. N.B.K., M.D.N., F.H., A.C.C., G.R.S., and K.M.M provided resources. B.A.A., F.J.O., N.G.B, J.D.S, G.R.S., and K.M.M. wrote the original draft. All the authors edited the final draft of the manuscript.

Lower brown adipose tissue activity is associated with non-alcoholic fatty liver disease (NAFLD) but not changes in the gut microbiota.

AUTHORS

Basma A. Ahmed^{1,2*}, Frank J. Ong^{1,3*}, Nicole G. Barra^{1,2,4}, Denis P. Blondin⁵, Elizabeth Gunn^{1,3}, Stephan M. Oreskovich^{1,3}, Jake C. Szamosi^{4,6}, Saad A. Syed², Emily K. Hutchings^{1,3}, Norman B. Konyer⁷, Nina P. Singh⁸, Julian M. Yabut^{1,9}, Eric M. Desjardins^{1,9}, Fernando F. Anhe^{1,2,4}, Kevin P. Foley^{1,2,4}, Alison C. Holloway^{1,10}, Michael D. Noseworthy^{1,7,8,11,12}, Francois Haman¹³, Andre C. Carpentier¹⁴, Michael G. Surette^{1,2,4,15}, Jonathan D. Schertzer^{1,2,4}, Zubin Punthakee^{1,3,9}, Gregory R. Steinberg^{1,2,9*}, Katherine M. Morrison^{1,3 * †}

AFFILIATIONS

1. *Centre for Metabolism, Obesity and Diabetes Research, McMaster University; Hamilton, ON, L8S 4L8; Canada*
2. *Department of Biochemistry and Biomedical Sciences, McMaster University; Hamilton, ON, L8S 4L8; Canada*
3. *Department of Pediatrics, McMaster University; Hamilton, ON, L8S 4L8; Canada*
4. *Farncombe Family Digestive Health Research Institute, McMaster University; Hamilton, ON, L8S 4L8; Canada*
5. *Faculty of Medicine and Health Sciences, Department of Medicine, Division of Neurology, Centre de recherche du CHUS, Université de Sherbrooke; Sherbrooke, QC, J1K 2R1; Canada*
6. *Farncombe Metagenomics Facility, Department of Medicine, McMaster University; Hamilton, ON, L8S 4L8; Canada*
7. *Imaging Research Centre, St. Joseph's Healthcare; Hamilton, ON, L8N 4A6; Canada*
8. *Department of Radiology, McMaster University; Hamilton, ON, L8S 4L8; Canada*
9. *Division of Endocrinology and Metabolism, Department of Medicine, McMaster University; Hamilton, ON, L8S 4L8; Canada*

10. *Department of Obstetrics and Gynecology, McMaster University; Hamilton, ON, L8S 4L8; Canada*

11. *Department of Electrical and Computer Engineering, McMaster University; Hamilton, ON, L8S 4K1; Canada*

12. *School of Biomedical Engineering, McMaster University; Hamilton, ON, L8S 4K1; Canada*

13. *Faculty of Health Sciences, University of Ottawa; Ottawa, ON, K1N 6N5; Canada*

14. *Division of Endocrinology, Department of Medicine, Centre de recherche du CHUS, Université de Sherbrooke; Sherbrooke, QC, J1K 2R1; Canada*

15. *Department of Medicine, McMaster University; Hamilton, ON, L8S 4L8; Canada*

* These authors made comparable contributions.

† Lead Contact

Correspondence to:

Dr. Gregory R. Steinberg - gsteinberg@mcmaster.ca

Dr. Katherine M. Morrison[†] - kmorrison@mcmaster.ca

DECLARATION OF INTERESTS

B.A.A. holds Lau's family scholarship for science and engineering and was funded by the Ontario graduate scholarship.

D.P.B. holds the GSK Chair in Diabetes of the *Université de Sherbrooke* that has been created in part through a donation of \$1 million by GSK to the *Université de Sherbrooke*. D.P.B. has received honoraria/consulting fees from Boehringer Ingelheim.

S.A.S. holds a Canadian Institutes of Health Research Vanier Canada Graduate Scholarship.

E.M.D. holds a Canadian Institutes of Health Research Vanier Canada Graduate Scholarship.

F.F.A. holds a CIHR postdoctoral fellowship and Diabetes Canada incentive funding.

A.C.H. holds research funding from the Canadian Institutes of Health Research and the Natural Sciences and Engineering Research Council of Canada.

A.C.C. holds the Canada Research Chair in Molecular Imaging of Diabetes and research funding from the Canadian Institutes of Health Research, *Fonds de recherche Québec – Santé*, and has participated in advisory boards for the companies Amgen, UniQure, Merck, Janssen, NovoNordisk, Novartis, HLS Therapeutics Inc., TVM Life Science Management, AstraZeneca, and Eli Lilly and made one conference sponsored by AstraZeneca.

M.G.S. is funded by the Canadian Institutes of Health Research, Genome Canada, and the W. Garfield Weston Foundation and holds a Tier 1 Canada Research Chair in Interdisciplinary Microbiome Research.

J.D.S. receives funding from the Canadian Institutes of Health Research (CIHR; FDN-154295) and holds a Canada Research Chair in Metabolic Inflammation.

Z.P. has received honoraria for advice and speaking from Abbott, Astra Zeneca/Bristol Myers Squibb, Boehringer Ingelheim/Eli Lilly, Janssen, Merck, NovoNordisk, Pfizer, and Sanofi. He has received research funds from Amgen, Astra Zeneca/Bristol Myers Squibb, Lexicon, Merck, NovoNordisk, Sanofi, and the Canadian Institutes of Health Research.

G.R.S. receives funding from the Canadian Institutes of Health Research (201709FDN-CEBA-116200 to GS), Diabetes Canada Investigator Award (DI-5-17-5302-GS)- a Tier 1 Canada Research Chair and the J Bruce Duncan Endowed Chair in Metabolic Diseases. He also receives research funding from Espervita Therapeutics, Esperion Therapeutics, and Poxel Pharma and honoraria/consulting fees from Astra Zeneca, Eli-Lilly, Esperion Therapeutics, Poxel, and Merck.

K.M.M. holds research funding from the Canadian Institutes of Health Research, Heart and Stroke Foundation of Canada, McMaster Children's Hospital Foundation, and McMaster University. She has received research funds from Astra Zeneca and is an advisory board member for Novo Nordisk and Akcea Therapeutics, Canada

ABSTRACT

In rodents, brown adipose tissue (BAT) contributes to whole-body energy expenditure and metabolic health. Lower BAT activity is related to hepatic fat content, partially attributable to the gut microbiome. Little is known about these relationships in humans. In adults (n=60), we assessed hepatic fat and cold-stimulated BAT activity utilizing magnetic resonance imaging and the gut microbiota with 16S sequencing. We transplanted gnotobiotic mice with feces from humans to assess the transferability of BAT activity through the microbiota. Individuals with NAFLD (n=29) had lower BAT activity than those without and BAT activity was inversely related to hepatic fat content. BAT activity was not related to the characteristics of the fecal microbiota and was not transmissible through fecal transplant to mice. Thus, low BAT activity is associated with higher hepatic fat accumulation in human adults, but this does not appear to have been mediated through the gut microbiota.

KEYWORDS

Non-alcoholic fatty liver disease; hepatic fat; brown adipose tissue; magnetic resonance imaging; proton density fat fraction; microbiota; germ free mice; adult humans; cold exposure

INTRODUCTION

Non-alcoholic fatty liver disease (NAFLD) is the leading cause of chronic liver disease and is an important risk factor for type 2 diabetes and cardiovascular disease²⁵⁹. NAFLD includes hepatic steatosis and non-alcoholic fatty steatohepatitis (NASH) which may progress to end-stage liver disease and hepatocarcinoma²¹. While numerous pharmacotherapies have been effective for treating NAFLD in rodents, none have been approved for use in humans²¹. The development of NAFLD occurs, in part, due to increased adipose tissue lipolysis and hepatic *de novo* lipogenesis²⁶⁰. The gut microbiome also plays an important role in the pathogenesis of NAFLD and its progression to more severe disease^{33,35,37,38,261}. Despite these important observations, therapies targeting lipolysis, lipogenesis, or the gut microbiome have had limited efficacy as stand-alone therapies for reducing NASH in humans, suggesting additional therapeutic strategies may be required²¹.

In numerous preclinical studies in rodents, enhancing the metabolic activity of brown adipose tissue (BAT) potentially reduces liver lipids^{211,262–264}. In mice housed at room temperature, BAT is a major contributor to whole-body energy expenditure due to thermogenesis mediated through uncoupling protein 1 (UCP1) and other futile cycles^{265,266}. Recent studies have found that the gut microbiome plays an important role in regulating BAT activity and the browning of white fat^{219,267,268} in rodents. However, it is not known if these findings are also present in humans.

In humans, BAT presents mainly in the neck and supraclavicular region (SCV)^{60–62}. Although BAT thermogenesis is a relatively minor contributor to whole-body energy expenditure^{59,269,270}, cold exposure increases human BAT activity and the clearance of circulating glucose, non-esterified fatty acids (NEFA), and triglycerides (TGs)^{66,67,99,105,152}. These data suggest that activating BAT may have positive effects on NAFLD. Consistent with this idea, retrospective

studies have noted a relationship between ^{18}F -fluorodeoxyglucose (^{18}F -FDG) uptake into the SCV area and NAFLD status^{193,194,212,213}. While interesting, it is important to note that in order to quantitate BAT activity it is essential that cold exposure be standardized between participants and to recognize that TGs and not glucose are likely the primary fuel source for activated BAT⁶⁶. Therefore, given previous studies in rodents and the potential influence of BAT activity on metabolic health in humans, it is important to determine if enhanced BAT activity may reduce hepatic fat content and if so, to determine whether the gut microbiota has a role in regulating this process.

In the current study, we have investigated if BAT activity is related to the hepatic fat content in adult humans. Compared to previous studies the use of a standardized cold exposure protocol and magnetic resonance imaging allows for detailed quantification of BAT activity. In addition, given previous studies in rodents, we investigated if the gut microbiota could be an intermediary factor regulating BAT activity. We find that low BAT activity is associated with increased liver lipids, but this is not related to differences in the gut microbiota.

RESULTS AND DISCUSSION

Participant Characteristics

This cross-sectional two-visit study was conducted in women and men, 18 – 57 years of age. Of the 483 people that inquired about the study, due to strict inclusion criteria described in the methods section, 73 (n=43 male) participants were enrolled, and 64 participants (n=39 male) completed both study visits (**Figure S1A**). Of the 9 participants that did not complete Visit 2, five were identified as ineligible at Visit 1 and four withdrew due to symptoms of claustrophobia during the MRI scan. Of the 64 participants with both visits, post-cold images for four participants were removed due to motion artifacts, leaving 60 participants (n=37 male) with useable pre- and post-cold MRI scans of the SCV region. Visits 1 and 2 occurred on average 18.5 days apart [range 14 – 29 days]. For premenopausal women, Visit 2 was scheduled around their menstrual cycle as described in the methods section. According to the American Diabetes Association guidelines for classification of glycemic status based on hemoglobin A1c (HbA1c) ²⁷¹, six participants had prediabetes and one had diabetes (HbA1c 8.0%). Diabetes had been previously identified in this individual, but they remained eligible as they were on no medications.

Proton Density Fat Fraction Declined in Supraclavicular but not in Subcutaneous Adipose Tissue

After a 3-hour cold exposure delivered through a water-perfused suit, set at 18°C ⁶⁶, the absolute decline in SCV PDFF was $3.0 \pm 2.4\%$ and the percent decline relative to baseline was $4.4 \pm 3.9\%$ (**Table 1**). In contrast, the PDFF in abdominal subcutaneous adipose tissue (SAT) remained unchanged after cold exposure (**Figure S1B**), consistent with expectations based on studies reported by us ²⁵⁵ and others ¹²³ in which PDFF of BAT and WAT had different responses to cold. The mean absolute decline in SCV PDFF in our participants was slightly greater than the

previously reported range of 0.4 – 2.2% (reviewed in Ong et al., 2018). This may be attributed to the more intense cold exposure (longer duration and lower temperature) and/or the application of cold to the whole body. The shivering intensity was < 3.0% of maximal voluntary contraction for all participants (**Table 1**), consistent with previous studies utilizing a similar standardized cold exposure protocol^{66,272}.

Given the variability in the baseline SCV PDFF, the decline in SCV PDFF that was relative to the baseline value was utilized as our primary measure of BAT activity (i.e., cold-induced percent decline in SCV PDFF). In studies in which BAT activity was measured with ¹⁸F-FDG uptake, individuals were classified as BAT positive or negative. Utilizing our measure, those who are BAT negative would be expected to have no cold-induced decline in SCV PDFF. Thus, we classified those with a cold-induced decline in SCV PDFF within one standard deviation of zero as having low BAT activity (n=33). A comparison of those with low vs high BAT activity is presented in Table S1. Neither shivering nor the delta change in outlet-inlet temperature were different between BAT groups (**Table S1**), suggesting that both groups were exposed to similar cold intensity^{108,255}. Consistent with previous literature, those with low BAT activity were older, more likely to be female, and had higher total body fat. No differences in macronutrient intake or dietary fibre were identified over the 24 hours prior to the measurement of BAT activity (**Table S2**).

Characteristics of those who were NAFLD positive

The median hepatic fat fraction in the 60 participants was 5.5% [4.6, 7.1%]. Hepatic fat exceeded 5.6%, the classification for hepatic steatosis (NAFLD positive)²⁷³, in 29 (48%) participants (**Table 1**). Those who were NAFLD positive were older and had higher body mass index (BMI), body fat percentage, visceral adipose tissue (VAT), and abdominal SAT (**Table 1**). They also had higher

serum alanine aminotransferase (ALT), gamma-glutamyl transferase (GGT), non-HDL cholesterol, fasting blood glucose levels, and higher blood pressure (**Table 1**). The participant with diabetes and four of the six participants with prediabetes were NAFLD positive.

Individuals with Hepatic Steatosis had Lower Cold-induced Percent Decline in Supraclavicular Proton Density Fat Fraction

Study participants that were NAFLD positive had lower BAT activity compared to NAFLD negative (2.5 [1.2, 5.7] % vs 4.7 [2.7, 8.1]; $p = 0.019$) (**Figure 1A**), (**Table 1**). Consistent with that, a lower cold-induced percent decline in SCV PDFF was associated with higher hepatic fat ($\rho = -0.41$; $p = 0.001$) (**Figure 1B**). The relationship of the decline in SCV PDFF with hepatic fat remained significant, independent of age, gender, and either total body fat or VAT area (**Table 2**). Our data suggest that in humans, as in rodents^{264,274,275}, higher BAT activity is associated with lower hepatic fat accumulation, and this relationship is not fully explained by age, biological sex, or adiposity.

Cold-induced Percent Decline in Supraclavicular Proton Density Fat Fraction, Age and Adiposity

We also confirmed that the cold-induced percent decline in SCV PDFF was related to demographic characteristics and measures of metabolic health previously reported to be related to ¹⁸F-FDG uptake measured with PET-CT⁷³. Lower age ($\rho = -0.48$; $p < 0.001$) (**Figure 2A**), total body fat ($r = -0.62$; $p < 0.001$) (**Figure 2B**), waist circumference ($r = -0.47$; $p < 0.001$) (**Figure 2C**), BMI ($r = -0.46$; $p < 0.001$) and VAT ($\rho = -0.60$; $p < 0.001$) were associated with greater cold-induced percent decline in SCV PDFF. Males had a greater cold-induced percent decline in SCV PDFF than females (mean difference = 2.3%; $p = 0.022$), but this relationship was no longer significant

($p = 0.479$) when age and total body fat were included in the multivariate regression model (**Table S3**).

Cold-induced Percent Decline in Supraclavicular Fat Fraction and Glucose Homeostasis

A greater cold-induced percent decline in SCV PDFF was associated with lower HbA1c ($\rho = -0.31$; $p = 0.017$), fasting plasma glucose ($\rho = -0.29$; $p = 0.026$) and 2-hour 75g oral glucose tolerance test (OGTT) plasma glucose ($\rho = -0.42$; $p = 0.018$) (**Figure 2D, E and F**). The latter remained related to cold-induced percent decline in SCV PDFF while controlling for age, sex, and total body fat ($\rho = -0.44$; $p = 0.022$). These data suggest that, in addition to the relationship with hepatic fat content, higher cold-stimulated BAT activity is linked to better glucose homeostasis.

Relationship of Gut Microbiota to Cold-induced Percent Decline in Supraclavicular Fat Fraction

To determine if gut microbiota characteristics might link lower BAT activity to the higher hepatic fat content in humans, as it does in rodents, we examined these relationships in our cohort. Alpha diversity of the fecal microbiota, as measured by Shannon and Inverse Simpson indices, was not related to cold-induced percent decline in SCV PDFF and was not different between high and low BAT groups, and this was true whether or not age and total body fat percentage were included in the model (**Figure 3A**), (**Table S4**). Further, there was no distinct clustering of BAT groups on a principal coordinates analysis (PCoA) plot using the Bray-Curtis dissimilarity metric (**Figure 3B**) and there was no significant relationship of BAT groups with microbial community structure; $p = 0.74$ (**Table S5**). The presence of three genera was related to cold-induced percent decline in SCV PDFF after controlling for age, although these relationships were tempered when total body fat was included in the regression model (**Table S6**) and these bacteria were present in only a few

participants in our cohort (**Figure S2**). The only genus with a different abundance between high and low BAT groups (**Figure 3C**) was *Succiniclaticum* which was more abundant in the low BAT group (**Table S6**). It was, however, only present in two participants in the cohort (**Figure S2**) and therefore does not appear in Figure 3C. Collectively, although the abundance of few bacteria was related to the cold-induced percent decline in SCV PDFF and different between BAT groups (**Table S6**), these bacteria were present in only a few participants in our cohort.

To examine whether these lack of differences between groups might be a function of our sample preparation and analysis, we compared microbiome signatures of people with and without NAFLD. Consistent with previous studies^{38,276}, gut microbiota characteristics differed based on NAFLD status in several distinct areas. Alpha diversity was lower in the fecal sample from individuals with NAFLD compared to those with normal hepatic fat content, independent of age and total body fat ($p=0.022$ and 0.046 for Shannon and Inverse Simpson respectively) (**Figure S3A**), (**Table S4**). Similarly, and consistent with previous reports^{276,277}, there was a distinct clustering between NAFLD groups on the PCoA plot (**Figure S3B**). Additionally, NAFLD status had a small (3%), but significant ($p=0.012$) effect on the variation in gut microbial community structure as measured with the Bray-Curtis dissimilarity index (**Table S5**). In summary, while we identified characteristics of the gut microbiota that differed in those with and without NAFLD, we identified no characteristics that were related to both BAT activity and hepatic steatosis.

Microbial Transfer to Mice

To assess whether BAT activity in humans is microbially transmissible, germ-free mice (3-4 per donor) were colonized with fecal material from human donors who had high BAT (n=3) or low BAT (n=4) activity (**Table S7**). Our laboratory has previously shown that this method of microbial transfer and the 8-week host exposure time is sufficient to transmit a microbial community that

can promote insulin resistance and poor glucose control when colonizing germ-free mice²⁷⁸. After 8 weeks, fecal microbiota of stool samples from the colonized mice was found to cluster with the stool sample from their respective donor (PERMANOVA $p=0.0001$; $R^2 = 0.39$; **Figure S4A**). Using an Upset plot to evaluate how many ASVs were shared between donor samples and recipient mice, we found 26 and 15 ASVs were uniquely shared between matched donors and recipients of high BAT or low BAT samples, respectively (**Figure S4B**). This was compared to 3 ASVs in discordant pairs of donors and recipients (i.e., high BAT donors and low BAT recipient mice), suggesting successful transfer of unique microbiota in each group. The colonized mice who received fecal material from high BAT donors had similar body mass (**Figure 4A**), fat mass (**Figure 4B**), and oxygen consumption (**Figure 4C**) as the colonized mice who received fecal material from low BAT donors. Also, recipient mice from high and low BAT donors had comparable oxygen consumption and interscapular surface temperature at baseline and when challenged with the β 3-adrenergic receptor agonist CL-316,243, which specifically increases UCP1-mediated thermogenesis²⁷⁹ (**Figure 4D, E, and F**). Similar results were collected using C57Bl6J colonized SPF mice gavaged with fecal material from human high or low BAT donors (**Figure S5**). These data indicate that transmission of fecal microbes from humans discordant for BAT activity did not result in alterations in body mass, fat mass, or BAT activity of the recipient mice.

Our findings contrast with studies done in rodents in which browning of white adipocytes and enhancement of BAT activity can be transmissible *via* fecal microbes. Cold-exposed mice have augmented BAT activity and distinctive gut microbial profiles^{216–218}. Microbiota transfer from cold-exposed mice to germ free mice promotes white adipocyte browning through the upregulation of UCP-1 expression²¹⁷. After cold stimulation, exposed mice have increased production of

bacterially derived compounds such as butyrate that can augment BAT function²¹⁹. While these results suggest that BAT metabolism can be altered via the gut microbiota in rodents, we have not identified similar findings in humans. No detectable changes in body composition, whole-body energy expenditure, or UCP-1 mediated thermogenesis were identified in mice that received gut microbes from humans with differing levels of BAT activity. These findings are consistent with the lack of association of the characteristics of the fecal microbiota with BAT activity.

STUDY LIMITATIONS

Although this study is one of the largest human studies to utilize MRI in the evaluation of BAT in cold-stimulated conditions, metabolic health, and gut microbiota, our study is not without limitations. It is uncertain how our findings might apply to groups who were not included in our study including older adults and individuals with diabetes or other conditions managed with pharmacotherapy. We also did not have individuals with severe obesity or high levels of liver fat in our study as the MRI could only accommodate individuals weighing less than 136kg. Although there were many similarities between our study and previous reports with respect to the relationship between the gut microbiome and NAFLD, the relatively low upper weight limit for the MRI and exclusion of individuals on medications may explain why some of our findings differed from others (**Figure S3C**)^{34,277}. We did not collect ethnicity data. Ethnicity has been shown to impact the gut microbiome²⁸⁰ but not BAT activity^{96,281} therefore it is unlikely this was a major factor dictating changes in BAT activity between groups. Lastly, the human microbiota can be influenced by diet²⁸². Although the self-reported macronutrient and dietary fibre intake did not differ between those with and without obesity (**Table S2**), we did not standardize the dietary intake and thus differences may have contributed to the lack of relationship between the fecal microbiota and BAT activity.

CONCLUSIONS

The current study demonstrates that, in human adults, lower BAT activity (cold-induced percent decline in SCV PDFF) is associated with greater hepatic fat content and higher measures of glycemia, independent of age, sex, and total body fat. Contrary to our hypothesis, we did not identify characteristics of the gut microbiota related to BAT activity, nor evidence that BAT activity can be transmitted via fecal transplant from humans to germ free mice. Thus, our findings highlight a clear link between BAT activity, and hepatic fat content supporting the premise that stimulation of BAT activity may be a potential therapeutic target for the management of NAFLD in humans. We did not, however, find evidence that the fecal microbiota plays an intermediary role in the relationship between BAT activity and NAFLD.

ACKNOWLEDGMENTS

This study was supported by grants from the Boris Family and the Canadian Institutes of Health Research (grant number 144625-1). We would like to thank the staff members of the Boris Clinic at McMaster University Medical Centre and the MRI technologists at the Imaging Research Centre (IRC) at St. Joseph's Healthcare Hamilton. We thank Prasiddha Parthasarathy and Stephanie Schwindt for their help in collecting the data, and Vivian Vaughan Williams for her assistance with study visits. We thank the McMaster Genome Facility and Laura Rossi who conducted the 16S amplification experiments. We also thank the computer server support provided by the laboratory of Dr. Andrew McArthur and the McMaster Service Lab and Repository (MSLR).

AUTHOR CONTRIBUTIONS

Conceptualization, F.J.O., B.A.A., G.R.S., and K.M.M.; Methodology, F.J.O., B.A.A., N.G.B., D.P.B., N.B.K., N.P.S., M.D.N., F.H., A.C.C., Z.P., S.A.S., J.M.Y., E.M.D., K.P.F., F.F.A., J.D.S.,

G.R.S., and K.M.M.; Formal Analysis, F.J.O., B.A.A., N.G.B., E.G., J.C.S.; Investigation, F.J.O., B.A.A., S.M.O., D.P.B., E.G., and E.K.H.; Resources, N.B.K., M.D.N., F.H., A.C.C., G.R.S., and K.M.M.; Writing – Original Draft, B.A.A., F.J.O., N.G.B., J.D.S., G.R.S., and K.M.M.; Writing – Review & Editing, B.A.A., F.J.O., N.G.B., E.G., J.C.S., D.P.B., S.M.O., E.K.H., N.B.K., N.P.S., S.A.S., J.M.Y., E.M.D., F.F.A., K.P.F., A.C.H., M.D.N., F.H., A.C.C., M.G.S., J.D.S., Z.P., G.R.S., and K.M.M.; Supervision, G.R.S., and K.M.M.; Funding Acquisition, G.R.S., and K.M.M.

METHODS

CONTACT FOR REAGENT AND RESOURCE SHARING

Requests for further information regarding resources utilized or data should be directed to and will be fulfilled by the Lead Contact, Dr. Katherine M. Morrison (kmorrison@mcmaster.ca).

MATERIALS AVAILABILITY

This study did not generate any new reagents or materials.

DATA AND SOFTWARE AVAILABILITY

Sequencing data from the fecal microbiota samples has been deposited in GEO (accession number: GSE162608). The clinical dataset supporting the current study has not been deposited in a public repository because the consent form signed by study participants noted that individualized data would not be published. Grouped data are available from the corresponding author on request.

EXPERIMENTAL MODEL AND PARTICIPANT DETAILS

Study Population

Participants in this two-visit, observational, cross-sectional study were enrolled from the City of Hamilton, Ontario, Canada, and the surrounding area between June 2016 and March 2018. Male

and female participants aged 18 to 60 years were included in the study unless they met any of the following exclusion criteria: use of nicotine or tobacco products, self-reported alcohol intake of ≥ 7 drinks/week and ≥ 3 drinks/day for males or ≥ 2 drinks/day for females, contraindications for MRI imaging (claustrophobic, implanted metal, metallic injuries, recent tattoos obtained outside of Canada), inability to fit inside or greater than the weight limit (i.e. more than 136 kg) of the MRI scanner, pregnancy or a breastfeeding mother, use of one of the excluded medications including adrenergic and serotonergic agents, metformin and other diabetes medications (**Table S8**), a history of bariatric surgery, liver transplantation or medical conditions i.e. liver diseases and untreated hormonal imbalance (**Table S8**).

METHOD DETAILS

Study Approval

This study was approved by the Hamilton Integrated Research Ethics Board (HiREB) and was conducted utilizing Good Clinical Practise (GCP) principles. All participants provided informed consent. All the animal experiments were approved by the McMaster University Animal Ethics Committee and conducted under the Canadian guidelines for animal research.

Study Visits

Participants were asked to fast for at least 8 hours, to refrain from vigorous physical activity for at least 48 hours, avoid intake of caffeine for at least 12 hours, and to abstain from serotonin-rich foods (e.g., banana, tomato, kiwi, walnut, avocado, pineapple, and plum) for at least 24 hours prior to both visits. Study participants completed a prospective, dietary diary for the 24-hour period prior to Visit 2. Visits 1 and 2 took place in the morning and were scheduled at least 7 days apart, but ideally within one month of each other. To standardize Visit 2 to the same point in the menstrual cycle for female participants who were pre-menopausal, the visit occurred within 7 days after the commencement of menstruation.

Visit 1 occurred at the McMaster University Medical Centre, Hamilton, ON, Canada. Measures included anthropometry (height, weight, and waist circumference), blood pressure, body composition assessment, and a 75g OGTT, with blood samples collected at baseline and 2 hours (**Figure S6**). The one study participant with a known diagnosis of type 2 diabetes (n=1) had a fasting blood sample only and no OGTT was done.

Visit 2 took place at the Imaging Research Centre at St. Josephs Healthcare, Hamilton. The mean outdoor temperature at 1 hour, 24 hours, and 7 days prior to this visit were obtained retrospectively from data collected at the McMaster Weather Station, operated by the Hydrometeorology and Climatology Lab in the School of Geography and Earth Sciences, McMaster University. Upon arrival, participants changed into standardized cotton tank tops and shorts. They were then acclimated to room temperature for 30 minutes. The temperature in the room where participants underwent acclimation and cold exposure was recorded (Wireless Forecast Station with Pressure History Model WS-9037U-IT; La Crosse Technology, La Crosse, WI, USA). The baseline (pre-cold) MRI scan was conducted of the SCV region, liver, and abdomen. Participants were then

exposed to a standardized cold exposure of 18°C for 3 hours using a whole-body water-perfused suit. Shivering intensity was measured using electromyography (EMG) as described below. The MRI scan of the neck was repeated immediately after the cold exposure.

Cold Exposure Protocol

The cold exposure protocol was based on a protocol previously shown to be adequate for BAT stimulation, measured using ^{18}F -FDG PET-CT ^{66,113,272}. Participants were fitted with a high-density liquid conditioned suit (LCS; Two Piece, Med-Eng, Ottawa, ON, Canada), and 18°C water was circulated for 3 hours using a temperature- and flow-controlled circulation bath (Isotemp 6200 R28, Fisher Scientific, Waltham, MA, USA). Inlet and outlet water temperature entering and exiting the suit were recorded during the cold exposure at 15-second intervals with a dynamic range of 16 bit using a data logger (PowerLab; ADInstruments, Sydney, Australia) connected to two quick-disconnect thermocouples (TMQSS-020G-2; OMEGA Engineering, Stamford, CT, USA) fixed to the inlet and outlet manifolds. The inlet to outlet temperature difference ($\Delta_{\text{Outlet-inlet}}$) of the suit was calculated for the last 30 minutes of the cold exposure.

Measurement of Shivering Intensity with electromyography (EMG)

The shivering intensity was measured at baseline and during cold exposure using surface EMG (Trigno Wireless System, Delsys, MA, USA with Trigno Snap-Lead Sensor connected to pre-jelled Norotrode 20 Bipolar SEMG electrodes, Myotronic, WA, USA). Electrodes were placed on the bellies of the trapezius, vastus lateralis, and vastus medialis muscles (right side only). A series of maximal voluntary contractions (MVC) were performed on each muscle (three trials of maximum contraction to be reached by verbal encouragement alternate with 30 seconds rest between trials) and the shivering intensity of each muscle was calculated from root-mean-square

(RMS) values calculated from raw sEMG, normalized to MVC RMS and corrected for baseline RMS measured at room temperature while lying down, as previously described ²⁸³.

MRI Acquisition Protocol

MRI-derived proton density fat fraction (MRI-PDFF) measures the ratio of the total density of fat mobile protons to the total density of fat and water mobile protons and therefore mirrors the triglyceride concentration in tissues¹⁷⁴. Accordingly, MRI-PDFF differentiates BAT and surrounding tissues including white adipose tissues and muscles based on their physical properties. Thus, BAT-containing depots showed lower PDFF than white adipose tissue^{101,136}.

MRI-PDFF can be used to measure BAT activity; the reduction in the supraclavicular (SCV) PDFF in response to cold exposure is correlated with ¹⁸F-FDG uptake measured using PET-CT^{123,136}. Further, cold-stimulated reductions in SCV-PDFF have been corroborated with histological findings, UCP1 immunohistochemistry^{173,179}, and observations that TG mobilization is central to BAT thermogenesis¹¹³. MRI-PDFF is also a well-established, non-invasive, quantitative, and accurate means to measure hepatic fat content²⁸⁴.

MRI scans were performed using a 3-Tesla (T) whole-body MRI scanner (Discovery 750; GE Healthcare, Waukesha, WI, USA). Quantitative Iterative Decomposition of water and fat with Echo Asymmetry and Least-squares estimation (IDEAL-IQ) was used since it is a confounder-corrected 3D gradient multi-echo MRI sequence that provides an accurate measure of tissue triglyceride content by using multiple spectral modeling of adipose tissues while accounting for T2* decay¹⁷⁴. This pulse sequence generates six distinct image contrasts: water-only, fat-only, in-phase, out-of-phase, corrected proton density fat fraction (PDFF), and R2* images. LAVA-FLEX is a 3D gradient dual-echo MRI sequence that generates four distinct image contrasts: water-only, fat-only, in-phase, and out-of-phase. Due to its nature, the LAVA-FLEX pulse sequence provides a higher resolution image with sharper tissue boundaries, compared to IDEAL-IQ.

BAT activity: Supraclavicular measurements of PDFF were acquired using the IDEAL-IQ pulse sequence. Using a Head/Neck/Spine (HNS) coil, with an additional attachment that provided signal from the anterior portion of the chest, axial images were taken from the C2/C3 disc to the T4/T5 disc (IDEAL-IQ, slice thickness 4mm, 50 slices, flip angle= 4°, TE/TR=1.2/7.8ms, FOV=380 mm, matrix size = 224x192 (i.e., image resolution = 1.70 x 1.98 x 4mm), acceleration factor 2, scan time = 2.7 min). Segmentation and analysis of all MRI images were conducted using Analyze Pro (Version 1; Mayo Clinic, Biomedical Imaging Resource, AnalyzeDirect, Overland Park, KS, USA) by a single reader. The SCV was segmented using semi-automated and manual segmentation tools and the accuracy of segmentation was confirmed by an experienced radiologist (NS). The vertebral column was used as the reference for the start (C5-C6 disc) and end (T1-T2 disc) of segmentation. A fat mask, generated from the fat-only images, was first applied to the PDFF map at the C7-T1 disc to isolate adipose tissues and exclude background noise from the MRI image. A FF threshold set at 30 to 100% was then applied to the PDFF image. A region of interest (ROI) was manually drawn over the SCV region defined by the trapezius muscle posteriorly, the sternocleidomastoid muscle medially, and the clavicle inferiorly¹⁷². The ROIs were then post-processed using a one-time 2D erosion (1x3 voxels) to correct for any inherent partial volume effects in the images. T2* images were generated from the R2* data by use of the relationship: $T2^* = 1/R2^*$. A T2* mask was applied to the FF map to help differentiate BAT from white adipose tissue (WAT) by isolating voxels with a T2* between 2 and 25ms, based on a published report that tissue with a T2* value of ≥ 26 ms consists mostly of muscle, fluid or white adipocytes²⁸⁵. The lower range of 2ms was selected due to the MRI sequence's limitation in detecting very low T2* values. All voxels that satisfied the above criteria were averaged and classified as SCV PDFF.

To evaluate BAT activity accounting for the pre-cold SCV PDFF, the percent change in SCV PDFF was calculated as $[(\text{pre-cold SCV PDFF} - \text{post-cold SCV PDFF}) / (\text{pre-cold SCV PDFF})] * 100$ and is introduced in the main text as cold-induced percent decline in SCV PDFF. For microbiota analysis, participants were categorized into high BAT (n= 27, male= 21) and low BAT (n= 33, male = 16) groups. Individuals were considered with low BAT activity if the cold-induced percent decline in SCV PDFF was within 1 SD of zero.

Hepatic fat: Hepatic fat was measured from axial scans obtained in a single breath-hold using a 32-channel torso array coil (NeoCoil, Pewaukee, WI, USA) from 7cm above to 7cm below the L4-L5 disc (IDEAL-IQ, slice thickness 8mm, 32 slices, flip angle = 3°, TE/TR=1.0/6.5ms, FOV=340 mm, matrix size = 160x160 (i.e., image resolution = 2.1 x 1.7 x 8mm), acceleration factor 2 x 1.5, scan time = 18 sec). A multi-slice segmentation that included the entire liver was undertaken using Analyze Pro software. ROIs were drawn over the entire liver using a tool that “snaps” to the edges of regions where changes in voxel intensities are high. The in-phase image was used as a reference when the boundaries of the liver were not clearly defined in the fat-fraction image. The ROIs were then post-processed using a 2D erosion (3x3 voxels) to correct for partial volume effects. All voxels that satisfied the above criteria were averaged and classified as hepatic fat.

Abdominal subcutaneous and visceral adipose tissue areas: For abdominal subcutaneous adipose tissue (SAT) and visceral adipose tissue (VAT) were measured from a single slice located 6 cm above the L4-L5 disc²⁸⁶. Abdominal SAT PDFF was calculated from a single slice at L4-L5 disc obtained in a single breath-hold scan (IDEAL-IQ, Slice thickness 5mm, 32 slices, flip angle 3°, TE 6.1ms, TR 0.9ms, FOV 400 mm, matrix size = 160x 160 (image resolution 2.5 x 2.0 x 5mm), acceleration factor 2 x 1.5, scan time = 18 sec). A semi-automated tool (i.e., 2D seeded region growing) was used to segment abdominal SAT. Voxels with low PDFF values (below 30%) were excluded to isolate adipose tissues from muscle. A 2D erosion (3x3 voxels) was applied to attenuate partial volume effects. All voxels that satisfied the above criteria were averaged and classified as SAT PDFF. To measure the area of abdominal SAT and VAT, the same slice was used from the higher resolution, single breath-hold LAVA-FLEX scan (LAVA-FLEX, slice thickness 5mm, 32 slices 32, flip angle = 3°, TE/TR=1.3/4.1ms, FOV=400mm, matrix=320x224 (i.e., spatial resolution = 1.25 x 1.78 x 5mm), acceleration factor 1.5, scan time = 14 sec). A fat

mask was applied to exclude non-adipose tissues from analysis while SAT and VAT were separated semi-automatically based on seed points. Retroperitoneal adipose tissue was excluded manually from VAT. Finally, the ROIs were post-processed using 2D erosion (3x3 voxels) to attenuate partial volume effects.

Anthropometric Measures

Weight, height, and waist circumference were each measured three times by trained research personnel and these values were averaged. Weight (kg) was measured using an electronic platform scale (BMI Scale Model 882; Seca, Hamburg, Germany) to the nearest 0.1 kg. Height (cm) was measured using a wall-mounted stadiometer (Height Measuring Rod Model 240; Seca, Hamburg, Germany) to the nearest 0.1 cm. BMI was calculated as weight in kilograms divided by height squared in meters. Waist circumference (cm) was measured at the midpoint between the costal margin and the iliac crest at the end of expiration using a weighted measuring tape (Pull Type Spring Scale; Ohaus, Parsippany, NJ, USA) set at 750g.

Body Composition

Body composition (total body fat (%), fat mass (kg), lean mass (kg)) was assessed using dual-energy x-ray absorptiometry (DEXA) (Lunar Prodigy Advance 8743; GE Healthcare, Waukesha, WI, USA). All scans were reviewed by one individual (KMM) to ensure the consistency of ROIs.

Blood Samples

Blood samples were collected at baseline (fasting) and 2-hours after the consumption of a 75g glucose drink and were analyzed in the Clinical Laboratory at Hamilton Health Sciences (Hamilton, ON, Canada). Fasting total cholesterol, HDL-cholesterol, and triglycerides were measured using Architect C16 (Abbott) on serum samples and LDL-cholesterol was calculated

using the Friedewald equation ²⁸⁷. Alanine aminotransferase (ALT), aspartate aminotransferase (AST), fasting, and 2-hour plasma glucose were measured using Architect C4000 or c4100 (Abbott, Chicago, IL, USA) on heparinized plasma samples. HbA1c was analyzed in whole-blood samples on the Capillary 2 Flex Piercing (Sebia, Lisses, France) instrument. Dysglycemia was based on HbA1c and was classified according to the American Diabetes Association guidelines, prediabetes (HbA1c= 5.7 – 6.4%) and diabetes (HbA1c \geq 6.5%) ²⁷¹.

Dietary intake

Information from the diet diary was entered into the nutritional software Food Processor by ESHA. Total calories, macronutrients (protein, carbohydrate, total and saturated fat), and dietary fibre intakes were calculated utilizing the software.

Stool Samples

Stool samples were collected by participants within 48 hours of Visit 2. Participants were instructed to immediately transfer 10-20g of fecal sample into the 50ml sterile specimen container and storage packaging provided, store in a cooler pack in their freezer, and bring the frozen samples to Visit 2. Samples were delivered frozen to the laboratory and stored at -20°C until thawed and aliquoted. One portion (approximately 200mg) was reserved for nucleic extraction and up to five 2-ml cryovials were stored for future analyses or experiments. All aliquots were kept frozen at -80°C.

Microbiota Profiling

DNA extraction was carried out as described previously (Stearns et al., 2015), with few modifications, from 0.2g of stool sample that was mechanically lysed with 2.8mm ceramic beads

(Mo Bio Laboratories Carlsbad, CA) and 0.1mm glass beads (Mo Bio Laboratories, Carlsbad, CA) for 2 cycles of 3 minutes at 3000rpm with a 45 seconds delay between cycles in 800µl of 200mM of monobasic NaPO₄ (pH=8) and 100µl of guanidinium thiocyanate buffer. Samples were further centrifuged at 13,500g for 5 minutes and processed using the MagMAX-96 DNA Multi-sample kit (Life Technologies, Carlsbad, CA) via the MagMAX Express 96-Deep Well Magnetic Particle Processor (Applied Biosystems, Foster City, CA). Purified DNA was used for amplification of the 16S rRNA gene using paired-end reads of the V3 region. Amplification of the bacterial 16S rRNA gene for the germ-free mice microbiota was done for the V3-V4 region. 50 ng of DNA was used as a template with 1U of Taq, 1x buffer, 1.5 mM MgCl₂, 0.4 mg/mL BSA, 0.2 mM dNTPs, and 5 pmoles each of 341F (CCTACGGGAGGCAGCAG) and 518R (ATTACCGCGGCTGCTGG) Illumina adapted primers, as previously described²⁹³. The reaction was carried out at 94°C for 5 minutes, 25 cycles of 94°C for 30 seconds, 50°C for 30 seconds, and 72°C for 30 seconds, with a final extension of 72°C for 10 minutes. PCR products were then visualized on a 1.5% agarose gel. Positive amplicons were normalized using the SequalPrep Normalization Plate kit (Thermo Fisher, Waltham, Massachusetts, USA). Triplicate amplifications were pooled for 250bp paired-end MiSeq Illumina sequencing in the McMaster Genomics Facility. Sequence data were processed through the DADA2 pipeline (divisive amplicon denoising algorithm 2) to produce ASVs (amplicon sequence variants)²⁹⁴. After processing, we had 4,881,511 reads representing 2,362 ASVs from the human stool samples. The number of reads per sample ranged from 11,497 to 143,413 with a median read number of 87,133.5. We removed all ASVs that were suspected to be host DNA including any ASVs (i) assigned to Kingdom Eukaryota, (ii) that lacked Phylum assignment, or (iii) that were assigned to Family Mitochondria. We also removed all ASVs with mean abundance < 5. After filtering, we had 4,771,682 reads

representing 574 ASVs. The number of reads per sample ranged from 10,160 to 141,152 with a median of 84,666.

Germ free mice samples were sequenced on a 2x300bp paired-end MiSeq Illumina run. To compare germ-free mice data with the human data, read 2 (R2) sequences from the mice microbiota sequencing data and donor stool sequencing data were trimmed to the V3 region using cutadapt²⁹⁵. This data underwent the same filtering steps as described above. After filtering, we had 2,927,423 reads representing 1291 ASVs. The number of reads per sample ranged from 27,010 to 134,635.

Filtered ASVs were processed for analysis using the phyloseq package in the R statistics software²⁹⁶. Alpha diversity (within-sample diversity) indices of community evenness and richness (Shannon Wiener index and Inverse Simpson index) were calculated after rarefying the samples to minimum sample depth. Bray-Curtis dissimilarity (between-sample diversity) on the relative abundance of all ASVs was calculated and principal coordinate analysis (PCoA) plots were generated with ggplot²⁹⁷ and were used to visualize the clustering of microbiota communities between BAT groups and NAFLD groups. Non-metric Multidimensional Scaling (NMDS) plots were generated and used to visualize the clustering of communities between human donor stool and stool from fecal transplant recipient mice. Upset plots were generated by considering any given ASV that appeared in any donor or recipient sample, grouped by high or low BAT, as presented, and visualized using UpsetR²⁹⁸. Relative abundance of genera was calculated by taking the ASV counts assigned for each member and dividing these counts by the sum of all ASV counts within a given sample. Stacked bar charts of the relative abundance of the top 25 genera were plotted using ggplot to visualize the differences within BAT and NAFLD groups.

Murine Fecal Microbiota Transfer Experiment

Male germ-free C57BL/6N mice (14-20 weeks old) were exported from McMaster University's Farncombe Gnotobiotic Unit and immediately and continually colonized twice weekly using fecal slurries from human donors over 8 weeks. Fecal material was diluted 1:10 (wt:vol.) in sterile saline and dissolved mechanically. A brief centrifugation separated undissolved fecal material from the supernatant, which was aliquoted and frozen at -80°C until needed. Mice were gavaged 200µL of the fecal slurry twice weekly from their assigned donor. Male donors were selected based on BAT and NAFLD status, and each donor colonized 3-4 germ free mice. Mice were housed individually at thermoneutrality (30°C), given access to irradiated standardized chow and autoclaved water *ad libitum*, and handled in a level II biosafety hood to prevent bacterial contamination²⁹⁹. Weekly body weight and adiposity measurements using the Bruker Minispec LF90-II BCA-Analyzer were taken. At week 5, metabolic monitoring was conducted at thermoneutrality using a Comprehensive Lab Animal Monitoring System (CLAMS, Columbus Instruments, OH, USA). Between weeks 6-7, UCP-1 mediated thermogenesis using CL-315,243 was assessed as previously outlined²⁷⁹. Briefly, anesthetized mice were injected i.p. with either saline or CL-316,243 and placed in an enclosed stationary treadmill dorsal side up. Oxygen uptake was monitored using CLAMs with air sampled every 5s. After twenty minutes, mice were removed from the treadmill and a dorsal thermal image was acquired using an infrared camera²⁷⁹. These experiments were also conducted in control, wildtype C57Bl/6J mice gavaged with fecal slurries three times a week from human high or low BAT donors, or from their fecal material (i.e., autologous controls). Non-moving VO₂ was calculated from CLAMS data. Mice were sacrificed between weeks 7-8 and harvested tissues were flash-frozen for further analyses. Hepatic TGs were

extracted from 50mg of tissue and quantified using an adapted Bligh and Dyer lipid extraction method and quantified using a glycerol assay.

STATISTICS

The sample size was determined using the rules outlined by Harris³⁰⁰ wherein the suggested number of participants should equal $50 + m$ (where m is the number of independent variables). Therefore, approximately 54 participants were needed to have enough power to assess independent associations between supraclavicular PDFF, liver fat, and metabolic health markers (adjusted for age, sex, and total body fat).

SPSS Statistics (version 27; IBM, North Castle, NY, USA), GraphPad Prism (version 8; GraphPad Software, La Jolla, CA, USA), RStudio (version 1.2.1335; R Core Team, 2013), and R (Foundation for Statistical Computing, Vienna, Austria) were used for all statistical analyses and for graphing. Normality was assessed by following the procedures outlined by Tabachnick and Fidell³⁰¹ where variables with $Z_{skewness}$ and/ or $Z_{kurtosis} \geq |3.29|$ were classified as non-normal. Non-parametric tests were used for analyses of non-normally distributed data. Data were presented as n (%) for categorical variables and mean (SD) for normally distributed variables or median [IQ1, IQ3] for skewed variables. Paired Student's t -test was used to compare MRI measures before and after cold exposure. Pearson (r) correlation coefficients were used to assess the linear association between normally distributed variables. Spearman (ρ) correlation coefficients were used to assess the association between non-normally distributed variables and for non-linear monotonic correlations. Independent Samples t -test and Mann-Whitney U test were used to compare differences of normally distributed and skewed variables respectively between NAFLD and BAT groups. Gender comparison between groups with and without NAFLD was assessed via the Chi-Square test. Hierarchical multivariate regression analysis was used to examine whether

associations between cold-induced percent decline in SCV PDFF (independent variable) and liver fat (dependent variable) are independent of covariates (age, sex, body fat, or VAT). Non-parametric partial correlation was used to examine the association between BAT activity and glycemia measures controlling for the effects of the covariates (age, sex, and body fat percentage). Multivariate regression analysis was used to determine the additional variance explained by age, gender, and body fat percentage (independent variables) in predicting BAT activity (dependent variable). Curve fitting was used to assess whether relationships between variables were linear or non-linear. A two-tailed p-value of less than 0.05 was considered significant.

Hierarchical regression was used to examine the difference in microbiota alpha diversity indices (the outcome) between BAT activity and NAFLD groups. Three models were used, model 1; without controlling for covariates, model 2; controlling for age, and model 3; controlling for age and total body fat. Permutational Analysis of Variance (PERMANOVA) test with 999 permutations using the adonis function in the vegan package of R software³⁰² was performed to test the effect of BAT and NAFLD groups on beta diversity controlling for age and total body fat.

DESeq2, a negative binomial generalized linear regression model³⁰³, was used to examine the differentially abundant genera in relation to cold-induced percent decline in SCV PDFF, between BAT and between NAFLD groups through three models (model 1; without controlling for covariates, model 2; controlling for age and model 3; controlling for age and total body fat). DESeq2 was reported to be one of the best tools for the analysis of count data for differentially expressed genes in terms of precision, accuracy, and sensitivity³⁰⁴. DESeq2 provides an estimate \log_2 fold of change (LFC) of the read counts for each bacterial gene. As pre-cold SCV PDFF and cold-induced percent decline in SCV PDFF have different scales, Z-scores of these two variables were used to make comparable effect sizes across them. As such, for each one-unit change (1 SD)

of the cold-induced percent decline in SCV PDFF, we reported the \log_2 (i.e., the change in each genus or the number of reads that are uniquely assigned for each gene). For BAT and NAFLD groups, we reported the \log_2 (the change in the ratio between the mean reads for high BAT activity or NAFLD positive to the mean of reads for low BAT activity or NAFLD negative). We used the library depth size factor, i.e., the number of bacterial reads in each sample in the presented analysis. DESeq2 uses a Wald test that is the shrunken estimate of LFC divided by its standard error to give a Z-statistic. To adjust for multiple testing, the false discovery rate was controlled using Benjamini and Hochberg's method. An adjusted p-value of < 0.05 was considered significant.

Table 1. Participant characteristics and study conditions of those with and without NAFLD

	All (n=60)	Normal liver fat (n=30)	Hepatic Steatosis (n=29)	<i>p</i>
Age (years)	25.9 [22.9, 36.4]	23.8 [21.2, 27.2]	31.02 [25.1, 43.4]	< 0.001 †
Sex (male)	37 (62%)	19 (63%)	18 (62%)	0.920
Weight (kg)	81.9 (18.6)	70.7 (13.6)	91.7 (14.8)	< 0.001 *
BMI (kg/m ²)	27.9 (6.8)	22.4 [21.0, 25.0]	30.40 [26.0, 35.9]	< 0.001 †
Waist Circumference (cm)	90.4 (16.9)	76.8 [72.5, 83.8]	101.4 [89.8, 110.2]	< 0.001 †
Body Fat (%) ^a	30.6 (12.6)	23.9 (9.6)	37.4 (11.8)	< 0.001 *
Hepatic Fat (%) ^b	5.5 [4.6, 7.1]	4.6 [4.0, 5.1]	7.1 [6.2, 8.5]	< 0.001 †
Pre-cold SCV PDFF (%)	72.4 (8.0)	67.9 (7.0)	76.7 (6.2)	< 0.001 *
Absolute cold-induced decline in SCV PDFF (%)	3.0 (2.4)	3.6 (2.2)	2.5 (2.4)	0.082
Cold induced percent decline in SCV PDFF (%)	4.4 (3.9)	4.7 [2.7, 8.1]	2.5 [1.2, 5.7]	0.019 †
VAT (cm ²) ^c	30.3 (26.1)	8.7 [5.2,17.2]	58.6 [22.7, 64.6]	< 0.001 †
SAT (cm ²) ^c	99.3 (68.1)	43.2 [29.3, 68.5]	150.1 [87.2, 188.3]	< 0.001 †
Fasting plasma glucose (mmol/L)	4.7 [4.4, 4.9]	4.6 [4.1, 4.8]	4.8 [4.6, 5.1]	0.005 †
2hr glucose (mmol/L) ^d	4.4 [3.8, 5.8]	4.4 (1.3)	5.00 (1.4)	0.299
HbA1c(%)	5.2 [4.9, 5.5]	5.1 [4.9, 5.3]	5.3 [4.9, 5.6]	0.112
Total cholesterol (mmol/L)	4.4 (0.8)	4.1 (0.6)	4.6 (0.8)	0.005 *
Triglycerides (mmol/L)	0.8 [0.6, 1.2]	0.8 (0.2)	1.3 (0.7)	<0.001*
HDL-cholesterol (mmol/L)	1.3 (0.3)	1.39 (0.3)	1.2 (0.3)	0.052
LDL-cholesterol (mmol/L)	2.6 (0.7)	2.35 (0.6)	2.8 (0.6)	0.004 *
Non-HDL-cholesterol (mmol/L)	3.1 (0.8)	2.7 (0.6)	3.4 (0.8)	< 0.001*
Systolic blood pressure (mmHg)	111.4 (12.1)	105.6 (10.7)	116.2 (9.9)	< 0.001*

	All (n=60)	Normal liver fat (n=30)	Hepatic Steatosis (n=29)	<i>p</i>
Diastolic blood pressure (mmHg)	74.4 (9.8)	70.7 (9.4)	77.8 (8.9)	0.004 *
AST (U/L)	18.5 [16.0, 21.0]	18.0 [16.0, 21.0]	19.0 [16.0, 25.5]	0.326
ALT (U/L)	20.0 [15, 25.8]	16.5 [13.0, 21.5]	25.0 [19.0, 35.5]	< 0.001 †
GGT (U/L)	18.5 [14.0, 25.0]	14.5 [11.0, 19.0]	20.0 [18.0, 29.5]	0.001 †
Outdoor temperature 1h before visit 2 (°C)	7.18 (10.0)	4.3 (7.7)	10.5 (11.2)	0.015 *
Shivering intensity (% MVC) ^e	1.95 [1.0, 2.9]	2.3 [1.3, 3.5]	1.2 [0.8, 2.6]	0.017 †
Δ Outlet-inlet of the suit (°C) ^F	1.6 (0.2)	1.6 (0.2)	1.5 (0.2)	0.671

Values are presented as n (%) for categorical variables and continuous variables are presented as mean (SD) for normally distributed variables or median [IQ1, IQ3] for non-normally distributed variables.

* - $p < 0.05$ via independent sample t-test; † - $p < 0.05$ via Mann-Whitney U test. Differences in sex was assessed via Chi-Square test.

^a one participant was above the weight threshold for body composition analysis via DEXA.

^b no liver scan for one participant as they did not fit inside the scanner.

^c no abdominal volume data for four participants (n=2: acquisition error; n=1: did not fit inside the scanner; n=1: motion issues).

^d 2hr glucose was not performed in 29 participants (n=2: fainted during their baseline bloodwork; n=1: known type 2 diabetic; n=26: glucose solution was later recalled so the test was not reliable).

^e Motion artifacts for one participant.

^F No outlet-inlet data for five participants (n=4: data were not acquired, n= 1: an error in the data acquisition).

BMI; body mass index, SCV PDFFF; supraclavicular proton density fat fraction, VAT; visceral adipose tissue, SAT; subcutaneous adipose tissue, HbA1c; hemoglobin A1c, HDL; high-density lipoprotein, LDL; low-density lipoprotein, Non-HDL; non-high-density lipoprotein, AST; aspartate aminotransferase, ALT; alanine aminotransferase, GGT; gamma-glutamyl transferase, MVC; maximal voluntary contraction.

Table 2. Hierarchical multivariate analysis for the predictors of hepatic fat (age, sex, cold-induced percent decline in SCV PDFF, total body fat, and visceral adipose tissue)

	Coefficients							Model		
	N	B	SE	β	95% CI		p	R ²	R ² Adj	p
					Lower Bound	Upper Bound				
Model 1A (+ Cold-induced percent decline in SCV PDFF)								0.338	0.289	<0.001*
Age (years)	59	0.085	0.049	0.221	-0.013	0.183	0.087			
Sex (male)		0.430	0.899	0.056	-1.373	2.233	0.635			
Cold-induced percent decline in SCV PDFF (%)		-1.153	0.318	-1.172	-1.790	-0.516	0.001*			
Cold-induced percent decline in SCV PDFF (%) ²		0.067	0.023	0.896	0.020	0.113	0.006*			
Model 1B (+ Body Fat Percentage)								0.433	0.380	<0.001*
Age (years)	59	0.051	0.047	0.132	-0.043	0.145	0.284			
Sex (male)		1.256	0.885	0.164	-0.519	3.031	0.162			
Cold-induced percent decline in SCV PDFF (%)		-0.885	0.310	-0.900	-1.507	-0.264	0.006*			
Cold-induced percent decline in SCV PDFF (%) ²		0.061	0.022	0.822	0.018	0.105	0.007*			
Body Fat (%)		0.129	0.043	0.435	0.042	0.216	0.004*			
Model 2B (+ VAT)								0.504	0.454	<0.001*
Age (years)	56	-0.013	0.061	-0.030	-0.135	0.109	0.836			
Sex (male)		-0.336	0.845	-0.043	-2.033	1.360	0.692			
Cold-induced percent decline in SCV PDFF (%)		-0.760	0.309	-0.769	-1.380	-0.139	0.017*			
Cold-induced percent decline in SCV PDFF (%) ²		0.051	0.022	0.690	0.008	0.095	0.021*			
VAT (cm) ²		0.081	0.022	0.556	0.036	0.126	0.001*			

Quadratic function of cold-induced percent decline in SCV PDFF (%) was used as it fits better than the linear model (R²Linear = 0.173 vs R²Quadratic = 0.301). * - p < 0.05. SCV PDFF; supraclavicular proton density fat fraction. VAT; visceral adipose tissue.

Figures

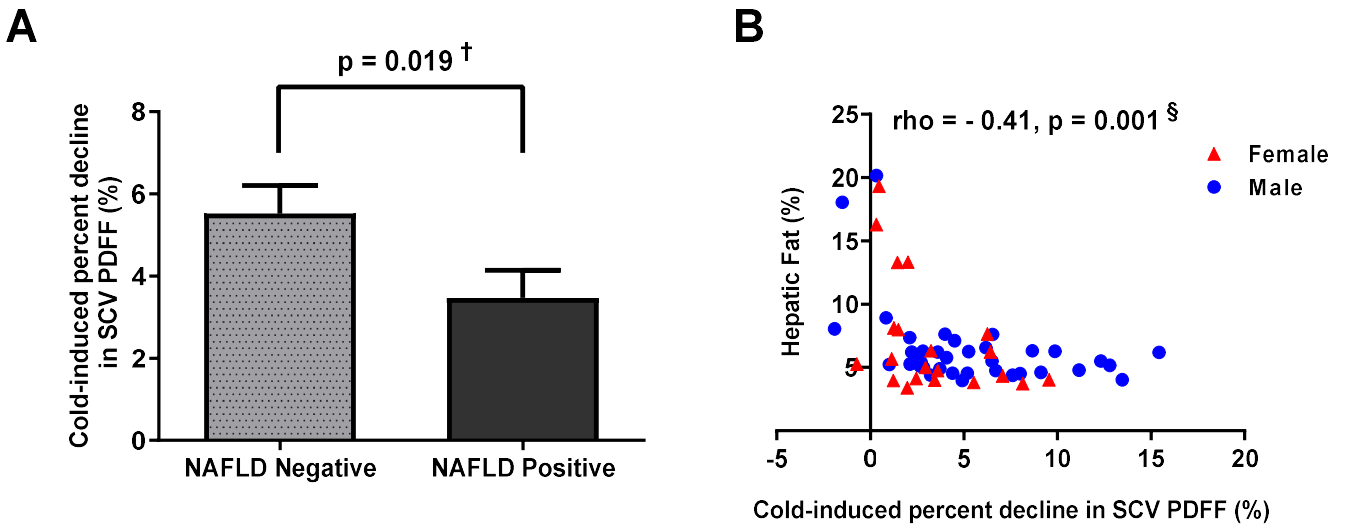


Figure 1. Cold-induced percent decline in SCV PDFF and hepatic fat fraction.

Comparison of the cold-induced percent decline in SCV PDFF (%) between those without (NAFLD negative, n= 30) and with hepatic steatosis (NAFLD positive, n= 29); data are presented as mean \pm standard error of the mean (SEM) for each group. **(A)** Relationship of the cold-induced percent decline in SCV PDFF (%) with hepatic PDFF (%) in males (blue circles) and females (red triangles). **(B)** \dagger - $p < 0.05$ via Mann-Whitney U test, \S - $p < 0.05$ via Spearman's Correlation; SCV PDFF - supraclavicular proton density fat fraction; NAFLD – non-alcoholic fatty liver disease.

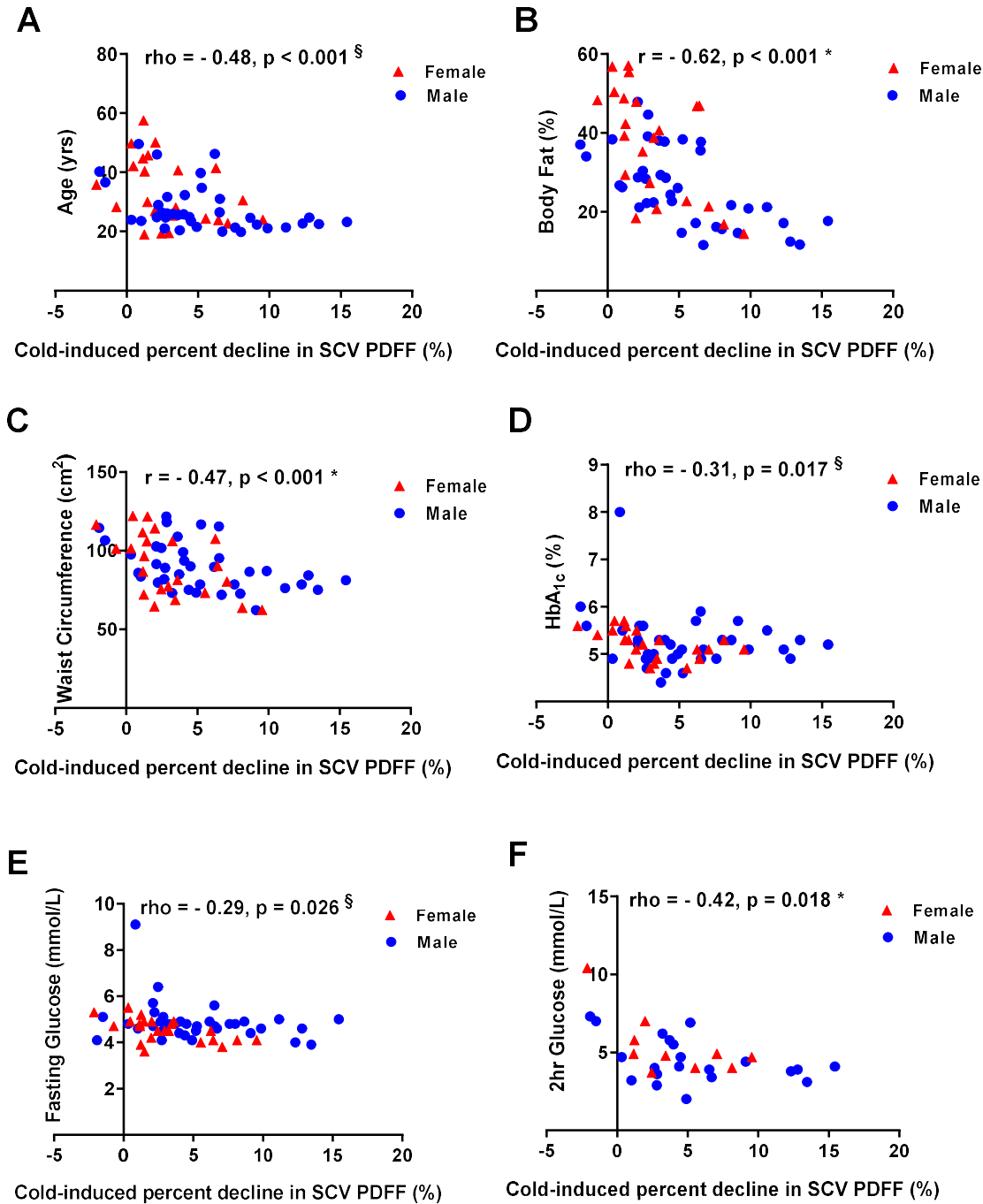


Figure 2. Cold-induced percent decline in SCV PDFF and health indicators in adults.

Relationship of the cold-induced percent decline in SCV PDFF (%) with age (A), body fat percentage (B), waist circumference (C), HbA_{1c} (D), fasting glucose (E), and 2-hour 75 g OGTT glucose (F) in males (blue circles) and females (red triangles). * - p<0.05 via Pearson's Correlation; § - p<0.05 via Spearman's Correlation. SCV PDFF; supraclavicular proton density fat fraction; HbA_{1c} - hemoglobin A_{1c}; OGTT – oral glucose tolerance test.

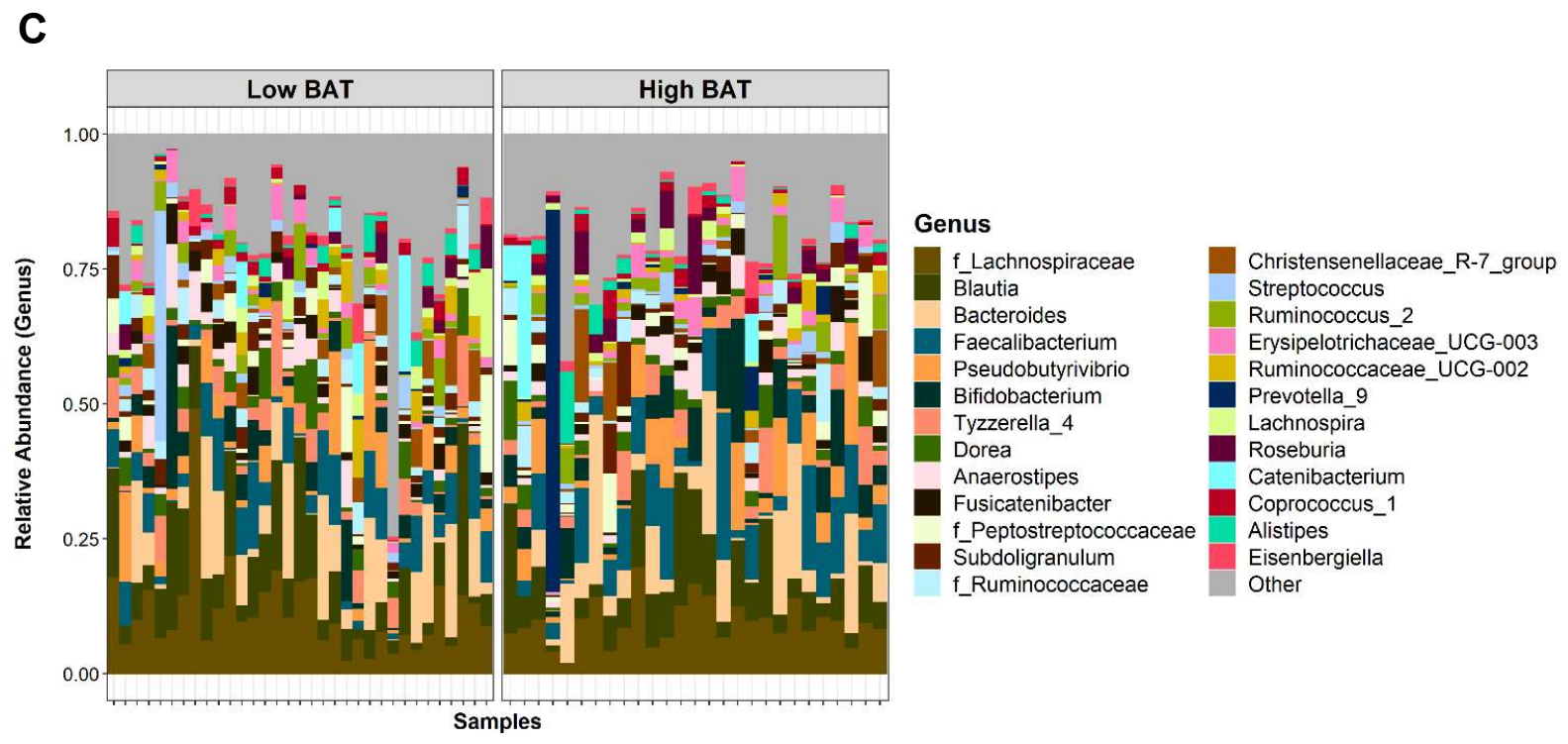
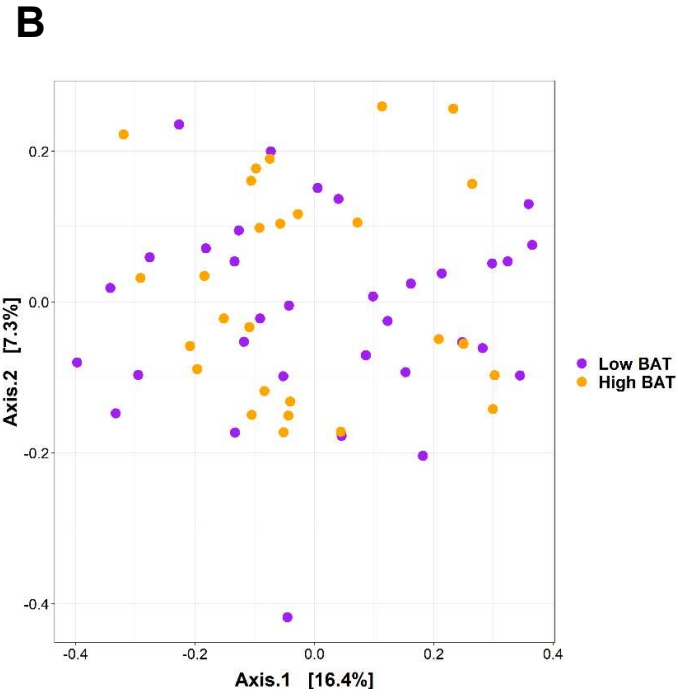
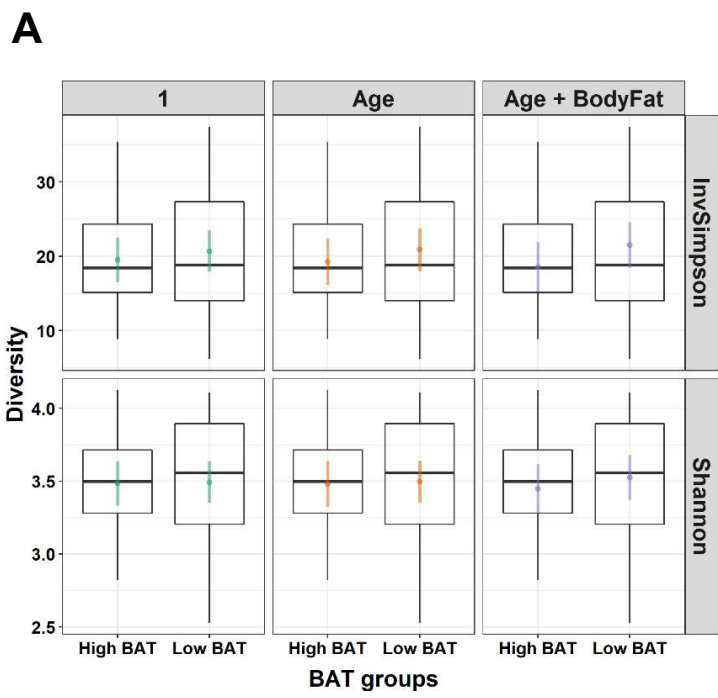


Figure 3. Gut microbiota between BAT groups.

Alpha diversity between BAT groups (low and high brown adipose tissue activity; Low BAT and high BAT respectively). (A) Principal coordinate analysis (PCoA) plot on Bray-Curtis dissimilarity distances between BAT groups. (B) Relative abundance of top 25 genera between BAT groups. (C) For A, data are represented as the median, interquartile range, and 95% range of the data. The colored points and lines are the point estimates of the means from the regression models and the 95% confidence intervals of the model estimates of the means, respectively. For B, axes 1 and 2 captured 16.4 and 7.3% in the variation between samples, respectively.

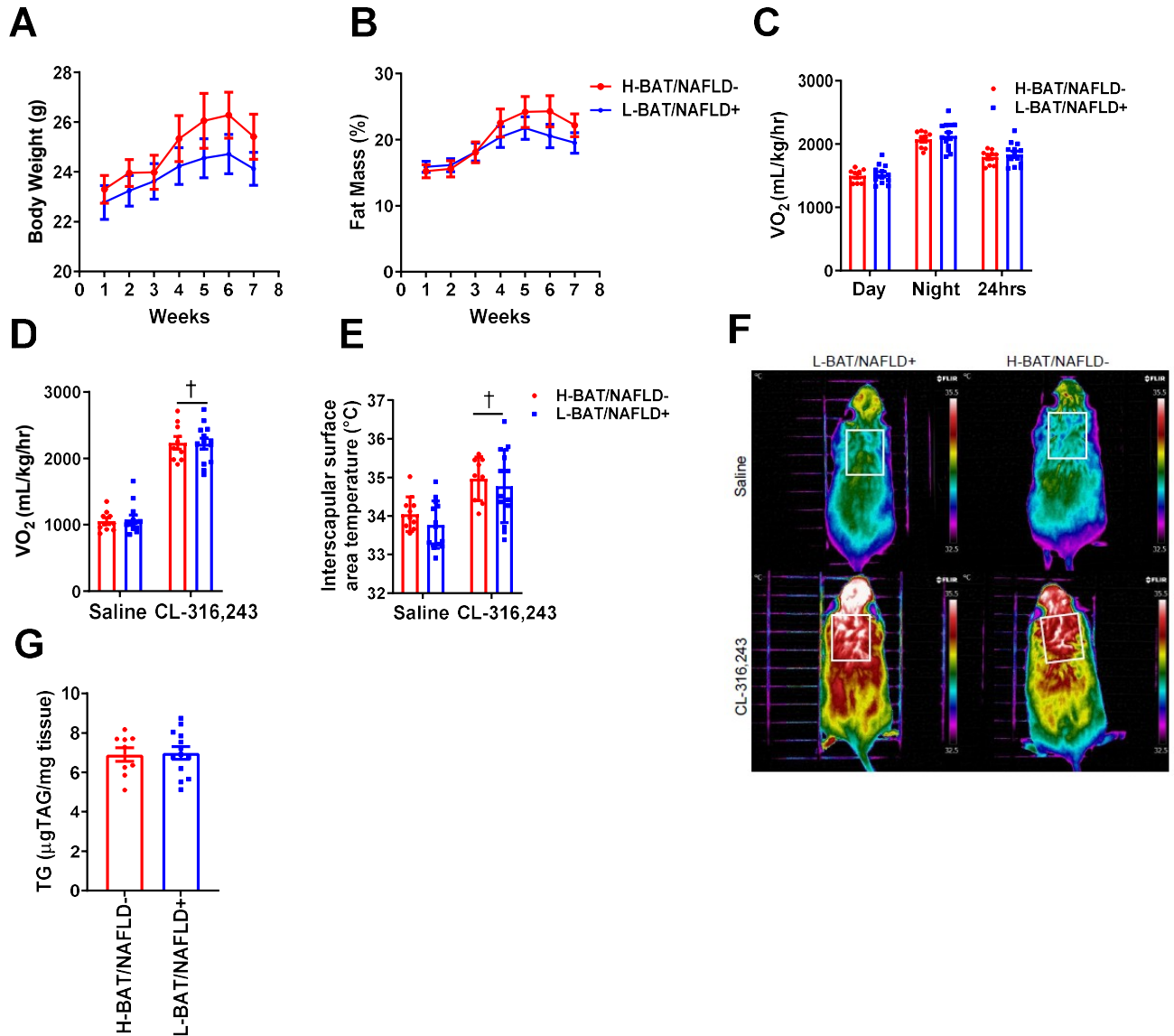


Figure 4. Human brown adipose tissue activity and NAFLD status are not transmissible via gut microbes in germ free mice.

Weekly body mass (A), and percent fat mass (B). Average oxygen consumption (VO_2) during light and dark cycles, and over a 24hr period (average of light and dark) after 5 weeks of colonization (C). Oxygen consumption (D) and dorsal interscapular surface temperature of anesthetized mice following saline or CL-316,243 administration after 6-7 weeks of colonization (E). Representative infrared images from each group after saline or CL-316,243 (F). Liver triglycerides after 7-8 weeks of colonization. (n=9 H-BAT/NAFLD- and n=12 L-BAT/NAFLD+) (G). Data are expressed as means \pm SEM. Significance determined using a Student's t-test or a two-way repeated measure analysis of variance (ANOVA) and Sidak's post hoc test; † - p<0.05 vs saline.

SUPPLEMENTARY ITEMS

Table S1. (Related to Proton Density Fat Fraction Declined in Supraclavicular but not in Subcutaneous Adipose Tissue). Participant and study characteristics between brown adipose tissue groups.

	Low BAT Activity (n= 33)	High BAT activity (n=27)	<i>p</i>
Age (years)	28.3 [24.8, 41.4]	23.9 [22.3, 30.6]	0.012†
Sex (male)	16 (48%)	21 (78%)	0.020 ^S
Weight (kg)	85.2 (21.1)	77.8 (14.4)	0.111
Waist (cm)	95.9 (17.0)	83.6 (14.4)	0.004*
BMI (kg/m ²)	30.2 (7.5)	25.1 (4.7)	0.002*
Body Fat (%) ^a	36.6 (11.2)	23.4 (10.5)	<0.001*
Hepatic fat (%) ^b	5.8 [5.0, 8.1]	5.2 [4.4, 6.3]	0.054
Absolute cold-induced decline in SCV PDFF (%)	1.2 (1.2)	5.1 (1.7)	<0.001*
Cold-induced percent decline in SCV PDFF (%)	1.7 (1.6)	7.8 (3.1)	<0.001*
VAT (cm ²) ^c	44.6 [15.0, 64.4]	8.54 [5.5, 23.3]	<0.001†
SAT (cm ²) ^c	121.4 (70.0)	73.8 (57.4)	0.008*
Fasting Glucose (mmol/L)	4.8 [4.5, 5.1]	4.6 [4.1, 4.8]	0.020†
2hr Glucose (mmol/L) ^d	5.4 (2.0)	4.2 (1.1)	0.049*
HbA1c (%)	5.3 [4.9, 5.6]	5.1 [4.9, 5.3]	0.171
TC (mmol/L)	4.4 (0.8)	4.3 (0.7)	0.490
TG (mmol/L)	0.9 [0.7, 1.6]	0.7 [0.6, 1.0]	0.078
HDL-cholesterol (mmol/L)	1.3 (0.3)	1.4 (0.3)	0.302
LDL-cholesterol (mmol/L)	2.6 (0.6)	2.6 (0.7)	0.616
Non-HDL-cholesterol (mmol/L)	3.2 (0.8)	2.9 (0.8)	0.263
Systolic blood pressure (mm HG)	113.5 (12.7)	108.7 (11.0)	0.130
Diastolic blood pressure (mm HG)	75.0 (9.3)	73.6 (10.5)	0.586
AST (U/L)	17.0 [15.5, 20.0]	21.0 [17.0, 23.0]	0.037†
ALT (U/L)	21.0 [16.0, 28.5]	19.0 [15.0, 25.0]	0.430
GGT (U/L)	20.0 [14.0, 33.5]	16.0 [13.0, 20.0]	0.108

Outdoor temperature 1hr before visit 2 (°C)	7.8 (10.3)	6.4 (9.7)	0.595
Muscles MVC (%) ^e	2.0 [1.1, 2.9]	2.0 [0.8, 2.9]	0.562
Δ Outlet-inlet of the suit (°C) ^F	1.5 (0.2)	1.6 (0.2)	0.309

Values are presented as n (%) for categorical variables and continuous variables are presented as mean (SD) for normally distributed variables or median [IQ1, IQ3] for non-normally distributed variables.

* - $p < 0.05$ via independent sample t-test; † - $p < 0.05$ via Mann-Whitney U test; § via Chi-Square test

^a one participant was above the weight threshold for body composition analysis via DEXA.

^b no liver scan for one participant as they did not fit inside the scanner.

^c no abdominal volume data for four participants (n=2: acquisition error; n=1: did not fit inside the scanner; n=1: motion issues).

^d 2hr glucose was not performed in 29 participants (n=2: fainted during their baseline bloodwork; n=1: known type 2 diabetic; n=26: recalled glucose solution).

^e Motion artifacts for one participant.

^F No inlet-outlet data for five participants (n=4: data were not acquired, n= 1: an error in the data acquisition).

BAT; brown adipose tissue, BMI; body mass index, SCV PDFF; supraclavicular proton density fat fraction, VAT; visceral adipose tissue, SAT; subcutaneous adipose tissue, HbA1c; hemoglobin A1c, HDL; high-density lipoprotein, LDL; low-density lipoprotein, Non-HDL; non-high-density lipoprotein, AST; aspartate aminotransferase, ALT; alanine aminotransferase, GGT; gamma-glutamyl transferase, MVC; maximal voluntary contraction.

Table S2. (Related to Proton Density Fat Fraction Declined in Supraclavicular but not in Subcutaneous Adipose Tissue). Macronutrient and dietary fibre intake 24 hours prior to measurement of BAT activity

	Normal liver fat (n=30)	Hepatic Steatosis (n=29)	<i>p</i>
Weight (kg)	70.7 (13.6)	91.7 (14.8)	< 0.001 *
Total calories (kcal)	2274.65 (712.6)	2384.63 (1026.4)	0.633
Total kcal (related to weight)	33.22 (11.8)	27.09 (13.2)	0.065
Protein			
Protein (kcal)	372.60 (135.9)	453.93 (245.4)	0.119
Calories from protein (%)	17.69 (8.7)	19.66 (8.4)	0.382
Fat			
Fat (kcal)	797.50 (437.8)	811.49 (376.7)	0.896
Calories from fat (%)	34.10 (13.9)	35.49 (11.4)	0.677
Carbohydrate			
Carbohydrate (kcal)	1117.39 (488.7)	1133.99 (713.7)	0.917
Calories from carbohydrate (%)	48.90 (14.7)	45.61 (14.5)	0.391
Fibre (g)			
Fibre (g)	23.12 (14.2)	22.59 (17.7)	0.899
Values are presented as mean (SD). * - $p < 0.05$ via independent sample t-test			

Table S3. (Related to Cold-induced Percent Decline in Supraclavicular Proton Density Fat Fraction, Age and Adiposity). Predictors of the cold-induced percent decline in supraclavicular proton density fat fraction in multivariate analysis

	Coefficients						Model			
	N	B	SE	β	95% CI		<i>p</i>	R ²	R ² Adj.	<i>p</i>
					Lower Bound	Upper Bound				
Cold-induced Percent Decline in SCV PDFF (%)								0.514	0.478	<0.001*
Age (years)	59	-0.083	0.043	-0.214	-0.169	0.002	0.056			
Sex (male)		0.604	0.846	0.078	-1.093	2.300	0.479			
Body Fat (%)		-0.702	0.160	-2.333	-1.022	-0.382	<0.001*			
Body Fat (%) ²		0.008	0.002	1.880	0.004	0.013	0.001*			

Quadratic function of body fat was used since it fits better than the linear model (R²Linear = 0.385 vs R²Quadratic = 0.474). * - *p* < 0.05.

Table S4. (Related to Relationship of Gut Microbiota to Cold-induced Percent Decline in Supraclavicular Fat Fraction). Hierarchical regression for alpha diversity indices in relation to cold-induced percent decline in supraclavicular proton density fat fraction, between BAT and between NAFLD groups.

Alpha diversity indices in relation to cold-induced percent decline in SCV PDFF								
	Shannon				Inverse Simpson			
	B	SE	T-Statistic	<i>p</i>	B	SE	T-Statistic	<i>p</i>
Model 1								
Percent decline in SCV PDFF	0.011	0.014	0.781	0.438	0.107	0.273	0.392	0.697
Model 2								
Age (years)	0.001	0.006	0.195	0.846	-0.035	0.119	-0.291	0.772
Percent decline in SCV PDFF	0.012	0.015	0.783	0.437	0.069	0.304	0.226	0.822
Model 3								
Age (years)	0.002	0.006	0.380	0.705	-0.007	0.125	-0.056	0.956
Body Fat	-0.004	0.006	-0.640	0.525	-0.080	0.111	-0.719	0.475
Percent decline in SCV PDFF	0.006	0.018	0.330	0.743	-0.066	0.359	-0.183	0.855
Alpha diversity indices between BAT groups								
	Shannon				Inverse Simpson			
	B	SE	T-Statistic	<i>p</i>	B	SE	T-Statistic	<i>p</i>
Model 1								
High BAT/ Low BAT	-0.008	0.103	-0.079	0.937	-1.186	2.058	-0.576	0.567
Model 2								
Age (years)	-0.001	0.006	-0.189	0.851	-0.072	0.113	-0.642	0.523
High BAT/ Low BAT	-0.015	0.109	-0.133	0.894	-1.622	2.178	-0.745	0.459
Model 3								
Age (years)	0.002	0.006	0.274	0.785	-0.014	0.122	-0.118	0.907
Body Fat	-0.006	0.005	-1.136	0.261	-0.126	0.105	-1.205	0.234
High BAT/ Low BAT	-0.077	0.122	-0.630	0.531	-2.937	2.428	-1.210	0.232
Alpha diversity indices between NAFLD groups								
	Shannon				Inverse Simpson			
	B	SE	T-Statistic	<i>p</i>	B	SE	T-Statistic	<i>p</i>
Model 1								
NAFLD positive/negative	-0.232	0.098	-2.36	0.022*	-4.283	1.977	-2.166	0.034*
Model 2								
Age (years)	0.006	0.006	1.04	0.303	0.071	0.116	0.614	0.542
NAFLD positive/negative	-0.284	0.110	-2.58	0.013*	-4.916	2.240	-2.195	0.032*
Model 3								

Age (years)	0.006	0.006	0.964	0.339	0.066	0.123	0.533	0.596
Body Fat	0.000	0.005	0.049	0.961	0.014	0.100	0.143	0.887
NAFLD positive/negative	-0.287	0.122	-2.351	0.022*	-5.061	2.475	-2.044	0.046*

Model 1, without adjusting to confounding variables, Model 2; controlling for age and Model 3, controlling for age and body fat percentage. * - $p < 0.05$. SCV PDFF; supraclavicular proton density fat fraction, BAT; brown adipose tissue, Low BAT; low BAT thermogenesis; High BAT; high BAT thermogenesis, NAFLD; non-acholic fatty liver disease, NAFLD positive; with hepatic steatosis, NAFLD negative; with normal hepatic fat.

Table S5. (Related Relationship of Gut Microbiota to Cold-induced Percent Decline in Supraclavicular Fat Fraction). Permutational multivariate analysis of variance (PERMANOVA) on Bray-Curtis dissimilarity matrices for BAT and NAFLD groups controlling for age and body fat percentage.

	R2	Pr (>F)
Brown adipose tissue (BAT) groups		
Age	0.017	0.359
Body fat percentage	0.065	0.003*
BAT groups (high/low BAT thermogenesis)	0.014	0.736
Non-alcoholic fatty liver disease (NAFLD) groups		
Age	0.017	0.332
Body fat percentage	0.065	0.001*
NAFLD groups (positive/negative)	0.030	0.012*

* - $p < 0.05$

Table S6. (Related to Relationship of Gut Microbiota to Cold-induced Percent Decline in Supraclavicular Fat Fraction). Differential gene expression analysis at the genus level.

Cold-induced percent decline in supraclavicular proton density fat fraction									
	Model 1			Model 2			Model 3		
Genera	LFC	<i>p</i> value	<i>p</i> adj	LFC	<i>P</i> value	<i>p</i> adj	LFC	<i>p</i> value	<i>p</i> adj
Catenisphaera	-2.94	0.045	0.515	-9.26	1.3E-08	1.7E-06*	1.04	0.584	0.990
Coriobacteriaceae UCG-003	- 2.80	0.056	0.523	-8.96	3.7E-08	2.5E-06*	0.984	0.606	0.990
Libanicoccus	-2.54	0.085	0.523	-8.29	3.5E-07	1.6E-05*	0.893	0.641	0.990
Brown adipose tissue (BAT) groups									
Succiniclasticum	0.00	1.00	NA	5.12	0.093	0.593	-26.39	1.9E-14	2.5E-12*
Non-acholic fatty liver disease (NAFLD) groups									
Catenisphaera	0	1	NA	-7.25	0.027	0.246	-30.0	9.6E-17	4.4E-15*
Coriobacteriaceae_UC G- 003	0	1	NA	-6.89	0.036	0.280	-30.0	9.6E-17	4.4E-15*
Libanicoccus	0	1	NA	-6.21	0.058	0.393	-30.0	9.7E-17	4.4E-15*
f_Muribaculaceae	0.68	0.817	NA	7.52	0.021	0.223	12.08	0.001	0.026*
Catenibacterium	8.38	5.2E-06	0.0004*	0.531	0.824	0.942	0.688	0.796	0.964
Dorea	1.35	1.7E-05	0.001*	1.36	0.0001	0.017*	1.15	0.003	0.058
Christensenellaceae_R- 7_group	-2.62	9.6E-05	0.002*	-1.78	0.039	0.282	-1.58	0.088	0.478
Lachnospira	-1.69	0.0002	0.003*	-1.79	0.001	0.039*	-1.83	0.002	0.055
Blautia	1	0.0003	0.005*	0.99	0.002	0.059	0.834	0.017	0.187
Bacteroides	-1.60	0.001	0.011*	-1.50	0.008	0.170	-1.44	0.020	0.208
Barnesiella	-3.97	0.002	0.016*	-3.17	0.034	0.280	-3.07	0.058	0.377
Lactococcus	2.68	0.003	0.030*	2.59	0.017	0.216	2.74	0.024	0.228

Unknown genus for Lachnospiraceae	0.56	0.005	0.042*	0.190	0.373	0.758	0.235	0.323	0.785
Alistipes	-1.85	0.006	0.042*	-1.36	0.095	0.446	-1.40	0.119	0.520
Tyzzarella_4	1.41	0.008	0.049*	1.12	0.068	0.403	0.99	0.145	0.520
Phascolarctobacterium	-2.62	0.008	0.049*	-1.93	0.098	0.446	-2.24	0.084	0.475
Unknown genus for Rhodospirillales order	-6.57	0.022	0.091	-8.52	0.0003	0.023*	-6.45	0.015	0.187

LCF; Log₂ fold of change, p-value; calculated via Wald test, *p* adj; adjusted *p*-value via Benjamini and Hochberg procedure. * - Adj *p* <0.05, Model 1, without adjusting to confounding variables, Model 2; controlling for age, and Model 3, controlling for age and body fat percentage. NA: *p*-value was not calculated as DESeq2 was not able to calculate the variance of the taxon.

Table S7. (Related to Microbial Transfer to Mice). Participant characteristics for donors of stool samples that were used for germ free mice colonization.

	Donors with high BAT activity			Donors with low BAT activity			
	A	B	C	D	E	F	G
Age (years)	24.7	22.7	22.5	36.6	24.0	49.6	24.8
Sex	Male	Male	Male	Male	Male	Male	Male
Weight (kg)	79.7	81.3	66.6	98.7	88.6	74.6	116.9
BMI (kg/m ²)	22.4	24.9	24.4	30.3	31.7	25.4	36.3
Waist circumference (cm)	84.4	78.5	75	106.6	97.5	85.8	102.7
Body Fat (%)	12.4	17.1	11.7	34	38.4	26.7	47.9
Hepatic fat (%)	5.2	5.5	4.0	18.1	20.2	8.9	7.4
Absolute cold-induced decline in SCV PDFF (%)	7.9	7.0	7.9	-1.2	0.3	0.7	1.5
Cold-induced percent decline in SCV PDFF (%)	12.8	12.3	13.5	-1.5	0.3	0.8	2.1
VAT (cm ²)	8.7	5.5	13.5	60.1	64.6	59.8	22.9
SAT (cm ²)	45.7	45.8	31.1	98.9	169.8	57.4	179.5
Fasting glucose (mmol/L)	4.6	4	3.9	5.1	4.8	9.1	5.7
2h glucose (mmol/L) ^a	3.9	3.8	3.1	7	4.7	-	-
HbA1c (%)	4.9	5.1	5.3	5.6	4.9	8	5.3
TC (mmol/L)	4.8	4.2	3.9	5.7	5.5	4.6	3.9
TG (mmol/L)	1.0	0.7	0.7	3.0	0.8	1.9	0.6
HDL-cholesterol (mmol/L)	1.7	1.3	1.4	1.3	1.5	1	1.3
LDL-cholesterol (mmol/L)	2.6	2.6	2.1	3.1	3.6	2.7	2.3
Non-HDL-cholesterol (mmol/L)	3.1	2.9	2.4	4.5	4.0	3.6	2.5
Systolic blood pressure (mmHg)	104	111	97	118	111	113	115
Diastolic blood pressure (mmHg)	79	74	63	78	75	78	61
AST (U/L)	31	21	16	19	50	15	12
ALT (U/L)	26	15	14	40	94	25	13
GGT (U/L)	17	16	43	37	55	25	20
NAFLD group	NAFLD negative	NAFLD negative	NAFLD negative	NAFLD positive	NAFLD positive	NAFLD positive	NAFLD positive

^a 2hr glucose was not performed for two participants (F; known type 2 diabetic and G; recalled glucose solution). BAT; brown adipose tissue, BMI; body mass index, SCV PDFF; supraclavicular proton density fat fraction, VAT; visceral adipose tissue, SAT; subcutaneous adipose tissue, HbA1c; hemoglobin A1c, HDL; high-density lipoprotein, LDL; low-density lipoprotein, Non-HDL-C; non-high-density lipoprotein, AST; aspartate aminotransferase, ALT; alanine aminotransferase, GGT; gamma-glutamyl transferase.

Table S8. (Related to STAR methods). List of excluded medications and conditions.

Class of Drugs	List
Drugs affecting β -adrenergic receptor	<p>β blockers</p> <ul style="list-style-type: none"> • Acebutolol (Sectral) • Atenolol (Tenormin) • Bisoprolol (Zebeta) • Metoprolol (Lopressor, Toprol-XL) • Nadolol (Corgard) • Propranolol (Inderal LA, InnoPran XL) <p>Asthma/COPD beta-adrenergic agonists</p> <ul style="list-style-type: none"> • Bambuterol (Bambec, Oxeol) • Bitolterol mesylate (Tornalate) • Clenbuterol (Dilaterol, Spiropent, Ventipulmin) • Fenoterol (Berotec N) • Formoterol (Foradil, Zenhale, Symbicort, Forpack Discair, Oxeze/Oxis) • Isoprenaline/ Isoproterenol (Isuprel) • Levosalbutamol (Levalbuterol, Xopenex) • Metaproterenol (Alupent) • Olodaterol (Striverdi) • Pirbuterol (Maxair) • Procaterol • Salbutamol (Albuterol, Ventolin) • Salmeterol (Serevent Diskus) • Terbutaline (Bricanyl) • Vilanterol (Breo Ellipta, Relvar Ellipta) <p>Others</p> <ul style="list-style-type: none"> • Mirabegron (Myrbetriq)
Drugs associated with hepatic steatosis	<p>Corticosteroids</p> <ul style="list-style-type: none"> • Betamethasone (Celestone) • Budesonide (Pulmicort, Entocort EC) • Cortone Acetate (Cortone) • Cotelone • Dexamethasone (Decadron) • Fludrocortisone (Florinef Acetate) • Methylprednisolone (Medrol, Methylpred-DP) • Prednisone (Bubpli-Pred, Deltasone, Prednicot, Prelone, Pediapred 5, Pms-prednisolone) • Triamcinolone (Aristocort) <p>Tetracycline</p> <ul style="list-style-type: none"> • Demeclocycline (Declomycin) • Doxycycline (Doryx, Vibramycin) • Minocycline (Dynacin, Minocin, Monodox)

	<ul style="list-style-type: none"> • Oxytetracycline (Terramycin) • Tetracycline (Achromycin) • Tigecycline (Tygacil) <p>Other</p> <ul style="list-style-type: none"> • Amiodarone (Cordarone, Nexterone, Pacerone) • L-asparaginase (Elspar) • Methotrexate (Rheumatrex, Trexall) • Tamoxifen (Nolvadex) • Valproic acid (Depakote, Depakote ER, Depakote Sprinkle, Depakene, Depacon, Stavzor)
<p>Anti-hyperglycemic drugs</p>	<p>Alpha-Glucosidase Inhibitor</p> <ul style="list-style-type: none"> • Acarbose (Precose) • Miglitol (Glyset) <p>Biguanides</p> <ul style="list-style-type: none"> • Metformin (Glucophage, Glucophage XR, Glumetza, Fortamet, Riomet) • Metformin combination drugs <ul style="list-style-type: none"> ○ Actoplus Met ○ Avandamet ○ Duetact ○ Glucovance ○ Janumet ○ Jentadueto ○ Komboglyze ○ Metaglip ○ PrandiMet <p>Dipeptidyl peptidase-4 (DPP-4) inhibitor</p> <ul style="list-style-type: none"> • Alogliptin (Nesina) • Canagliflozin (Invokana) • Dapagliflozin (Farxiga) • Linagliptin (Tradjenta) • Saxagliptin (Onglyza) • Sitagliptin (Januvia) <p>Glucagon-like peptide</p> <ul style="list-style-type: none"> • Exenatide (Exendin-4, Byetta) • Liraglutide (Victoza) • Lixisenatide (Lyxumia) <p>Meglitinides</p> <ul style="list-style-type: none"> • Repaglinide (GlucoNorm, Prandin, NovoNorm) • Nateglinide (Starlix)

	<p>Insulin</p> <p>Sulfonylurea</p> <ul style="list-style-type: none"> • Chlorpropamide (Diabinese) • Glimepiride (Amaryl) • Glipizide (Glucotrol, Glucotrol XL) • Glyburide (DiaBeta, Glynase PresTab, Micronase) • Tolbutamide • Yolazamide <p>Thiazolidinediones</p> <ul style="list-style-type: none"> • Pioglitazone (Actos) • Rosiglitazone (Avandia)
HIV drugs	<ul style="list-style-type: none"> • HAART
Antidepressants, anxiolytic drugs, anti-psychotic drugs	<p>5-HT₂ Receptor Antagonists</p> <ul style="list-style-type: none"> • Trazodone (Desyrel, Oleptro, Trazorel, Trialodine, Trittico) <p>5-HT₃ Receptor Antagonists</p> <ul style="list-style-type: none"> • Vortioxetine (Brintellix, Trintellix) <p>Dopamine Reuptake Blocker</p> <ul style="list-style-type: none"> • Bupropion (Wellbutrin) <p>MAOIs (Monoamine oxidase inhibitors)</p> <ul style="list-style-type: none"> • Isocarboxazid (Marplan) • Phenelzine (Nardil) • Selegiline (Emsam) • Tranylcypromine (Parnate) <p>SNRIs (Serotonin and norepinephrine reuptake inhibitors)</p> <ul style="list-style-type: none"> • Desvenlafaxine (Pristiq) • Duloxetine (Cymbalta) • Venlafaxine (Effexor XR) <p>SSRIs (Selective serotonin reuptake inhibitor)</p> <ul style="list-style-type: none"> • Citalopram (Celexa) • Escitalopram (Lexapro) • Fluoxetine (Prozac) • Fluvoxamine (Luvox) • Paroxetine (Paxil) • Sertraline (Zoloft) <p>Tetracyclic Antidepressant</p> <ul style="list-style-type: none"> • Maprotiline (Teva-Maprotiline) • Mirtazapine (Tera-Mirtazapine)

	<p>Tricyclic medication</p> <ul style="list-style-type: none"> • Amitriptyline (Elavil) • Amoxapine (Asendin) • Clomipramine (Anafranil) • Desipramine (Norpramin) • Doxepin (Silenor) • Imipramine (Tofranil) • Nortriptyline (Pamelor) • Protriptyline (Vivactil) • Trimipramine (Surmontil)
Thyroid drugs	<p>Anti-thyroid</p> <ul style="list-style-type: none"> • Methimazole (Tapazole) • Propylthiouracil (Propyl-Thyracil or PTU) <p>Thyroid</p> <ul style="list-style-type: none"> • levothyroxine (T4) (Levothroid, Levoxyl, Synthroid, Tirosint, Unithroid) • liothyronine (T3) (Cytomel) • Liotrix (T3 and T4) (Thyrolar)
Antiemetic (5HT3 antagonists)	<ul style="list-style-type: none"> • Dolasetron (Anzemet) • Granisetron (Granisetron Hydrochloride) • Ondansetron (Zofran) • Palonosetron (Aloxi)
Drugs associated with serotonin metabolism	<ul style="list-style-type: none"> • Amphetamine • Dextromethorphan • Metoclopramide
Conditions	List
Diseases associated with brown adipose tissue dysfunction	<ul style="list-style-type: none"> • Adrenal gland disorder (i.e., pheochromocytoma) • Hibernoma
Diseases associated with hepatic steatosis and liver disorders	<ul style="list-style-type: none"> • Abetalipoproteinemia • Celiac disease • Cystic fibrosis • Galactosemia • Glycogen storage disease • Hemochromatosis • Hepatitis B or C • Hepatocellular carcinoma (HCC) • Homocystinuria • Inflammatory bowel disease • Lipodystrophy • Polycystic liver disease • Tyrosinemia

	<ul style="list-style-type: none">• Weber-Christian syndromeWilson's disease
--	---

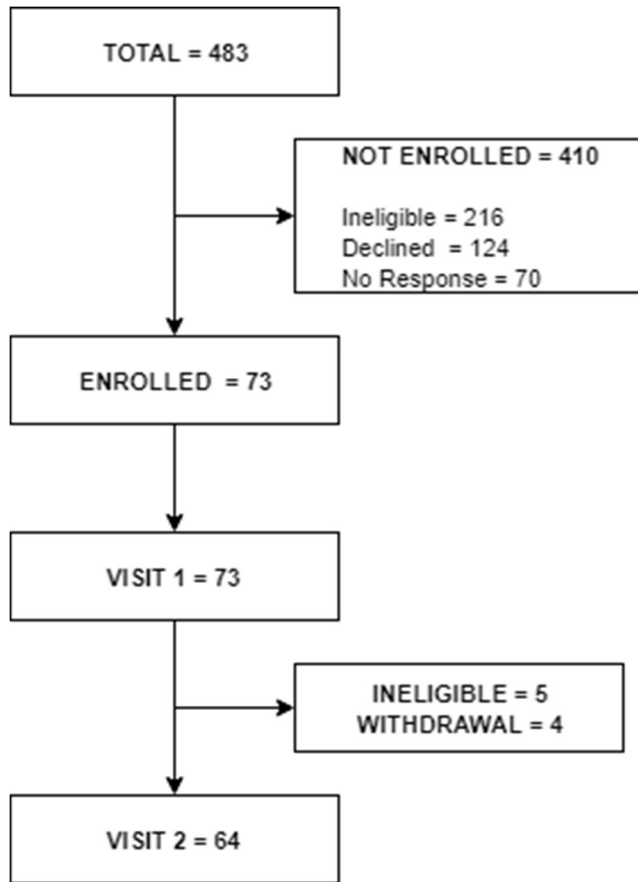


Figure S1A. (Related to Participant Characteristics). Recruitment Flow Chart.

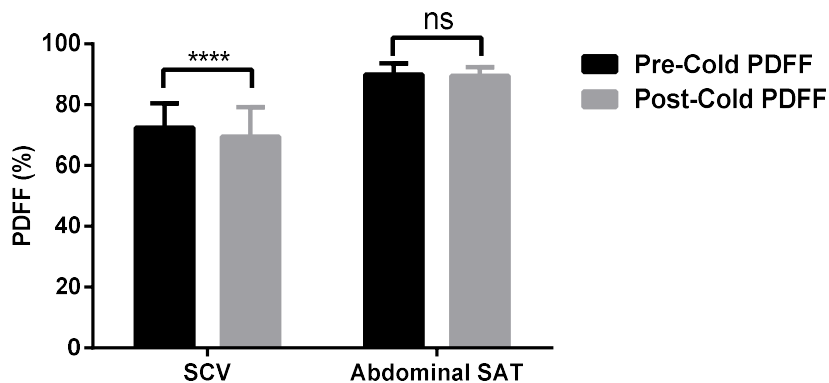


Figure S1B. (Related to Proton Density Fat Fraction Declined in Supraclavicular but not in Subcutaneous Adipose Tissue). Proton density fat fraction in brown adipose tissue and white adipose tissue before and after cold exposure. Proton density fat fraction (PDFF) in supraclavicular (SCV) brown adipose tissue (n= 60) and abdominal subcutaneous adipose tissue (SAT) (n=37) before (pre-cold) and after (post-cold) cold exposure. **** - $p < 0.001$ via paired Student's t-test.

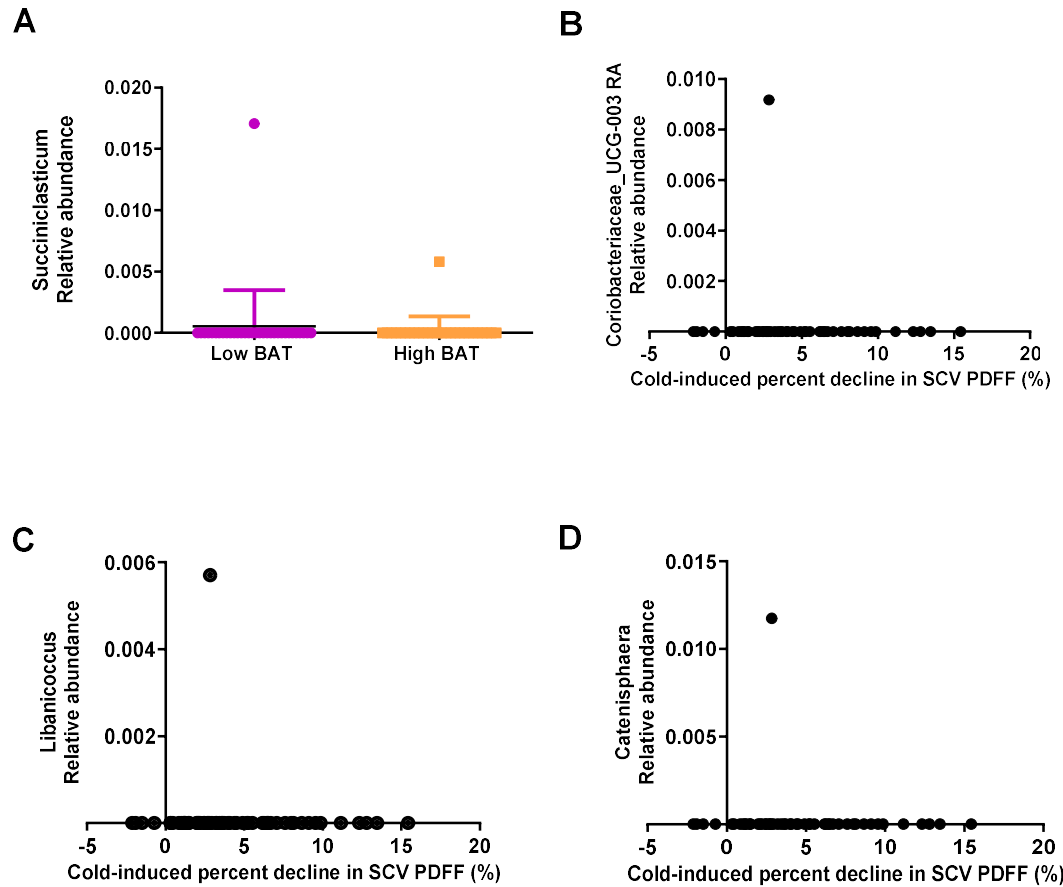


Figure S2. (Related to Relationship of Gut Microbiota to Cold-induced Percent Decline in Supraclavicular Fat Fraction). Relative abundances of genera related to cold-induced percent decline in supraclavicular proton density fat fraction. Relative abundance of *Succiniclasticum* between BAT groups; low brown adipose tissue thermogenesis (Low BAT) and high BAT thermogenesis (High BAT) (A), the relative abundance of *Coriobacteriaceae UCG-003* (B) *Libanicoccus* (C), and *Catenisphaera* (D) in relation to cold-induced percent decline in supraclavicular proton density fat fraction (SCV PDFF) (%).

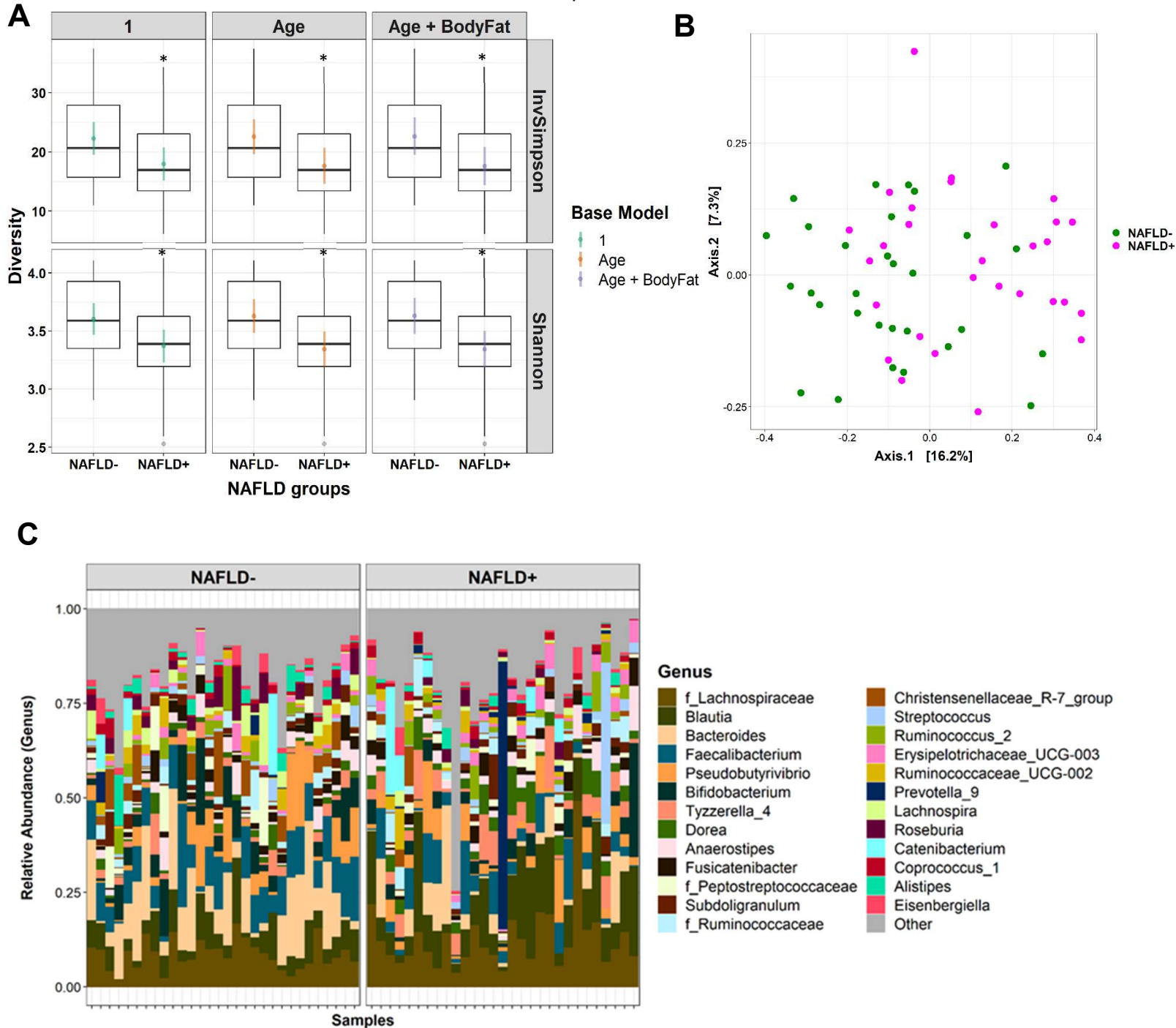


Figure S3. (Relationship of Gut Microbiota to Cold-induced Percent Decline in Supraclavicular Fat Fraction). Gut microbiota between NAFLD groups. Alpha diversity between NAFLD groups (without and with hepatic steatosis; NAFLD- and NAFLD+ respectively). **(A)** PCoA on Bray-Curtis dissimilarity distances between NAFLD groups. **(B)** Relative abundance of top 25 genera between NAFLD groups. **(C)** For A, data are represented as the median, IQ range, and 95% range of the data. The colored points and lines are the point estimates of the means from the regression models and the 95% confidence intervals of the model estimates of the means, respectively. For B, axes 1 and 2 captured 16.2 and 7.3% in the variation between samples, respectively. * - $p < 0.05$.

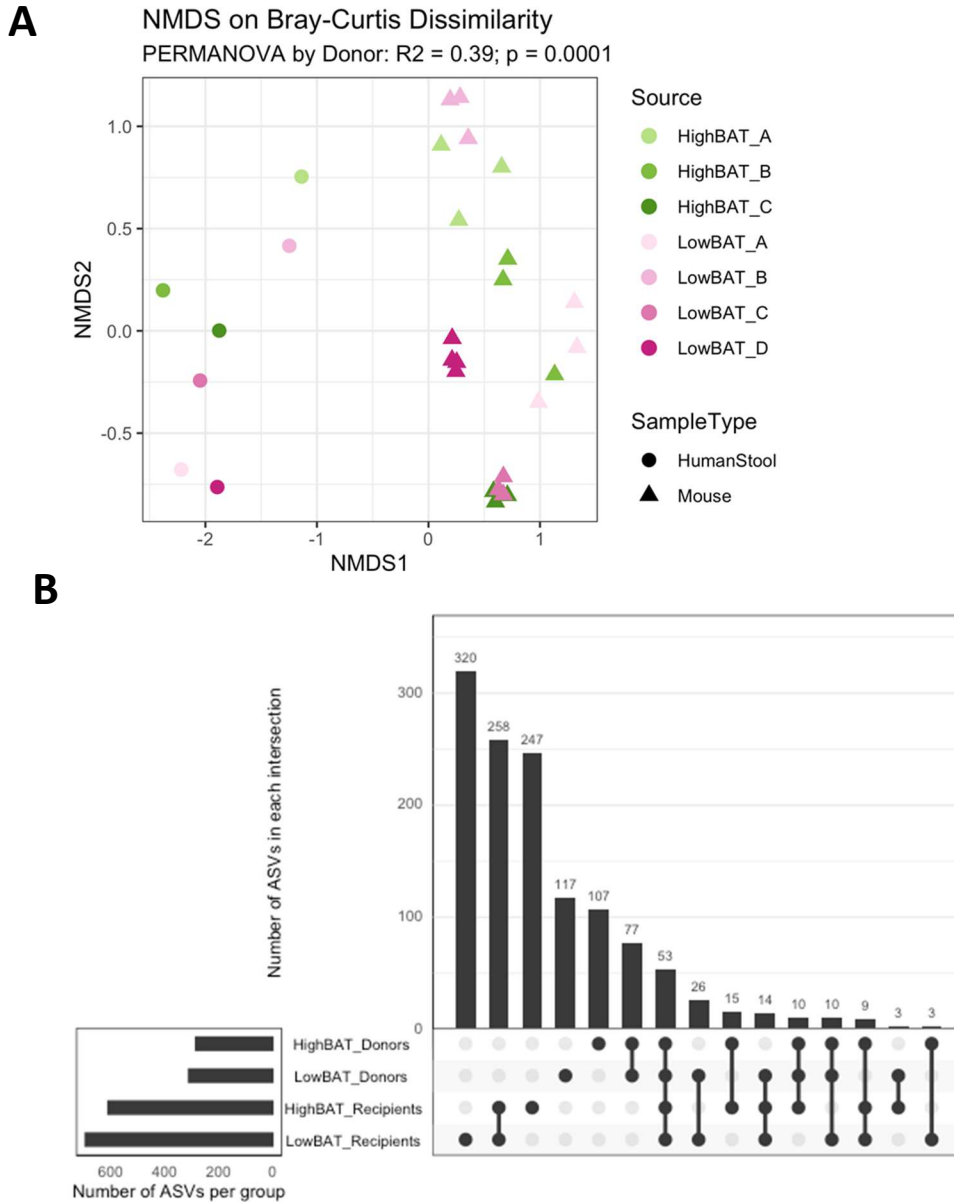


Figure S4. (Related to Microbial Transfer to Mice). Fecal microbiota transfer from fecal samples of participants with high and low BAT activity to axenic mice. The fecal microbiota of fecal transplanted axenic mice and their human fecal sample sources. Each donor and their fecal sample were classified as either High BAT activity (labeled HighBAT_A, HighBAT_B, or HighBAT_C) or Low BAT activity (labeled LowBAT_A, LowBAT_B, LowBAT_C, LowBAT_D). Non-metric multidimensional scaling (NMDS) plot of the Bray-Curtis dissimilarity metric colored by the source of stool to denote BAT activity classification and different donors, and with shapes to denote either the human stool donor or the axenic mice recipients (A). Upset plot comparing ASVs present in each group, where the y-axis shows the number of ASVs common between the groups identified along the x-axis. The bar graph beside the x-axis shows the total number of ASVs detected in each group (B).

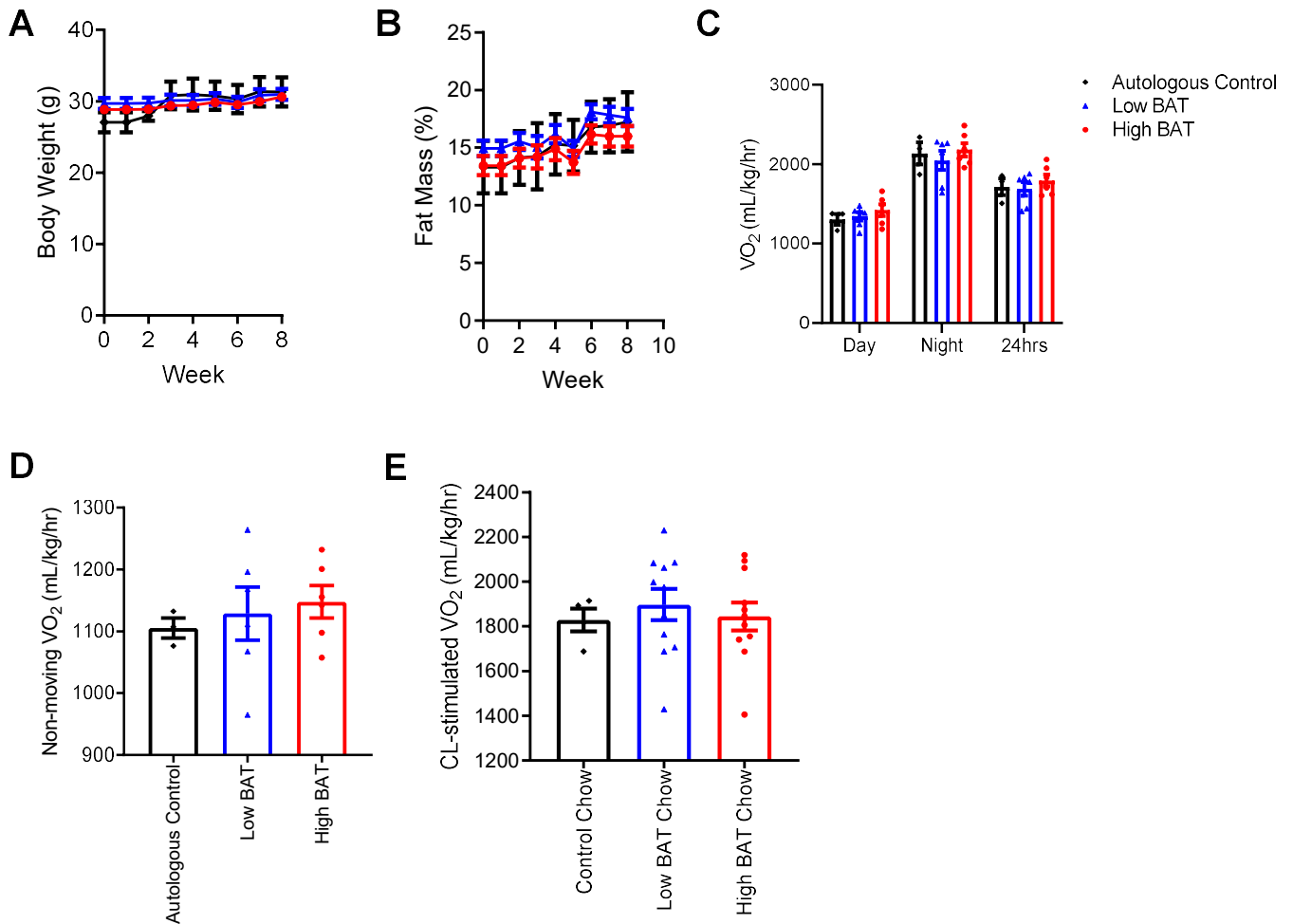
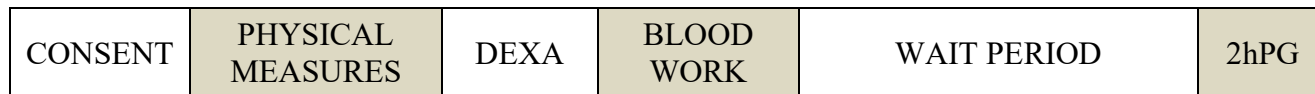


Figure S5: (Related to Microbial Transfer to Mice). Human brown adipose tissue activity is not transmissible via gut microbes in SPF mice. Weekly (A) body mass and (B) percent fat mass. (C) Average oxygen consumption (VO_2) during light and dark cycles, and over a 24hr period (average of light and dark), along with (D) non-moving VO_2 measures after 5 weeks of colonization. Oxygen consumption of anesthetized mice following CL-316,243 administration after 7 weeks of colonization. Data are expressed as means \pm SEM. Significance was determined using a One-Way ANOVA and Tukey's multiple comparison test. n=3-12/group.

A



B

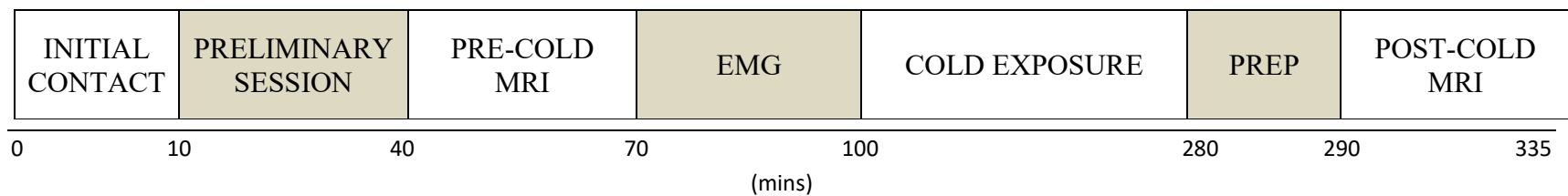


Figure S6. (Related to STAR methods) Timelines for the study visits. Visit 1 at McMaster University Medical Centre (A). Visit 2 at St. Joseph's Healthcare Hamilton (B)

CHAPTER THREE

Impaired cold stimulated supraclavicular brown adipose tissue activity in young boys with obesity

Basma A. Ahmed, Nina Varah, Frank J. Ong, Denis P. Blondin, Elizabeth Gunn, Norman B. Konyer, Nina P. Singh, Michael D. Noseworthy, Francois Haman, Andre C. Carpentier, Zubin Punthakee, Gregory R. Steinberg*, Katherine M. Morrison*

*These authors contributed equally to this work

Prepared for publication.

3.1 Preface and significance to the thesis

In adults, reductions in cold-stimulated BAT activity are related to obesity and type 2 diabetes, however little is known about whether this relationship exists in children. In this chapter, we examined cold-stimulated BAT activity via MRI, in 26 boys (8-10 years), after one hour of standardized whole-body cold exposure at 18°C. We show that boys with overweight/obesity have less responsive BAT when exposed to cold compared to boys with normal BMI. Additionally, higher cold-stimulated BAT activity was related to lower BMI, waist circumference, and visceral fat. These findings are important as they show that, like in adults, delivering whole-body cold exposure to young children allows the evaluation of BAT characteristics via MRI and that increasing BAT activity in children with overweight/obesity could be important.

3.2 Author contribution

B.A.A. was the primary contributor to all the figures and the tables in this manuscript. B.A.A. wrote the manuscript with G.R.S. and K.M.M. Other contributions are listed below:

B.A.A., F.J.O., G.R.S., and K.M.M. conceptualized the study. B.A.A., N.V., F.J.O., and E.G. conducted the experiments. F.J.O., D.P.B., N.B.K., N.P.S., M.D.N., F.H., A.C.C., Z.P., G.R.S., and K.M.M contributed to the methodology. B.A.A., D.P.B., N.V., and E.G. ran the formal Analysis. N.B.K., M.D.N., F.H., A.C.C., G.R.S., and K.M.M provided resources. All the authors edited the final version of the manuscript.

Impaired cold stimulated supraclavicular brown adipose tissue activity in young boys with obesity

Basma A. Ahmed^{1,2}, Nina Varah^{1,3}, Frank J. Ong^{1,3}, Denis P. Blondin⁴, Elizabeth Gunn^{1,3}, Norman B. Konyer⁵, Nina P. Singh⁶, Michael D. Noseworthy^{1,5,6,7,8}, Francois Haman⁹, Andre C. Carpentier¹⁰, Zubin Punthakee^{1,3,11}, Gregory R. Steinberg^{1,2,11*}, Katherine M. Morrison^{1,3*†}

AFFILIATIONS

- 1- *Centre for Metabolism, Obesity and Diabetes Research, McMaster University; Hamilton, ON, L8S 4L8; Canada*
- 2- *Department of Biochemistry and Biomedical Sciences, McMaster University; Hamilton, ON, L8S 4L8; Canada*
- 3- *Department of Pediatrics, McMaster University; Hamilton, ON, L8S 4L8; Canada*
- 4- *Faculty of Medicine and Health Sciences, Department of Medicine, Division of Neurology, Centre de recherche du CHUS, Université de Sherbrooke; Sherbrooke, QC, J1K 2R1; Canada*
- 5- *Imaging Research Centre, St. Joseph's Healthcare; Hamilton, ON, L8N 4A6; Canada*
- 6- *Department of Radiology, McMaster University; Hamilton, ON, L8S 4L8; Canada*
- 7- *Department of Electrical and Computer Engineering, McMaster University; Hamilton, ON, L8S 4K1; Canada*
- 8- *School of Biomedical Engineering, McMaster University; Hamilton, ON, L8S 4K1; Canada*
- 9- *Faculty of Health Sciences, University of Ottawa; Ottawa, ON, K1N 6N5; Canada*
- 10- *Division of Endocrinology, Department of Medicine, Centre de recherche du CHUS, Université de Sherbrooke; Sherbrooke, QC, J1K 2R1; Canada*
- 11- *Department of Medicine, McMaster University; Hamilton, ON, L8S 4L8; Canada*

* These authors made comparable contributions.

† Lead Contact

Short title: Cold-stimulated BAT activity in boys

Correspondence to:

Dr. Katherine M. Morrison[†] - kmorrison@mcmaster.ca

Reprint requests to:

Dr. Katherine M. Morrison[†] - kmorrison@mcmaster.ca

Background: Childhood obesity is a growing worldwide problem. In adults, lower cold-induced brown adipose tissue (BAT) activity is linked to obesity and metabolic dysfunction. It is not known whether this relationship exists in children. This study aimed to compare cold-induced supraclavicular (SCV) BAT activity in prepubertal boys with and without overweight/obesity.

Methods: This is a cross-sectional study of 26 boys aged 8-10 years; 13 with normal body mass index (BMI) and 13 with overweight/obesity based on the WHO BMI definition. Magnetic resonance imaging (MRI) proton density fat fraction (PDFF) was used to assess SCV BAT activity after one hour of whole-body cold exposure (via a water-perfused suit (18°C)). Anthropometry, body composition, fasting lipids, oral glucose tolerance test, insulin resistance, shivering intensity with electromyography and, MRI measurement of hepatic and abdominal fat were assessed. The main outcome measure was the cold-induced percent decline in SCV PDFF as a measure of BAT activity.

Results: Cold exposure reduced the PDFF in the SCV region but not in either the posterior neck fat or the abdominal subcutaneous fat. Boys with overweight/obesity have lower cold-stimulated BAT activity compared to those with normal BMI (percent decline in SCV PDFF $1.6 \pm 0.8\%$ versus $4.7 \pm 1.2\%$, respectively). BAT activity is inversely related to BMI ($r = -0.39$, $p = 0.047$), waist circumference ($r = -0.48$, $p = 0.014$), and visceral fat area ($\rho = -0.47$, $p = 0.014$).

Conclusion: BAT activity in young boys, as in adults, is lower in those with overweight/obesity, consistent with the consideration of BAT as a potential therapeutic target for childhood obesity treatment.

HIGHLIGHTS

- Delivering a standardized whole-body cold exposure to young children is feasible in a manner that allows the evaluation of BAT characteristics via MRI.
- Cold-stimulated BAT PDFF in young boys with overweight/obesity is lower compared to boys with normal BMI.

KEYWORDS

Brown adipose tissue, children, cold exposure, MRI, obesity

INTRODUCTION

Pediatric obesity is a growing worldwide problem. The World Health Organization has suggested that the rate of obesity in childhood has reached ‘‘alarming proportions’’³⁰⁵. Childhood obesity is linked to unfavorable health outcomes including type 2 diabetes, non-alcoholic fatty liver disease (NAFLD), and the development of other cardiovascular disease risk factors^{306–308} in adulthood. Interventions to treat childhood obesity have generally focussed on changes in health behaviors to achieve alterations in energy balance; these have had moderate efficacy and have been challenging to sustain, highlighting the need to identify novel approaches³⁰⁹.

Brown adipose tissue (BAT) contributes to energy expenditure through its ability to produce heat by uncoupling mitochondrial oxidative phosphorylation through uncoupling protein 1 (UCP-1)²⁵³ and possibly other futile cycles³¹⁰. BAT is detectable in the supraclavicular (SCV) region of the neck in children, adolescents^{202,206,207,247,311}, and adults^{60,62,255,312}. Mild cold exposure has been reported to be the most powerful stimulus for BAT activity as it enhances BAT oxidative metabolism⁶⁶. Cold stimulation is used in BAT PET-CT imaging studies examining F-18 labeled fluorodeoxyglucose (¹⁸F-FDG uptake) as a measure of the accumulation of glucose in BAT⁸³. Both retrospective and prospective studies report that adults with obesity and with diabetes have lower cold stimulated BAT glucose uptake than those without^{67,77,142,145,157}. In children, PET-CT scans obtained for clinical purposes (oncological follow-up) have been used to examine spontaneous BAT ¹⁸F-FDG uptake under standard room temperature conditions^{202,206,207}. In these reports, ¹⁸F-FDG uptake at ambient temperature was lower in children with obesity²⁰², higher during puberty²⁰⁶, and was directly related to the child’s muscle volume²⁰⁷. Due to exposure to ionizing radiation, no studies have been done using cold-stimulated PET-CT to assess BAT activity in otherwise healthy children.

To date, the only cold-stimulated imaging studies of BAT activity in the pediatric population have measured skin temperature with infrared thermography^{84,146,208,251}. Although these studies have noted that children with higher BMI⁸⁴ or higher liver fat²⁰⁸ had less of an increase in skin temperature after cold-stimulation, this method has significant limitations. BAT is not the sole source of heat in the SCV region during cold exposure i.e, neck muscle tension and big blood vessels can contribute to SCV temperature. Also, the variability in the thickness of the subcutaneous fat overlying BAT in the SCV region cannot be accounted for. Thus, those with higher SCV subcutaneous fat thickness may have less change in skin temperature resulting in underestimation of BAT activity²⁵⁴.

One method which has been developed to measure BAT activity that avoids the ionizing radiation of PET-CT and the influence of superficial subcutaneous fat involves the use of magnetic resonance imaging (MRI) in which the proton density fat fraction (PDFF) is measured⁵⁹. In adults, PDFF reduction was reported in the SCV region after cold stimulation, which suggests an increase in intracellular triglyceride utilization^{101,102,138}. Using whole-body cold exposure, known to stimulate BAT activity in adults^{67,102,113}, we have demonstrated that PDFF in the SCV region of young adults begins to decline after 10 minutes of cold exposure and reaches its lowest level within the first hour of exposure²⁵⁵.

In infants, lower PDFF in the SCV region at ambient temperature predicted less gain in body fat during the first 6 months of life¹⁹⁷. In preschool children, the presence of more BAT in the SCV region, measured by PDFF, is associated with lower BMI, lower hepatic fat, and abdominal obesity¹⁹⁶. Similarly, young boys with higher adiposity and adolescents with higher 2-hour glucose levels had higher SCV PDFF at ambient temperature^{256,258}. These data suggest a relationship

between BAT, obesity and, glucose homeostasis in children and adolescents but whether PDFF at ambient temperature accurately reflects BAT activity in children is not known.

In the current study, we examined cold-stimulated changes in SCV PDFF as a measure of BAT activity in prepubertal boys. Our objectives were to 1. evaluate the change in SCV PDFF with a 1-hour whole-body cold exposure (18°C); 2. compare the cold-stimulated changes in SCV PDFF between boys with and without obesity, and 3. examine the relationship of BAT activity to adiposity and metabolic health in young boys.

METHODS

Study Population

Boys aged 8 to 10 years were recruited to this two-visit, cross-sectional study. Participants were recruited through public announcements and from the pediatric weight management clinic at McMaster Children's Hospital between February 2018 and August 2019. The study was approved by the Hamilton Integrated Research Ethics Board (HiREB). All participants provided informed assent; informed consents were provided by the child's guardian. Exclusion criteria included: contraindications for MRI (claustrophobia, implanted metal, metallic injuries, recent tattoo or weight > 300lbs), prior bariatric surgery or liver transplant, and use of medications likely to influence BAT activity or metabolic health (β adrenergic, steatogenic, anti-hyperglycemic, antidepressant, anti-psychotic, anxiolytic, thyroid hormone, antiemetic – 5HT3 antagonists or serotonergic drugs).

Study Visits

Participants were asked to fast for at least 8 hours, to avoid intake of caffeine for at least 12 hours, and to abstain from serotonin-rich foods (e.g., banana, tomato, kiwi, walnut, avocado,

pineapple, and plum) for at least 24 hours prior to each study visit²¹¹. Visits 1 and 2

(Supplementary Figure 1) took place in the morning and were scheduled at least 8 days apart, but ideally within one month of each other.

Anthropometric/ metabolic Visit: Visit 1, the anthropometric/ metabolic visit, took place at the McMaster University Medical Centre, Hamilton, ON, Canada. This visit included the evaluation of anthropometric indices, body composition, 2-hour oral glucose tolerance test (1.75 g/kg to a maximum of 75 g glucose), fasting lipid profile, fasting insulin, and blood pressure as detailed in **Supplementary Material 1**.

Imaging Visit: Visit 2, the imaging visit, took place at the Imaging Research Centre at St. Josephs Healthcare, Hamilton, ON, Canada. It involved MR imaging of the SCV BAT, liver, and abdomen before and after a standardized cold exposure protocol. The cooling protocol was based on published methodology^{113,272}, with a modification in the length of cold exposure from 3 hours to 1 hour, consistent with our findings in young adults²⁵⁵. Participants were fitted with a high-density liquid conditioned suit (LCG; Two Pieces with zippers and open access neck, Med-Eng, Ottawa, ON, Canada), and 18°C water was circulated using a temperature- and flow-controlled circulation bath (Isotemp 6200 R28, Fisher Scientific, Waltham, MA, USA). During cold exposure, participants stayed in a hospital bed in a semi-reclined position with access to a device to watch a movie but were not permitted to type or do any activities that required movement. Continuous evaluation of skin temperature and shivering activity was done during the cold exposure as detailed in **Supplementary Material 2**.

MRI was performed using a 3-Tesla (T) whole-body scanner (Discovery 750; GE Healthcare, Waukesha, WI, USA). MRI acquisitions are detailed in **Supplementary Material 2**. MRI

outcomes included cold-stimulated change in SCV PDFF (BAT activity) and quantification of abdominal fat (liver, subcutaneous (SAT), and visceral (VAT) adipose tissues).

Post-imaging analysis: Segmentation and analysis of all MR images were conducted using Analyze Pro (Version 1; Mayo Clinic, Biomedical Imaging Resource, AnalyzeDirect, Overland Park, KS, USA) by one reader (BA). The SCV region was segmented as previously described²⁵⁵. To evaluate BAT activity accounting for the pre-cold SCV PDFF, the percent change in SCV PDFF was calculated as $[(\text{pre-cold SCV PDFF} - \text{post-cold SCV PDFF}) / (\text{pre-cold SCV PDFF})] * 100$ and is noted as cold-induced percent decline in SCV PDFF – our measure of BAT activity. For comparison, the PDFF of posterior neck fat was analyzed at three MRI slices: C5-C6, C6-C7, and T1-T2 using manual tracing and the criteria that were used for SCV BAT. Analysis for abdominal fat is detailed in **Supplementary Material 2**.

Statistical Analyses

SPSS Statistics (version 27; IBM, North Castle, NY, USA) was used for all statistical analyses. Normality was assessed by following the procedures outlined by Tabachnick and Fidell³⁰¹ where variables with Z_{skewness} and/ or $Z_{\text{kurtosis}} \geq |3.29|$ were classified as non-normal. Non-parametric tests were used for analyses if data were non-normally distributed. Data were presented as mean (standard error of the mean; SEM) or median [Q1, Q3] for skewed variables. Parametric paired Student's t-test was used to determine the effects of cold exposure on normally distributed MRI outcomes (before and after cold exposure). Assuming the independence of the observations, independent Samples t-test and Mann-Whitney U test were used to assess the differences in the means of normally distributed continuous variables and the differences in the mean rank of skewed continuous variables, respectively, between boys with and without overweight/obesity (categorical

variable) and results of Levene's test for equality in variances between groups were considered to assess the p-value of independent Samples t-test for equality in the mean. Pearson's correlation coefficient was used to assess the association between normally distributed variables. Spearman's correlation coefficient was used to assess the association between skewed variables and for non-linear monotonic relationships. Multivariate regression models were used to examine if cold-induced percent decline in SCV PDFF (independent variable) was associated with significant correlates (dependent variables) after controlling for shivering in the trapezius muscle at 60 minutes of cold exposure. A two-tailed p-value of less than 0.05 was considered significant.

RESULTS

Participant enrollment and characteristics

Of the 98 participants who inquired about the study, 35 were enrolled and attended the anthropometric/ metabolic study visit (**Figure 1**). Of these, 33 attended the imaging visit after a median of 12 days [range 8 – 43 days]. Of the 33, 28 had a pre-cold image taken and 26 completed both the pre-and post-cold MRI scans. Seven participants were unable to complete the MRI measurements due to claustrophobia. The cold exposure was 60 minutes in 25 children and was terminated at 38 minutes in one child. The cold stimulus was similar between boys with and without overweight/obesity as measured by the temperature difference between outlet and inlet temperature to the cooling bath ($p= 0.362$) and the decline in skin temperature ($p= 0.333$) (**Supplementary Table 1**).

Of the 26 boys with pre-and post-cold scans, 10 boys were obese and 3 were overweight based on BMI Z-score. There was no significant difference in age between boys with normal BMI and those with overweight/obesity ($p= 0.151$). Boys with overweight/obesity had, as expected, higher body

weight, waist circumference, and total body adiposity than those with normal BMI (**Table 1**). As expected, boys with overweight/obesity had higher hepatic fat content (4.6 [3.5, 8.7] vs 3.0 [2.5, 3.2] %; $p < 0.001$) and higher VAT area (24.3 ± 4.5 vs 4.7 ± 0.6 cm²; $p = 0.001$) compared to boys with normal BMI. Boys with overweight/obesity also had lower HDL-cholesterol and higher triglycerides, non-HDL-cholesterol, LDL-cholesterol, and gamma-glutamyl transferase (GGT) than boys with normal BMI (**Table 1**). Although there were no differences between groups in fasting or 2-hour blood glucose, boys with overweight/obesity had lower insulin sensitivity compared to boys with normal BMI (**Table 1**).

Cold-induced change in SCV adipose tissue (BAT activity)

Boys with overweight/obesity had higher pre-cold SCV PDFF compared to those with normal BMI; 72.7 ± 2.2 vs $56.6 \pm 1.4\%$ respectively, $p < 0.001$. With cold exposure, the percent decline in SCV PDFF was less in boys with overweight/obesity compared to the normal BMI group (1.6 ± 0.8 vs $4.7 \pm 1.2\%$, $p = 0.044$ respectively) (**Figure 2**). In the entire cohort, there was a significant reduction in SCV PDFF after cold exposure (pre-cold PDFF 64.7 ± 2.1 vs $62.7 \pm 2.2\%$ post-cold PDFF, $p < 0.001$). No significant changes in PDFF after cold exposure were identified in either the posterior neck fat (pre-cold PDFF 78.8 ± 2.2 vs $78.7 \pm 2.1\%$ post-cold PDFF, $p = 0.558$) or in the abdominal SAT (pre-cold PDFF 87.9 ± 1.0 vs $87.9 \pm 1.0\%$ post-cold PDFF, $p = 0.721$) (**Figure 3A and B**). These data indicate that cold exposure reduces PDFF within the BAT but not in either the posterior neck fat or abdominal SAT. Consistent with these findings, the cold-induced percent decline in SCV PDFF was inversely related to BMI ($r = -0.39$, $p = 0.047$), waist circumference ($r = -0.48$, $p = 0.014$) and VAT area ($\rho = -0.47$, $p = 0.014$), but the relationships to BMI Z-score, total body fat, and hepatic fat were not statistically significant; $r = -0.37$, $p = 0.065$, $\rho = -0.28$, $p = 0.167$ and $\rho = -0.34$, $p = 0.088$ respectively (**Figure 4**).

The percent decline in SCV PDFF was unrelated to shivering measured in the vastus lateralis or vastus medialis muscles at any time point during the cold exposure. Boys with greater decline in SCV PDFF had more shivering in the trapezius muscle, which was observed at 20, 30, 40, and 60 minutes of cold exposure (**Supplementary Figure 2**) and boys with normal BMI had higher EMG shivering signals in the trapezius and the vastus lateralis muscles compared to boys with overweight/obesity; $p= 0.035$ and 0.034 respectively (**Supplementary Table 1**).

To evaluate whether SCV PDFF was related to the anthropometric and body composition variables independent of shivering intensity in the trapezius muscle, a multivariate regression analysis was done. As demonstrated (**Supplementary Table 2**), cold-induced percent decline in SCV PDFF controlling for shivering activity in the trapezius muscle was not related to BMI ($p= 0.078$) or VAT area ($p= 0.064$) but explained 25% of the variance in waist circumference; $p= 0.045$, and R^2 adjusted= 0.246.

Cold-induced BAT activity and obesity-related health parameters

The relationship of the cold-induced percent decline in SCV PDFF to measures of metabolic health is demonstrated in Figure 4 and Supplementary Figure 3. Statistically, there was no relationship with glycemia, insulin levels, insulin sensitivity indices, components of the plasma lipid profile, or hepatic fat. There was also no significant relationship to serum transaminases (AST; $\rho=-0.16$, $p= 0.443$, ALT; $\rho= -0.16$, $p= 0.451$, and GGT; -0.37 , $p= 0.064$).

DISCUSSION

We have demonstrated that young boys with overweight/obesity have lower BAT activity, measured as the cold-induced decline in SCV PDFF, than age and sex-matched controls with normal BMI. Further, as this is the first evaluation of cold-induced change in SCV PDFF in

children, we have demonstrated the feasibility of carrying this out in a standardized manner as is done in adults²⁵⁵. A higher PDFF in this region is consistent with a “whiter” fat phenotype and the decline in PDFF is a measure of triglyceride lipolysis in response to stimulation of brown adipocytes. Consistent with this assertion is the observation that there was no change in the PDFF in either the posterior neck fat or in the abdominal SAT. Our findings are consistent with previous studies in adults using the same methodology^{102,255,313}.

Our findings suggest that even at a young age and before puberty, boys with overweight/obesity have lower cold-induced BAT activity. Further, there is an inverse relationship between VAT area and waist circumference, particularly in boys with obesity. Boys with normal BMI have more variability in their cold-induced BAT activity (percent decline in PDFF ranges -1.9 to 12%) than boys with overweight/obesity (-3.0 to 6.1%). Little is known of the trajectory of BAT activity in children and longitudinal studies should be undertaken to determine the relationship between low BAT activity and metabolic health over time.

The only previous studies of cold-induced BAT activity in children utilized SCV skin temperature as the measure of BAT activity^{84,146,208,251}, a method made unreliable as introduced earlier²⁵⁴. Cold-induced BAT activity, measured either with ¹⁸F-FDG uptake using PET-CT imaging or change in SCV PDFF is lower in adults with obesity^{123,157} and diabetes^{115,127}. Further, in studies in adults utilizing either PET-CT or MRI SCV PDFF, cold-induced BAT activity was inversely related to glycemia^{77,199,314,315}, circulating lipid levels^{199,316}, and hepatic fat^{195,212} but was not related to HOMA-IR in 25 young men³¹⁵. In our cohort of young boys, cold-induced BAT activity is not related to glycemia, insulin sensitivity, or circulating lipid levels. However, the lack of variability in our metabolic measures would make it challenging to identify a relationship to BAT activity with the small number of children that had metabolic abnormalities. While it will be interesting to

examine in future studies whether glycemia, insulin sensitivity, or circulating lipid levels are related to changes in BAT activity this may be challenging to complete in children not taking medications that have been shown to affect BAT activity (e.g., metformin).

We found that boys with overweight/obesity have a higher pre-cold SCV PDFF than those with normal BMI. This finding is consistent with previous reports suggesting children with obesity have higher SCV FF at ambient temperature^{172,182}. Also consistent with this was the demonstration of lower BMI in preschool children with more BAT at ambient temperature¹⁹⁶. In the latter study, boys had SCV PDFF of 50%¹⁹⁶. The mean pre-cold SCV PDFF in our entire sample is higher than in the work by Andersson et al in a group of 7-year-old children (64.7 ± 2.1 vs 57.2 ± 5.2 %). This likely stems from differences in the extent of obesity – only 3 of 63 children in the Andersson study had obesity, one had morbid obesity and 19 were overweight. In our study, ambient SCV PDFF in the boys with normal BMI is very comparable to their group ($56.6 \pm 1.4\%$)²⁵⁶.

The absolute reduction in SCV PDFF in this cohort is lower than what has been reported in young adults by us and others^{131,255}. Similarly, the percent change in SCV PDFF in this cohort is lower than what we noticed in young adult males that we previously studied (3.2 ± 0.8 , n= 26 vs $6.6 \pm 0.9\%$, n=23 respectively). Interestingly, boys with normal BMI have lower pre-cold SCV PDFF to start with compared to young adult males with normal BMI (56.5 ± 1.4 , n=13 vs $64.6 \pm 1.4\%$, n= 16). These observations raise interesting questions about the trajectory of BAT activity over time from childhood to adulthood. It has been suggested that BAT is most abundant in infancy³¹⁷ and declines with time, though we have not, to date, had sufficient data to enable closer inspection of this trajectory. This study supports the feasibility of conducting studies in children examining the factors that influence cold-induced BAT activity as children mature.

Study limitations

In this first study to examine cold-induced BAT activity using MRI in children, we have demonstrated the feasibility of this methodology in children and noted that lower BAT activity is seen in prepubertal boys with overweight/obesity. We cannot however generalize our findings to females or other age groups. The change in SCV temperature, using IRT, after 5 minutes of hand cold exposure was reported to be higher in prepubertal girls than in boys²⁰⁸, thus exploring cold-stimulated BAT in prepubertal girls after whole-body cold exposure is warranted. We also note that these young children have a lower decline in cold-stimulated SCV PDFF than young adult males we have studied, highlighting the importance of future longitudinal studies across a broader age range to help understand the pattern of change in BAT activity during development and the factors that contribute to it. Puberty has been described as a factor that increases the ¹⁸F-FDG uptake in PET-CT scans obtained at ambient temperature for cancer surveillance^{202,247,249,250}. In addition to larger sample sizes, it will be important to measure energy expenditure during the cold stimulation and relate that to the BAT activity, something we were unable to do because of the lack of availability of infrastructure to conduct this study where the MRI is housed. Finally, larger studies in children with metabolic abnormalities will be needed to ascertain the relationship between BAT activity and metabolic health in the pediatric population.

CONCLUSION

We have identified smaller changes in cold-stimulated BAT PDFF in young boys with overweight/obesity compared to boys with normal BMI. Further, we have demonstrated the

feasibility of delivering a standardized whole-body cold exposure to young children in a manner that is compatible with the evaluation of the characteristics of BAT with MRI. This early work will enable future studies to further examine these relationships in girls and children of other ages such that we may better understand the factors impacting BAT activity in the early years of life, the trajectory of BAT activity over time, and the relationship of BAT activity to obesity-related health indicators. Together, this data will inform the hypothesis that BAT may be a promising therapeutic target for obesity-related illnesses.

ACKNOWLEDGMENT

We would like to thank our Boris Family and the Canadian Institutes of Health Research (grant number 144625-1) for the supporting grants. We also thank our participants and their families. We thank the MRI technologists at the Imaging Research Centre (IRC) at St. Joseph's Healthcare Hamilton. We thank Prasiddha Parthasarathy and Emily Hutchings for their contributions toward data collection and management. We also thank the computer server support provided by the laboratory of Dr. Andrew McArthur and the McMaster Service Lab and Repository (MSLR).

DISCLOSURE SUMMARY

B.A.A. holds Lau's family scholarship for science and engineering and was funded by the Ontario graduate scholarship.

N.V. holds the Canadian Institutes of Health Research Graduate Scholarship and was funded by the Ontario Graduate Scholarship.

D.P.B. holds the GSK Chair in Diabetes of the *Université de Sherbrooke* that has been created in part through a donation of \$1 million by GSK to the *Université de Sherbrooke*. D.P.B. has received honoraria/consulting fees from Boehringer Ingelheim.

A.C.C. holds the Canada Research Chair in Molecular Imaging of Diabetes and research funding from the Canadian Institutes of Health Research, *Fonds de recherche Québec – Santé*, and has participated in advisory boards for the companies Amgen, UniQure, Merck, Janssen, NovoNordisk, Novartis, HLS Therapeutics Inc., TVM Life Science Management, AstraZeneca, and Eli Lilly and made one conference sponsored by AstraZeneca.

M.G.S. is funded by the Canadian Institutes of Health Research, Genome Canada, and the W. Garfield Weston Foundation and holds a Tier 1 Canada Research Chair in Interdisciplinary Microbiome Research.

Z.P. has received honoraria for advice and speaking from Abbott, Astra Zeneca/Bristol Myers Squibb, Boehringer Ingelheim/Eli Lilly, Janssen, Merck, NovoNordisk, Pfizer, and Sanofi. He has received research funds from Amgen, Astra Zeneca/Bristol Myers Squibb, Lexicon, Merck, NovoNordisk, Sanofi, and the Canadian Institutes of Health Research.

G.R.S. receives funding from the Canadian Institutes of Health Research (201709FDN-CEBA-116200 to GS), Diabetes Canada Investigator Award (DI-5-17-5302-GS)- a Tier 1 Canada Research Chair and the J Bruce Duncan Endowed Chair in Metabolic Diseases. He also receives research funding from Espervita Therapeutics, Esperion Therapeutics, Poxel Pharma, and Novo Nordisk and honoraria/consulting fees from Eli-Lilly, Esperion Therapeutics, Poxel, and Merck.

K.M.M. holds research funding from the Canadian Institutes of Health Research, Heart and Stroke Foundation of Canada, McMaster Children's Hospital Foundation, and McMaster University. She has received research funds from Astra Zeneca and is an advisory board member for Novo Nordisk and Akcea Therapeutics, Canada.

FIGURE LEGENDS

Figure 1: Participants' recruitment and study flow

This figure demonstrates the number of children who expressed interest in the study, the number consented, and the number who completed each of the visits.

Figure 2: Cold-induced percent decline in SCV PDFF between obesity groups

Cold-induced percent decline in SCV PDFF in boys with normal BMI (black circles, n= 13) and those with overweight/obesity (white cones, n= 13). Data are presented as the mean \pm standard errors of the mean, $p < 0.05$ via Paired Student's t-test. SCV PDFF; supraclavicular proton density fat fraction.

Figure 3: Proton density fat fraction in different fat pads before and after cold exposure

Comparison between Proton density fat fraction (PDFF) before and after cold exposure in supraclavicular brown adipose tissue (BAT, n= 26), subcutaneous adipose tissue (SAT) in the posterior neck region (Neck SAT, n= 25) and SAT in the abdomen (Abd. SAT, n= 24) **(A)**. A representation of the mean absolute cold-induced decline between different fat pads **(B)**. Data are presented as mean \pm standard errors of the mean. * - $p < 0.05$ using Paired Student's t-test. ns: differences did not reach statistical significance using Paired Student's t-test.

Figure 4: The relationships of cold-induced percent decline in SCV PDFF, measures of adiposity, and hepatic fat

The relationship between cold-induced percent decline in SCV PDFF and waist circumference **(A)**, total body fat **(B)**, hepatic fat **(C)**, and visceral fat (VAT) **(D)** in boys with normal BMI (black circles) and those with overweight/obesity (white cones). § - $p < 0.05$ via Pearson's Correlation; \$ - $p < 0.05$ via Spearman's Correlation. SCV PDFF; supraclavicular proton density fat fraction.

Table 1: Participant characteristics and metabolic profile.

	All (n=26)	Normal BMI (n=13)	Overweight/obesity (n= 13)	p
Age (years)	9.7 (0.2)	10.0 (0.2)	9.5 (0.3)	0.151
Weight (kg)	39.9 (2.9)	30.1 (0.9)	49.8 (4.2)	0.001*
Height (cm)	140.1 (1.5)	138.2 (1.5)	142.0 (2.4)	0.204
Waist Circumference (cm)	69.3 (3.3)	57.9 (1.5)	80.7 (4.5)	<0.001*
BMI (kg/m ²)	20.0 (1.1)	15.7 (0.3)	24.2 (1.3)	<0.001*
BMI Z-score	1.1 (0.4)	-0.5 (0.2)	2.7 (0.2)	<0.001*
Body Fat (%)	27.2 (2.6)	16.2 (1.3)	38.1 (2.7)	<0.001*
Fasting Glucose (mmol/L) ^a	4.6 (0.1)	4.7 (0.1)	4.5 (0.1)	0.485
2hr Glucose (mmol/L) ^b	5.6 [4.5, 6.2]	5.3 [4.4, 6.2]	5.7 [5.1, 6.4]	0.379
Insulin (mU/L)	4.8 [3.6, 7.2]	4.2 (0.6)	10.0 (2.5)	0.040*
HOMA_IR ^a	0.9 [0.8, 1.4]	0.8 [0.6, 1.0]	1.2 [0.9, 3.1]	0.005†
QUICKI ^a	0.38 (0.01)	0.41 (0.01)	0.36 (0.01)	0.008*
Total cholesterol (mmol/L)	4.1 [3.7, 4.5]	4.0 (0.1)	4.4 (0.3)	0.223
Triglycerides (mmol/L)	0.7 [0.5, 0.9]	0.6 [0.5, 0.7]	0.8 [0.6, 1.3]	0.044†
HDL-cholesterol (mmol/L)	1.4 (0.1)	1.6 (0.1)	1.3 (0.1)	0.005*
LDL-cholesterol (mmol/L)	2.3 [1.2, 2.6]	2.1 (0.1)	2.6 (0.2)	0.0125*
Non-HDL-cholesterol	2.6 [2.3, 2.9]	2.4 (0.1)	3.1 (0.3)	0.029*
AST (U/L)	27.0 [21.8, 31]	27 [22.0, 31.0]	27 [21.5, 31.5]	0.960
ALT (U/L)	17.5 [14.0, 21.0]	16.0 [12.5,	20.0 [14.5, 31.0]	0.101
GGT (U/L)	14.0 [11.0, 15.3]	12.0 [10.5,	15.0 [13.5, 20.0]	0.019†
VAT (cm) ²	7.3 [4.1, 19.5]	4.7 (0.6)	24.3 (4.5)	0.001*
Hepatic fat (%)	3.2 [2.8, 4.6]	3.0 [2.5, 3.2]	4.6 [3.5, 8.7]	<0.001†

Values are presented as mean (SEM) for normally distributed variables or median [IQ1, IQ3] for non-normally distributed variables.

* - $p < 0.05$ via independent sample t-test; † - $p < 0.05$ via Mann-Whitney U test.

^a Fasting blood glucose is not available for one sample due to laboratory error.

^b Two-hour glucose is not available for three participants (child refusal).

BMI; body mass index, SCV PDFFF; supraclavicular proton density fat fraction, HOMA-IR; homeostatic model assessment of insulin resistance, QUICKI; quantitative insulin-sensitivity check index, HDL; high-density lipoprotein, LDL; low-density lipoprotein, Non-HDL; non-high-density lipoprotein, AST; aspartate aminotransferase, ALT; alanine aminotransferase, GGT; gamma-glutamyl transferase, VAT; visceral adipose tissue.

Figures

Figure 1

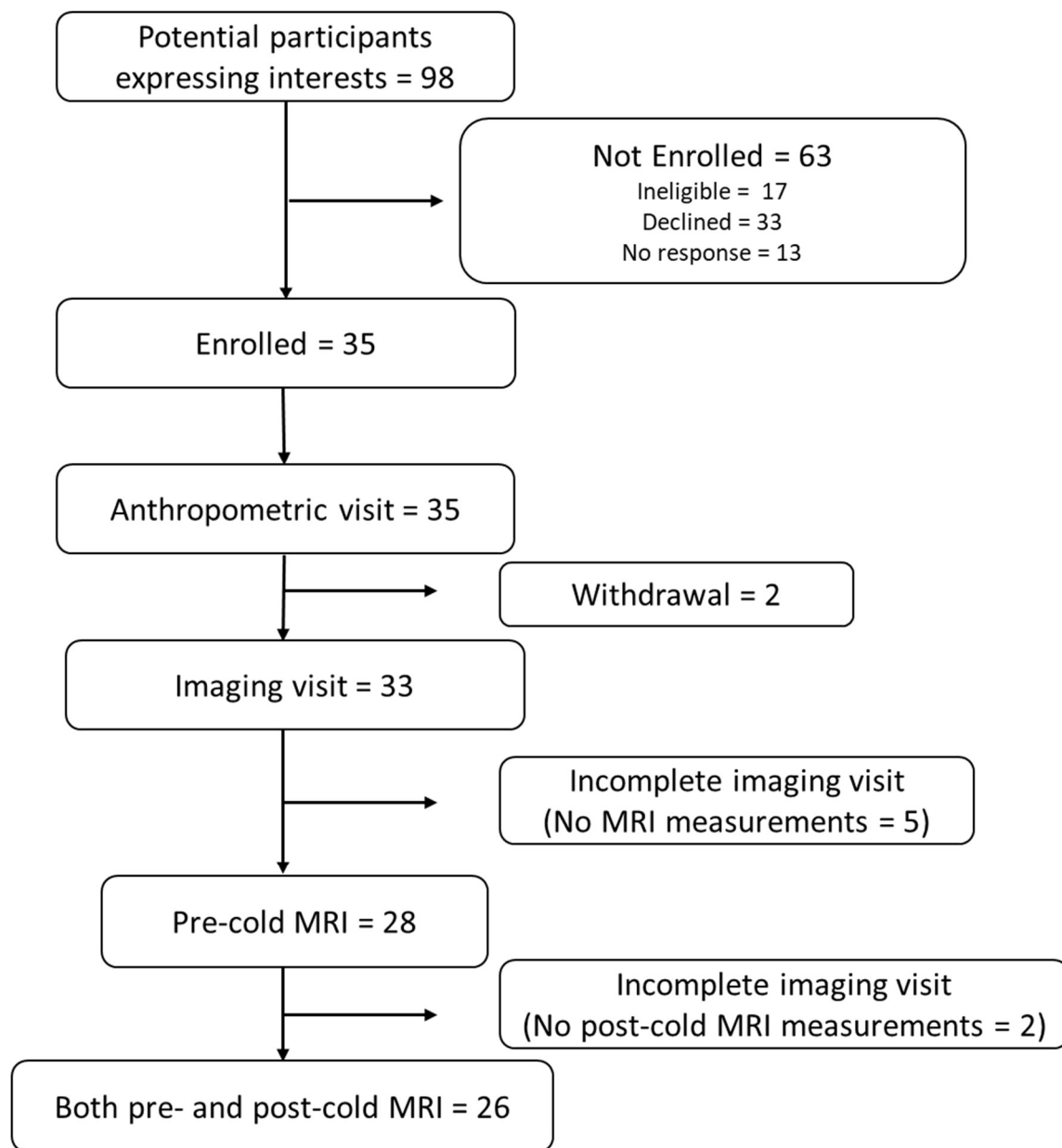


Figure 2

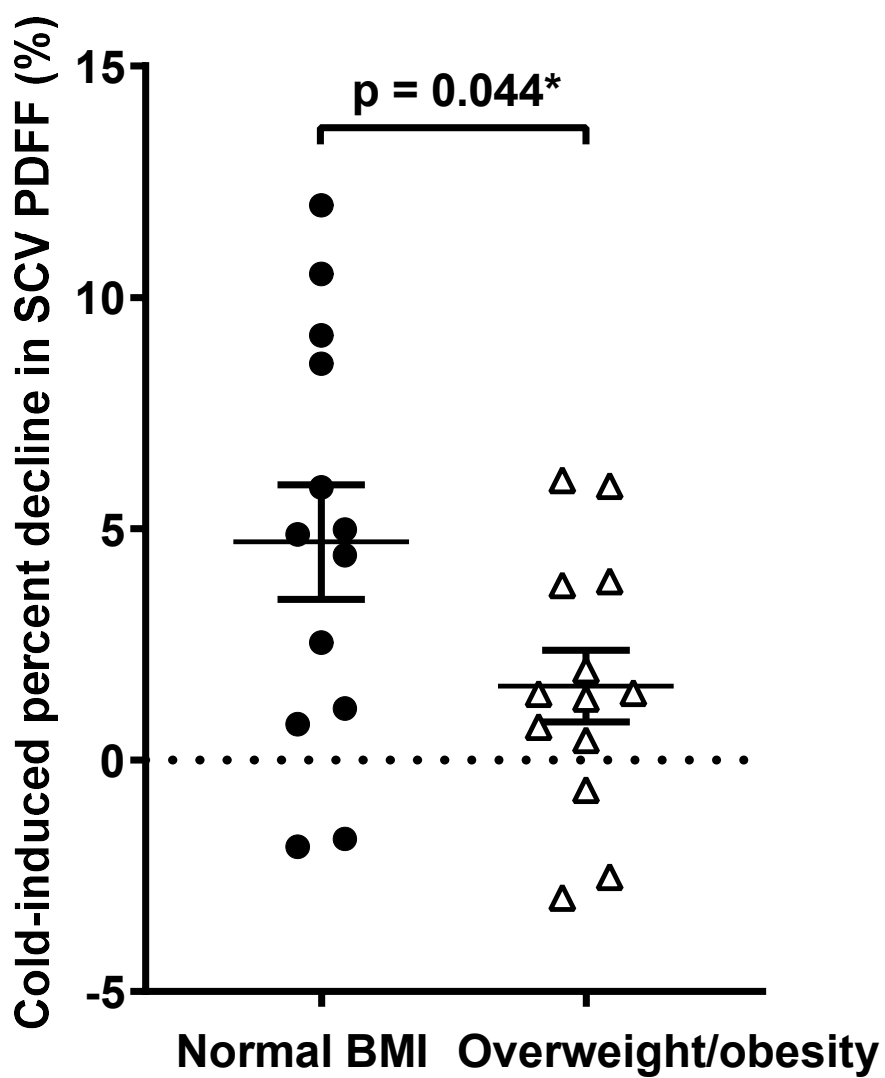


Figure 3

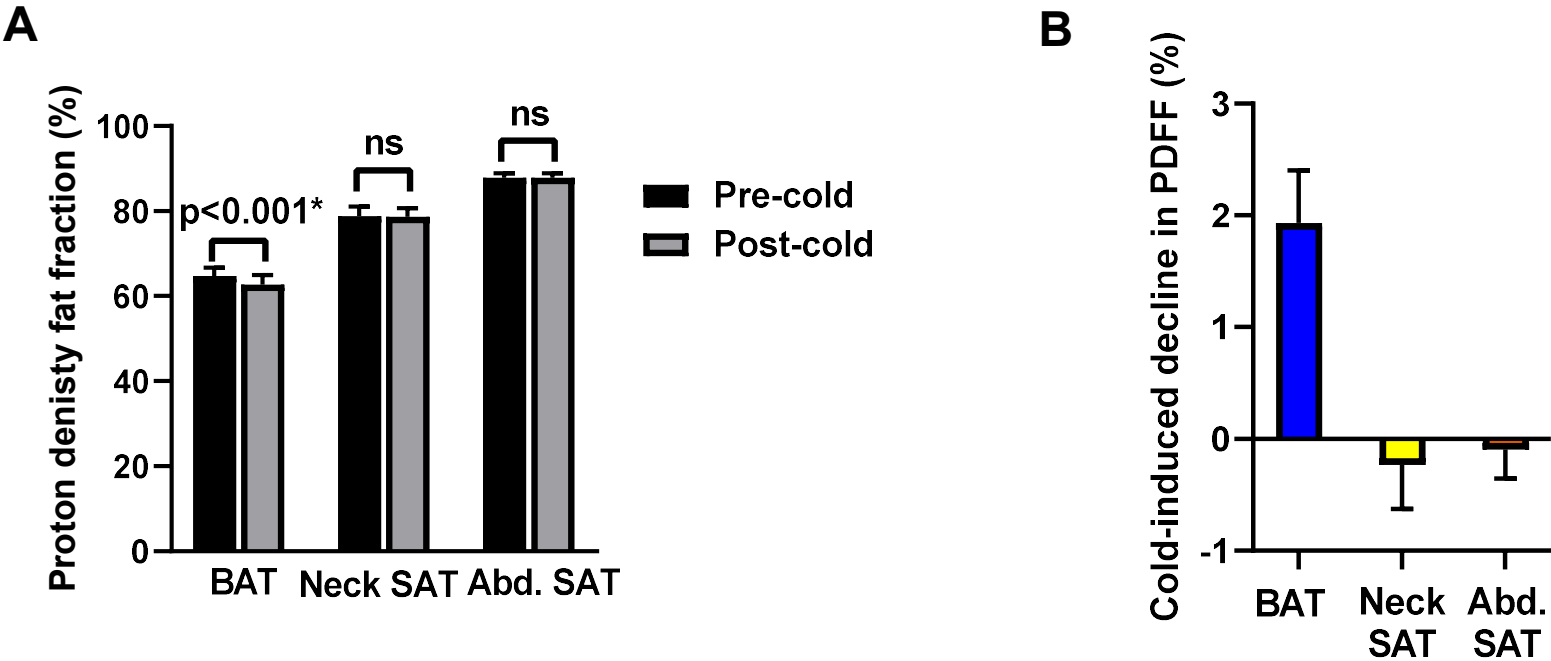
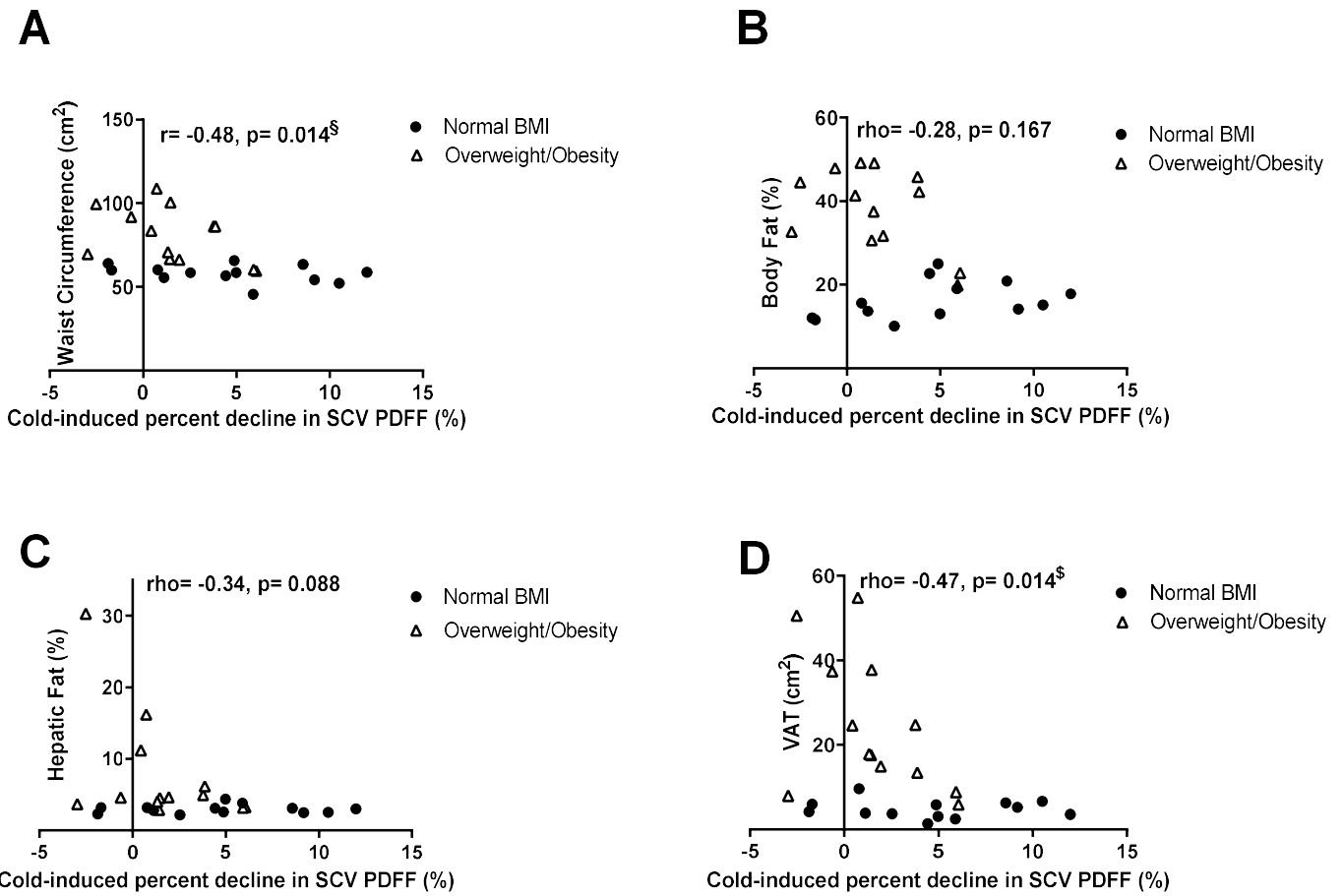


Figure 4



SUPPLEMENTARY MATERIAL 1

Anthropometric/ metabolic Visit

Anthropometrics and body composition: Weight (kg) was measured by trained research personnel using an electronic platform scale (BMI Scale Model 882; Seca, Hamburg, Germany) to the nearest 0.1 kg. Height (cm) was measured using a wall-mounted stadiometer (Height Measuring Rod Model 240; Seca, Hamburg, Germany) to the nearest 0.1 cm. Body mass index (BMI) was calculated as weight in kilograms divided by height squared in meters. BMI Z-score was calculated using the WHO AnthroPlus anthropometric calculator, with the World Health Organization defining normal weight as a Z-score < 1, and as overweight and obese as a Z-score ≥ 1 . Waist circumference (cm) was measured at the midpoint between the costal margin and the iliac crest at the end of expiration using a weighted measuring tape (Pull Type Spring Scale; Ohaus, Parsippany, NJ, USA) set at 750g. Weight, height, and waist circumference were each measured three times and the average was utilized. Body composition (Body Fat (%), Fat Mass (kg), Lean Mass (kg)) was assessed using a dual-energy x-ray absorptiometry (DXA) scanner (Lunar Prodigy Advance 8743; GE Healthcare, Waukesha, WI, USA). All scans were reviewed by one individual (KMM) to ensure the consistency of the regions of interest (ROIs).

Metabolic health: Blood samples were collected at baseline (fasting) and 2-hours after the consumption of the glucose drink. In the Clinical Laboratory at Hamilton Health Sciences (Hamilton, ON, Canada), fasting total cholesterol, high-density lipoprotein (HDL) cholesterol, triglycerides were measured using Architect C16 (Abbott) on serum samples and low-density lipoprotein (LDL) cholesterol was calculated using the Friedewald equation²⁸⁷. Fasting and 2-hour plasma glucose were measured using Architect C4000 or c4100 (Abbott, Chicago, IL, USA) on heparinized plasma samples. Serum fasting insulin levels were measured using the Immunometric

(non-competitive) methodology on the Ortho Vitros XT7600 Microwell (Rochester, NY). Homeostatic model assessment of insulin resistance (HOMA-IR) was calculated as fasting insulin (mU/L) times fasting glucose (mmol/L) divided by 22.5. Quantitative insulin sensitivity check index (QUICKI) was calculated as 1 divided by the sum of log fasting insulin (mU/L) and log fasting glucose (mg/dl). HOMA-IR and QUICKI are presented herein as surrogate measures for insulin sensitivity³¹⁸.

SUPPLEMENTARY MATERIAL 2

Imaging visit

Skin temperature measurement:

Upon arrival, participants wearing a standardized cotton tank top and shorts, and were acclimated to room temperature for 30 minutes. The temperature in the room was recorded (Wireless Forecast Station with Pressure History Model WS-9037U-IT; La Crosse Technology, La Crosse, WI, USA). During this temperature acclimation, the participants were instructed on the use of a 9-point thermal sensation scale based on the International Organization for Standardization 10551³¹⁹ and a 4-point thermal comfort scale (Modified from Fanger et al, 1972). After the baseline MRI scans, 15 autonomous temperature sensors (Thermochron iButtons DS1922L; Maxim Integrated, San Jose, CA, USA)³²⁰ were placed over the abdomen, biceps, cheek, chest, foot, forearm, forehead, front and back of the lower leg, hamstring, hand, occiput, quadriceps, and the upper and lower back, on the left side of the participants' body to calculate the arithmetic mean skin temperature³²¹. Skin temperature was monitored continuously during the experimental protocol. The change in skin temperature was calculated: $\Delta T_{\text{skin}} = \text{post-cold } T_{\text{skin}} (\text{mean of last 10 minutes}) - \text{pre-cold } T_{\text{skin}} (\text{mean of 10 minutes before the start of cold exposure})$.

The outlet-inlet temperature of the cooling suit:

Afferent (entering) and efferent (exiting) water temperature were recorded during the cold exposure at 15-second intervals with a dynamic range of 16 bit using a data logger (PowerLab; ADInstruments, Sydney, Australia) connected to thermocouples (TMQSS-020G-2; OMEGA Engineering, Stamford, CT, USA) fixed to the inlet and outlet manifolds. The difference between the efferent and afferent temperatures (ΔT) was calculated from data collected during the last 10 minutes of the cold exposure.

Shivering activity:

To estimate shivering during the cold exposure, surface electrodes were placed on the trapezius, vastus lateralis, and vastus medialis muscles. EMG signals were recorded at baseline and continuously during cold exposure using surface EMG (Trigno Wireless System, Delsys, MA, USA with Trigno Snap-Lead Sensor connected to pre-jelled Norotrode 20 Bipolar SEMG electrodes, Myotronic, WA, USA). Voluntary muscle activity was minimized as much as possible throughout the cold exposure by asking participants to avoid voluntary movements during the recording periods.

Raw EMG signals were collected at a sampling rate of 2148 Hz, filtered to remove spectral components below 20 Hz and above 500 Hz as well as 60 Hz contamination and related harmonics, and analyzed using custom-designed MATLAB algorithms (Mathworks, Natick, MA, USA). The shivering intensity of individual muscles was determined from root-mean-square (RMS) values calculated from raw EMG signals using a 50 ms overlapping window (50%). In brief, baseline RMS values (RMS_{baseline}: 15 min RMS average measured before cold exposure) were subtracted from shivering RMS (RMS_{shiv}) values.

MRI outcomes:

Cold-stimulated change in SCV PDFF (BAT activity): SCV measurements of PDFF were acquired using the **I**terative **D**ecomposition of water and fat with **E**cho **A**symmetry and **L**east-squares estimation (IDEAL-IQ) pulse sequence. IDEAL-IQ is a confounder-corrected 3D gradient multi-echo MRI sequence that provides an accurate measure of tissue triglyceride content by using multiple spectral modeling of adipose tissues while accounting for T2* decay¹⁷⁴. This pulse sequence generates six distinct image contrasts: water-only, fat-only, in-phase, out-of-phase, corrected proton density fat fraction (PDFF), and R2* images. Using a Head/Neck/Spine (HNS) coil, with an additional attachment that provided signal from the anterior portion of the chest, axial images were taken from the C2/C3 disc to the T4/T5 disc (IDEAL-IQ, slice thickness 3mm, 50 slices, flip angle 4°, TE 1.3ms, TR 8.4ms, FOV 340 mm, image resolution 1.52 x 1.42 x 3mm, acceleration factor 2, scan time = 2.4 min).

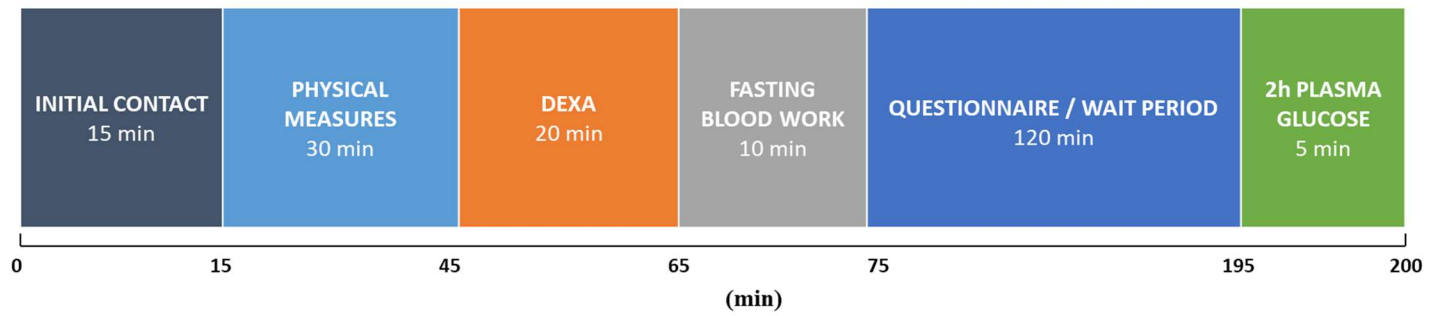
Abdominal fat: Hepatic fat was measured from pre-cold axial scans obtained in a single breath-hold using a 32-channel torso array coil (NeoCoil, Pewaukee, WI, USA) from 7cm above to 7cm below the L4-L5 disc (IDEAL-IQ, slice thickness 8mm, 32 slices, flip angle 3°, TE 1.0ms, TR 6.5ms, FOV 340 mm, image resolution 2.13 x 1.86 x 8 mm, acceleration factor 2 x 2, scan time = 14 sec). In the post-imaging analysis, a multi-slice segmentation that included the entire liver was undertaken to measure PDFF% ($\frac{Fat}{Water+Fat} * 100$). ROIs were drawn over the entire liver using a tool that “snaps” to the edges of regions where changes in voxel intensities are high. The in-phase image was used as a reference when the boundaries of the liver were not clearly defined in the fat-fraction image. The ROIs were then post-processed using a 2D erosion (3x3 voxels) to correct for partial volume effects. All voxels that satisfy the above criteria were averaged and classified as hepatic fat. Abdominal subcutaneous adipose tissue (SAT) PDFF was calculated from a single

slice at the level of the umbilicus obtained in a single breath-hold scan (IDEAL-IQ, Slice thickness 5mm, 32 slices, flip angle 3°, TE 6.3ms, TR 1.0ms, FOV 360 mm, image resolution 2.25 x 1.97 x 5mm, acceleration factor 2 x 2, scan time = 14 sec). A manual tracing tool was used to segment abdominal SAT. Voxels with low PDFF values (below 30%) were excluded to isolate adipose tissues from muscle. A 2D erosion (3x3 voxels) was applied to attenuate partial volume effects. All voxels that satisfied the above criteria were averaged and classified as SAT PDFF.

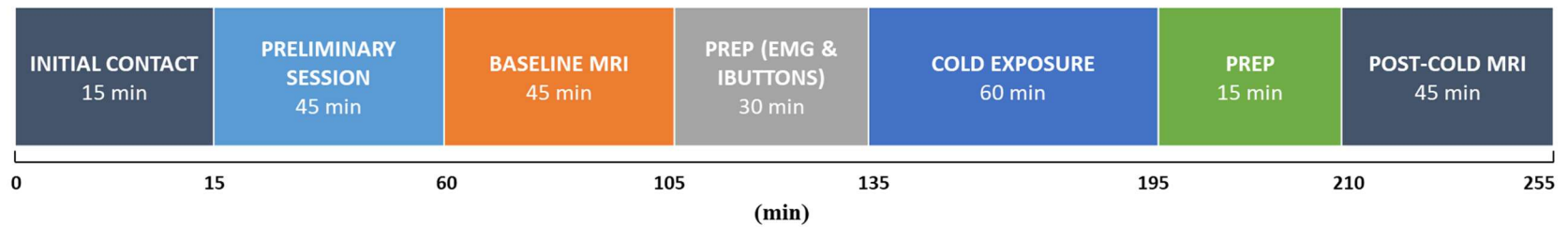
Visceral adipose tissue (VAT) area was measured from a single slice located at the level of the umbilicus³²² obtained from a single breath-hold LAVA-FLEX scan (LAVA-FLEX, slice thickness 5mm, 32 slices, flip angle 3°, TE 1.3ms, TR 4.2ms, FOV 360mm, spatial resolution 1.13 x 1.29 x 5mm, acceleration factor 1.5, scan time = 12 sec). A fat mask was applied to exclude non-adipose tissues from analysis while SAT and VAT were separated semi-automatically based on seed points. Manual tracing was used to include parts that may have been missed from the seeding. Retroperitoneal adipose tissue was excluded manually from VAT. Finally, the ROIs were post-processed using 2D erosion (3x3 voxels) to attenuate partial volume effects. LAVA-FLEX is a 3D gradient dual-echo MRI sequence that generates four distinct image contrasts: water-only, fat-only, in-phase, and out-of-phase. It provides a higher resolution image than IDEAL-IQ with sharper tissue boundaries.

SUPPLEMENTARY FIGURE 1: Timeline for the study visits

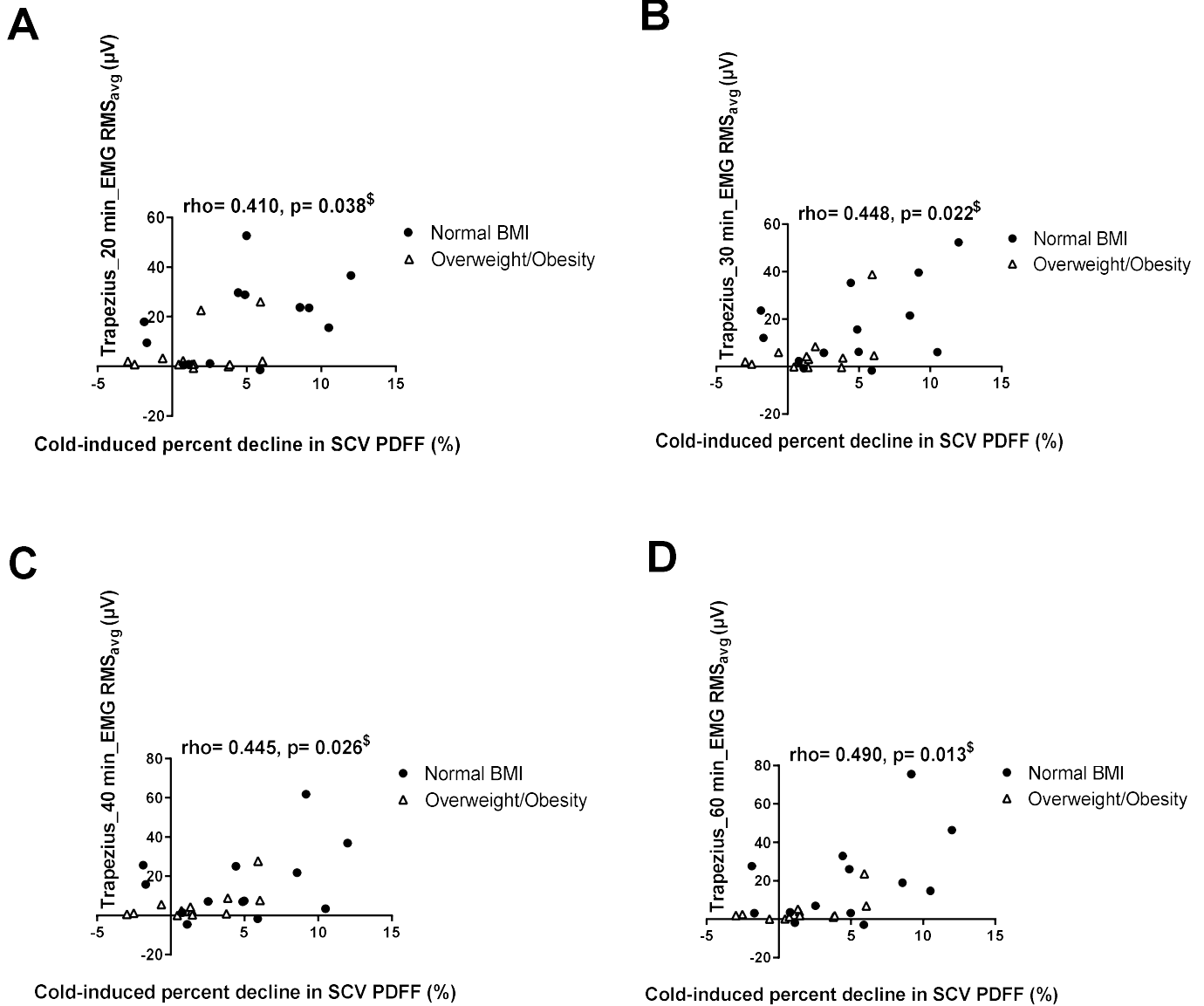
ANTHROPOMETRIC/ METABOLIC STUDY VISIT



IMAGING STUDY VISIT

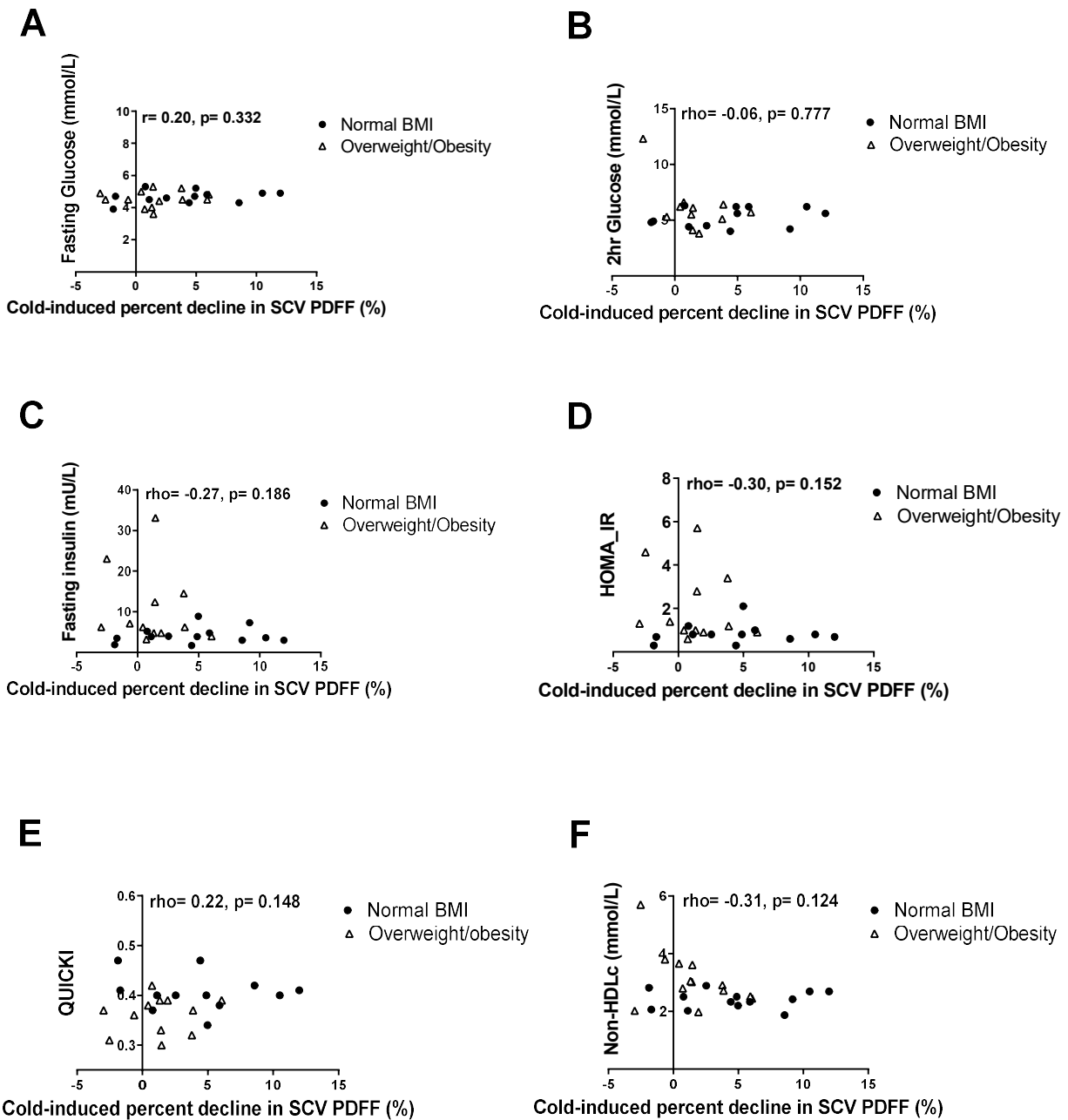


SUPPLEMENTARY FIGURE 2: Relationship of the cold-induced percent decline in SCV PDFF and shivering in the trapezius muscle.



The relationship between cold-induced percent decline in SCV PDFF and shivering signal in the trapezius muscle at 20 minutes of cold exposure (**A**), 30 minutes of cold exposure (**B**), 40 minutes of cold exposure (**C**), and 60 minutes of cold exposure (**D**) in boys with normal BMI (black circles) and with overweight/obesity (white cones). \$ - p < 0.05 via Spearman's Correlation. SCV PDFF; supraclavicular proton density fat fraction, EMG RMS_{avg}; electromyogram root-mean-square average.

SUPPLEMENTARY FIGURE 3: Relationship of the cold-induced percent decline in SCV PDFF and circulating metabolic measures



The relationship between cold-induced percent decline in SCV PDFF and fasting plasma glucose (A), two hours post-prandial plasma glucose (B), and fasting insulin (C), HOMA-IR (D), QUICKI (E), and non-HDLc (F) in boys with normal BMI (black circles) and with overweight/obesity (white cones). r - via Pearson's Correlation; ρ - via Spearman's Correlation. SCV PDFF; supraclavicular proton density fat fraction. HOMA-IR; homeostatic model assessment of insulin resistance, QUICKI; quantitative insulin-sensitivity check index, Non-HDL-C; non-high-density lipoprotein cholesterol.

SUPPLEMENTARY TABLE 1: Temperature and shivering measurements

	All (n=26)	Normal BMI (n=13)	Overweight/obesity (n= 13)	p
Outdoor temperature 1h before visit 2 (°C)	11.8 (1.7)	13.7 (2.5)	9.9 (2.2)	0.310
Δ outlet-inlet of the suit (°C)	1.6 (0.1)	1.5 (0.1)	1.7 (0.1)	0.362
Delta changes in skin temperature (°C)	-3.2 (0.1)	-3.3 (0.1)	-3.2 (0.1)	0.333
Trapezius shivering activity at the end of cold exposure (μ V).	3.6 [1.5, 21.3]	14.7 [3.2, 30.2]	1.9 [1.1, 1.9]	0.035†
Vastus medialis shivering activity at the end of cold exposure (μ V).	1.2 [0.24, 4.1]	2.6 [0.94, 8.3]	0.6 [0.07, 2.6]	0.052
Vastus lateralis shivering activity at the end of cold exposure (μ V).	1.6 [0.11, 4.7]	6.9 (2.4)	1.01 (0.5)	0.034*

Values are presented as mean (SEM) for normally distributed variables or median [IQ1, IQ3] for non-normally distributed variables. * - $p < 0.05$ via independent sample t-test; † - $p < 0.05$ via Mann-Whitney U test.

SUPPLEMENTARY TABLE 2: Regression analysis for the prediction of adiposity parameters by cold-induced percent decline in SCV PDFF (%).

	Coefficients						Model		
	N	B	SE	β	95% CI		R ²	R ² Adj	p
					Lower Bound	Upper Bound			
Waist circumference (cm)							0.246	0.178	0.045*
Trapezius shivering activity		-0.144	0.210	-0.155	-0.580	0.292			
Cold-induced percent decline in SCV PDFF (%)	25 ^a	-1.637	0.946	-0.391	-3.600	0.325			
VAT (cm)²							0.221	0.150	0.064
Trapezius shivering activity		-0.147	0.193	-0.175	-0.548	0.254			
Cold-induced percent decline in SCV PDFF (%)	25 ^a	-1.316	0.869	-0.348	-3.119	0.487			
BMI (kg/m²)							0.207	0.135	0.078
Trapezius shivering activity		-0.086	0.071	-0.279	-0.233	0.062			
Cold-induced percent decline in SCV PDFF (%)	25 ^a	-0.323	0.320	-0.234	-0.986	0.340			

^a One participant did not have a measurement for the trapezius shivering at 60 minutes (had 38 minutes of cold exposure). * P < 0.05. VAT; visceral adipose tissue area, BMI; body mass index.

CHAPTER FOUR

Boys with obesity have low concentrations of 5-hydroxyindole acetic acid (5-HIAA) in the urine.

Basma A. Ahmed, Nina Varah, Frank J. Ong, Elizabeth Gunn, Julian M. Yabut, Denis P. Blondin, Norman B. Konyer, Nina P. Singh, Michael D. Noseworthy, Francois Haman, Andre C. Carpentier, Zubin Punthakee, Gregory R. Steinberg*, Katherine M. Morrison*

*These authors contributed equally to the work

Prepared for publication as a short report.

4.1 Preface and significance to the thesis

In chapter three, we show that young boys with overweight/obesity have a lower cold-stimulated BAT activity compared to boys with normal BMI. However, little is known about potential regulatory factors that could contribute to this finding. In rodents, increases in peripheral serotonin reduce BAT thermogenic function²¹¹, but whether this is important in children is not known. In this chapter, we demonstrate that circulating serotonin (PPP-serotonin and 5-HIAA/creatinine in the urine) is not related to cold-stimulated BAT activity in young boys. However, young boys with overweight/obesity have lower levels of urinary 5-HIAA/creatinine. Both measures of circulating serotonin are negatively related to BMI Z-score and total body fat. 5-HIAA/creatinine, but not PPP-serotonin, correlates negatively to hepatic fat, and VAT. These results show that, contrary to preclinical studies, circulating serotonin does not seem to be linked to cold-stimulated BAT activity in young boys.

4.2 Author contribution

B.A.A. was the primary contributor to all the figures and tables in this manuscript. B.A.A. wrote the manuscript with G.R.S. and K.M.M. Other contributions are listed below:

B.A.A., G.R.S., and K.M.M. conceptualized the study. B.A.A, N.V., F.J.O., J.M.Y, and E.G., conducted the experiments. F.J.O., D.P.B., N.B.K., N.P.S., M.D.N., F.H., A.C.C., Z.P., G.R.S., and K.M.M contributed to the methodology. B.A.A. ran the formal Analysis. N.B.K., M.D.N., F.H., A.C.C., G.R.S., and K.M.M provided resources. All the authors edited the final version of the manuscript.

Boys with obesity have low concentrations of 5-hydroxyindole acetic acid (5-HIAA) in the urine.

Basma A. Ahmed^{1,2}, Nina Varah^{1,3}, Frank J. Ong^{1,3}, Elizabeth Gunn^{1,3}, Julian M. Yabut^{1,4}, Denis P. Blondin⁵, Norman B. Konyer⁶, Nina P. Singh⁷, Michael D. Noseworthy^{1,6,7,8,9}, Francois Haman¹⁰, Andre C. Carpentier¹¹, Zubin Punthakee^{1,3,4}, Gregory R. Steinberg^{1,2,4*}, Katherine M. Morrison^{1,3*†}

Affiliations

- 1- *Centre for Metabolism, Obesity and Diabetes Research, McMaster University, Hamilton, ON, Canada*
- 2- *Department of Biochemistry and Biomedical Sciences, McMaster University, Hamilton, ON, Canada*
- 3- *Department of Pediatrics, McMaster University, Hamilton, ON, Canada*
- 4- *Division of Endocrinology and Metabolism, Department of Medicine, McMaster University, Hamilton, ON, Canada*
- 5- *Faculty of Medicine and Health Sciences, Department of Medicine, Division of Neurology, Centre de recherche du CHUS, Université de Sherbrooke, Sherbrooke, QC, Canada*
- 6- *Imaging Research Centre, St. Joseph's Healthcare, Hamilton, ON, Canada*
- 7- *Department of Radiology, McMaster University, Hamilton, ON, Canada*
- 8- *Department of Electrical and Computer Engineering, McMaster University, Hamilton, ON, Canada*
- 9- *School of Biomedical Engineering, McMaster University, Hamilton, ON, Canada*
- 10- *Faculty of Health Sciences, University of Ottawa, Ottawa, ON, Canada*
- 11- *Division of Endocrinology, Department of Medicine, Centre de recherche du CHUS, Université de Sherbrooke, Sherbrooke, QC, Canada*

* These authors made comparable contributions.

† Lead Contact

Correspondence to:

Dr. Gregory R. Steinberg - gsteinberg@mcmaster.ca

Dr. Katherine M. Morrison[†] - kmorrison@mcmaster.ca

Disclosure summary

B.A.A. holds the Lau family scholarship for science and engineering and was funded by the Ontario graduate scholarship.

N.V. holds the Canadian Institutes of Health Research Graduate Scholarship and was funded by the Ontario Graduate Scholarship.

D.P.B. holds the GSK Chair in Diabetes of the Université de Sherbrooke that has been created in part through a donation of \$1 million by GSK to the Université de Sherbrooke. D.P.B. has received honoraria/consulting fees from Boehringer Ingelheim.

A.C.C. holds the Canada Research Chair in Molecular Imaging of Diabetes and research funding from the Canadian Institutes of Health Research, Fonds de recherche Québec – Santé, and has participated in advisory boards for the companies Amgen, UniQure, Merck, Janssen, NovoNordisk, Novartis, HLS Therapeutics Inc., TVM Life Science Management, AstraZeneca, and Eli Lilly and made one conference sponsored by AstraZeneca.

Z.P. has received honoraria for advice and speaking from Abbott, Astra Zeneca/Bristol Myers Squibb, Boehringer Ingelheim/Eli Lilly, Janssen, Merck, NovoNordisk, Pfizer, and Sanofi. He has received research funds from Amgen, Astra Zeneca/Bristol Myers Squibb, Lexicon, Merck, NovoNordisk, Sanofi, and the Canadian Institutes of Health Research.

G.R.S. receives funding from the Canadian Institutes of Health Research (201709FDN-CEBA-116200 to GS), Diabetes Canada Investigator Award (DI-5-17-5302-GS)- a Tier 1 Canada Research Chair and the J Bruce Duncan Endowed Chair in Metabolic Diseases. He also receives research funding from Espervita Therapeutics, Esperion Therapeutics, Poxel Pharma, and Novo Nordisk and honoraria/consulting fees from Eli-Lilly, Esperion Therapeutics, Poxel, and Merck.

K.M.M. holds research funding from the Canadian Institutes of Health Research, Heart and Stroke Foundation of Canada, McMaster Children's Hospital Foundation, and McMaster University. She has received research funds from Astra Zeneca and is an advisory board member for Novo Nordisk and Akcea Therapeutics, Canada.

Abstract

Circulating serotonin inhibits brown adipose tissue (BAT) and increases adiposity in mice. It is uncertain if circulating serotonin impairs BAT and increases adiposity in children. We measured serotonin in platelet-poor plasma (PPP) and the ratio of its metabolite, 5-hydroxyindole acetic acid (5-HIAA), to creatinine (Crt) in the first-morning urine of boys (aged 8-10 years). We investigated if these measures were a) related to cold-induced BAT activity (assessed via MRI), b) related to adiposity, and c) different in boys with overweight/obesity compared to control. 5-HIAA/Crt, not PPP-serotonin, was lower in boys with overweight/obesity compared to boys with normal BMI. 5-HIAA/Crt and PPP-serotonin were inversely correlated with BMI Z-score and percent body fat. 5-HIAA/Crt, not PPP-serotonin, was inversely related to visceral adipose tissue ($\rho = -0.44$, $p = 0.021$) and hepatic fat ($\rho = -0.55$, $p = 0.003$). Neither of the serotonin measures was related to BAT activity. These data indicate that lower circulating serotonin is associated with greater adiposity suggesting a potential role in childhood obesity.

Keywords:

Childhood obesity, serotonin, 5-hydroxyindole acetic acid, brown adipose tissue, hepatic fat

Introduction

The high prevalence of obesity in childhood is of global concern given the link to adverse influence on physical and mental health³⁰⁹. These concerns are exacerbated by challenges in identifying sustainable, efficacious treatment modalities.

Brown adipose tissue (BAT), is a thermogenic organ present mostly in the supraclavicular (SCV) region of the neck in children²⁰⁸, adolescents²⁰⁷, and adults²⁵⁵. BAT contributes to energy expenditure through its heat production ability via uncoupling mitochondrial oxidative

phosphorylation²⁵³ and other futile cycles³¹⁰. Cold-stimulated BAT activity is inversely related to adiposity and diabetes in adults^{67,123} and children⁸⁴, and hepatic fat^{195,208}. However, factors that modulate BAT activity, and potentially impact hepatic fat accumulation are not well understood.

In rodents, a key hormone inhibiting the metabolic activity of BAT is serotonin. Circulating serotonin is a monoamine secreted mainly by gut enterochromaffin cells by the enzyme tryptophan hydroxylase 1 (*Tph1*)³²³. After its release, most of the serotonin is taken up and stored in the platelets but approximately 2% remains unbound and can be measured in platelet-poor plasma (PPP)²²⁸. 5-hydroxyindole acetic acid (5-HIAA) is the major metabolic end-product of serotonin and is excreted in the urine³²⁴. In mice, inhibiting *Tph1* leads to increases in BAT activity and protection from diet-induced obesity, fatty liver, and insulin resistance²¹¹. Consistent with these findings, plasma serotonin was higher in adults with obesity compared to controls and was directly related to body mass index (BMI) and HbA1c²³³. Whether PPP-serotonin and/or 5-HIAA are related to BAT activity in humans and how this relationship impacts adiposity is still not known.

We hypothesized that PPP-serotonin and urinary 5-HIAA (will be referred to together as circulating serotonin) would be negatively correlated with BAT activity in children. Accordingly, we further hypothesized that PPP-serotonin and urinary 5-HIAA would be directly related to adiposity and liver fat in children.

Methodology

This study involved healthy boys (8 -10 years), who were recruited for the pediatric GETBAT cohort; an observational, cross-sectional study. Consents and assents were obtained from the guardians and the children, respectively. The study was approved by the Hamilton Integrated Research Ethics Board (HiREB, Project 0575). The boys were instructed to avoid serotonin-rich

foods (e.g., banana, tomato, kiwi, walnut, avocado, pineapple, and plum) for 24 hours before visits 1 and 2 (metabolic and imaging visits, respectively). Exclusion criteria included any conditions or medications that impact BAT, serotonin, or hepatic fat. Both visits occurred after an overnight fast.

Body composition (assessed via dual-energy x-ray) and anthropometry were evaluated during visit 1 at the McMaster University Medical Centre, Canada as previously described²⁵⁵. BMI was calculated from height and weight (weight (kg)/height² (m)), and BMI Z-score was calculated utilizing the World Health Organization anthropometric calculator. Participants were classified with normal BMI if BMI Z-score < 1 or with overweight/obesity if BMI Z-score ≥ 1.

5-HIAA was measured in the first-morning urine samples^{325,326}. These samples were collected in sterile plastic containers on the morning of both study visits. Samples were kept at 4°C and were sent on the collection day to the Core Laboratory at Hamilton Health Sciences (HHS). 5-HIAA and creatinine (Crt) were measured by high-performance liquid chromatography (HPLC) on a C18 column with electrochemical detection. 5-HIAA/Crt ratio was calculated and used in the analysis to control for variations in urine concentration³²⁷.

Fasting blood samples were collected during visit 1 for PPP extraction in BD Medical vacutainers containing 7.2mg K₂EDTA then were centrifuged (4000 xg for 10 minutes) at room temperature. 200ul of the top ¾ of the supernatant was transferred to 0.5 ml microtubes without disruption of the white blood cell layer and were kept frozen at -80°C. Platelet count was evaluated in 300ul of the supernatant by the Core Laboratory at HHS to ensure the absence of platelet contamination. These samples were used for serotonin measurement using undiluted PPP (in duplicate) via an ELISA kit as per the manufacturer's instructions (Serotonin EIA kit Beckman Coulter; IM1749).

The imaging visit took place at the Imaging Research Centre (IRC), St. Josephs Healthcare Hamilton (SJHH). MRI scans were conducted for the SCV region, liver, and abdomen before and after one hour of standardized cold exposure at 18°C²⁵⁵ using a high-density liquid conditioned suit (LCG; Two Pieces with zippers and open access neck, Med-Eng, Ottawa, ON, Canada). MRI acquisition and analysis, to evaluate proton density fat fraction (PDFF), were done similar to our published protocol²⁵⁵ with the following IDEAL-IQ parameters for SCV region and liver: slice thickness 3mm and 8mm; 50 and 32 slices; flip angle 4° and 3°; TE 1.3ms, TR 8.4ms and 1.0ms; FOV 340 and 340 mm; image resolution 1.52 x 1.42 x 3mm and 2.13 x 1.86 x 8 mm; acceleration factor 2 and 2 x 2; scan time = 2.4 min and 14 sec respectively. VAT area was retrieved from a slice at the level of the umbilicus at a single breath-hold LAVA-FLEX scan (LAVA-FLEX, slice thickness 5mm, 32 slices, flip angle 3°, TE 1.3ms, TR 4.2ms, FOV 360mm, spatial resolution 1.13 x 1.29 x 5mm, acceleration factor 1.5, scan time = 12 sec). A fat mask was applied to exclude non-adipose tissues while SAT and VAT were separated semi-automatically based on seed points. Regions of interest were post-processed using 2D erosion (3x3 voxels). BAT activity is reported as the percent change in SCV PDFF from pre-cold SCV PDFF.

Statistical Analyses

SPSS Statistics (version 27; IBM, North Castle, NY, USA) and GraphPad Prism (version 6; GraphPad Software, La Jolla, CA, USA) were used for statistical analysis and graphing, respectively. Normality was assessed via the procedures outlined by Tabachnick and Fidell³⁰¹. Data are presented as mean (SEM) for normally distributed and as median [Q1, Q3] for skewed variables. Assuming the independence of the observations, independent Samples t-test and Mann-Whitney U test were used to assess the differences in the means of normally distributed continuous variables and the differences in the mean rank of skewed continuous variables, respectively,

between boys with and without overweight/obesity (categorical variable) and results of Levene's test for equality in variances between groups were considered to assess the p-value of independent Samples t-test for equality in the mean. Pearson and Spearman's correlations were used for assessing the relationships between normally distributed and skewed variables, respectively. A two-tailed p-value of less than 0.05 was considered significant.

Results

Participant demographics

The pediatric GETBAT cohort included thirty-five boys: 16 control and 19 with overweight/obesity. Of these, 26 (13 control and 13 with overweight/obesity), matched for age, had pre and post SCV MRI scans for evaluation of BAT activity. Body composition and MRI variables are included in Table 1.

Urinary 5-HIAA

Of the 35 boys, 32 had a urine sample available from both study visits. Boys with overweight/obesity had lower 5-HIAA/Crt compared to controls (mean difference = 0.49 $\mu\text{mol}/\text{mmol}$, $p= 0.003$) (**Figure 1A**). The percent coefficient of variation (CV) was calculated to assess the variability in 5-HIAA/Crt levels between visits and was 12.2% so, the average value of 5-HIAA/Crt from both visits was used in subsequent analyses. The mean 5-HIAA/Crt was 2.5 ± 0.1 $\mu\text{mol}/\text{mmol}$, consistent with previously reported levels in children (aged 4-18 years)³²⁶.

Serotonin levels in platelet-poor plasma

After excluding one sample with high platelets, the platelet count in all PPP samples was $\leq 1 \times 10^9/L$, confirming the absence of platelet contamination²²⁸. In addition to this one sample, serotonin level was also not measured in samples from three participants (signs of hemolysis, n= 1 and not enough sample to run ELISA, n= 2). In the remaining 31 samples, PPP-serotonin was 12.0 ± 1.9 nmol/L. PPP-serotonin was directly related to 5-HIAA/Crt ($r = 0.41$, $p = 0.022$). There was no difference in PPP-serotonin levels between boys with overweight/obesity and controls, $p = 0.213$ (**Figure 1B**).

Peripheral serotonin, adiposity, and brown adipose tissue activity

Urine 5-HIAA/Crt was negatively related to BMI ($\rho = -0.56$, $p < 0.001$), BMI Z-score ($r = -0.56$, $p < 0.001$) (**Figure 1C**), and total body fat ($r = -0.53$, $p = 0.001$) (**Figure 1D**). PPP-serotonin was negatively related to BMI Z-score ($r = -0.41$, $p = 0.023$) and total body fat ($r = -0.39$, $p = 0.030$). 5-HIAA/Crt was negatively related to waist circumference ($r = -0.45$, $p = 0.007$), VAT ($\rho = -0.44$, $p = 0.021$) (**Figure 1E**) and hepatic fat ($\rho = -0.55$, $p = 0.003$) (**Figure 1F**), but PPP-serotonin was not. Percent change in SCV PDFF was not related to 5-HIAA/Crt; $r = -0.027$, $p = 0.896$ ($n = 26$) or PPP-serotonin; $r = 0.048$, $p = 0.827$ ($n = 23$).

Discussion

To the best of our knowledge, this is the first study to investigate the relationships between peripheral serotonin, adiposity, and BAT activity in a pediatric population. Boys with overweight/obesity had lower levels of urinary 5-HIAA/Crt compared to boys with normal BMI but both groups did not differ in PPP-serotonin. Inverse associations between measures of

adiposity and both PPP-serotonin and its metabolite in urine (5-HIAA) were identified. Contrary to our hypothesis, we did not find an association between circulating serotonin and BAT activity. Reduced activity of adipose tissue Monoamine oxidases (MAOs), the enzymes that regulate the catabolism of serotonin to form 5-HIAA, was reported in obese human adults and may explain the lower levels of urinary 5-HIAA/Crt in boys with overweight/obesity compared without³²⁸. Our finding of a negative association between circulating serotonin and adiposity is consistent with previous findings of a negative relationship between plasma serotonin and BMI in children with obesity²³⁹. Consistent with this, serum and whole blood serotonin levels were inversely related to BMI and total body fat in human adults^{237,238}. Women with morbid obesity had lower serum serotonin compared to those with normal weight³²⁹. Conversely, other studies showed that plasma serotonin was higher in adults with obesity compared to controls and was directly related to BMI and HbA1c²³³. Similarly, plasma 5-HIAA was positively related to plasma triglycerides and waist circumference in adults with metabolic syndrome²³⁶. The discrepancies between previously mentioned reports may have been attributed to methodological differences i.e., avoidance of serotonergic food and medications before sample collection, the fraction of blood in which serotonin and/or its metabolites were measured, and the used analytical methods. Additionally, pubertal status influences circulating serotonin in the context of other disorders like autism³³⁰ however the puberty impact on circulating serotonin in the context of obesity is yet to be explored. It was reported that adolescents with diabetes and obesity had lower urinary 5-HIAA compared to controls²⁴⁰.

We did not find an association between circulating serotonin and BAT activity in this cohort. Studies have shown that human BAT is most closely related to rodent beige/brite adipose tissue (AT) than it is to rodent classical BAT. Initial studies showed that inhibiting Tph1 in all tissues

leads to increased metabolic activity of both BAT and beige AT, however, the key contributing tissues/cell types were not delineated²¹¹. White AT (WAT) derived synthesis of serotonin, rather than gut-derived serotonin synthesis was critical for inhibiting the browning of white fat³³¹. Recently, it was indicated that with obesity, WAT is infiltrated with mast cells that are enriched in Tph1 and that this local production of serotonin is critical for inhibiting the metabolic activity of beige AT in obesity³³². Thus, local production of serotonin may also be more important than circulating serotonin in BAT, future studies involving AT biopsies will be required to test this effect.

We found herein a negative association between circulating serotonin and adiposity in young boys with no relation to BAT activity, further studies are needed to investigate the same relationship in a larger and more diverse pediatric population, in adolescents and adults.

Acknowledgment: We would like to thank the Boris Family and the Canadian Institutes of Health Research (grant number 144625-1), brave participants and their families, the staff members of the core laboratory at HHS, the MRI technologists at the IRC, Prasiddha Parthasarathy and Emily Hutchings for their contributions in the data collecting, Dr. Andrew McArthur's laboratory, and the McMaster Service Laboratory and Repository for the computer server support.

Table 1: Participant characteristics and study variables.

	All (n=35)	Normal BMI (n=16)	overweight/obesity (n= 19)	p
Age (years)	9.6 (0.2)	9.9 (0.2)	9.4 (0.3)	0.092
Weight (kg)	35 [30, 46.9]	29.9 (0.8)	49.7 (3.5)	<0.001*
Height (cm)	140.4 (1.2)	138.6 (1.4)	141.8 (1.7)	0.172
Waist Circumference (cm)	69.4 (2.8)	57.5 (1.3)	79.5 (3.6)	<0.001*
BMI (kg/m ²)	19 [15.7, 23]	15.5 (0.3)	24.3 (1.3)	<0.001*
BMI Z-score	1.3 (0.3)	-0.6 (0.2)	2.8 (0.3)	<0.001*
Body Fat (%)	28.2 (2.2)	16.7 (1.2)	37.9 (2.2)	<0.001*
Urine creatinine (mmol/L)	10.3 (0.5)	9.8 (0.7)	10.6 (0.8)	0.507
Pre-cold SCV PDFF (%) ^a	64.7 (2.1)	56.1 (1.4)	73.3 (2.1)	<0.001*
Post-cold SCV PDFF (%) ^{a, b}	62.7 (2.2)	53.9 (1.3)	71.6 (2.4)	<0.001*
Cold-induced percent decline in SCV PDFF (%) ^{a, b}	3.2 (0.8)	4.7 (1.2)	1.6 (0.8)	0.044*
Hepatic fat (%) ^{a, c}	3.2 [2.8, 4.6]	3.0 [2.5, 3.2]	4.6 [3.5, 8.7]	<0.001†
VAT (cm) ^{2 a, d}	6.6 [4.2, 17.8]	4.9 (0.6)	24.3 (4.5)	0.001*

Values are presented as mean (standard errors of the mean) for normally distributed variables or median [IQ1, IQ3] for skewed variables.

* - p < 0.05 via independent sample t-test; † - p < 0.05 via Mann-Whitney U test.

^a No pre-cold MRI scans for seven participants (Withdrawal after the metabolic visit, n=2 and incomplete imaging visit, n=5).

^b No post-cold MRI scans for two participants (symptoms of claustrophobia)

^c No liver MRI measurements for two participants (symptoms of claustrophobia, n= 1 and motion artifacts, n=1)

^d No abdominal MRI scans for one participant (symptoms of claustrophobia, n= 1)

BMI; body mass index, SCV PDFF; supraclavicular proton density fat fraction, VAT; visceral adipose tissue.

Figure 1

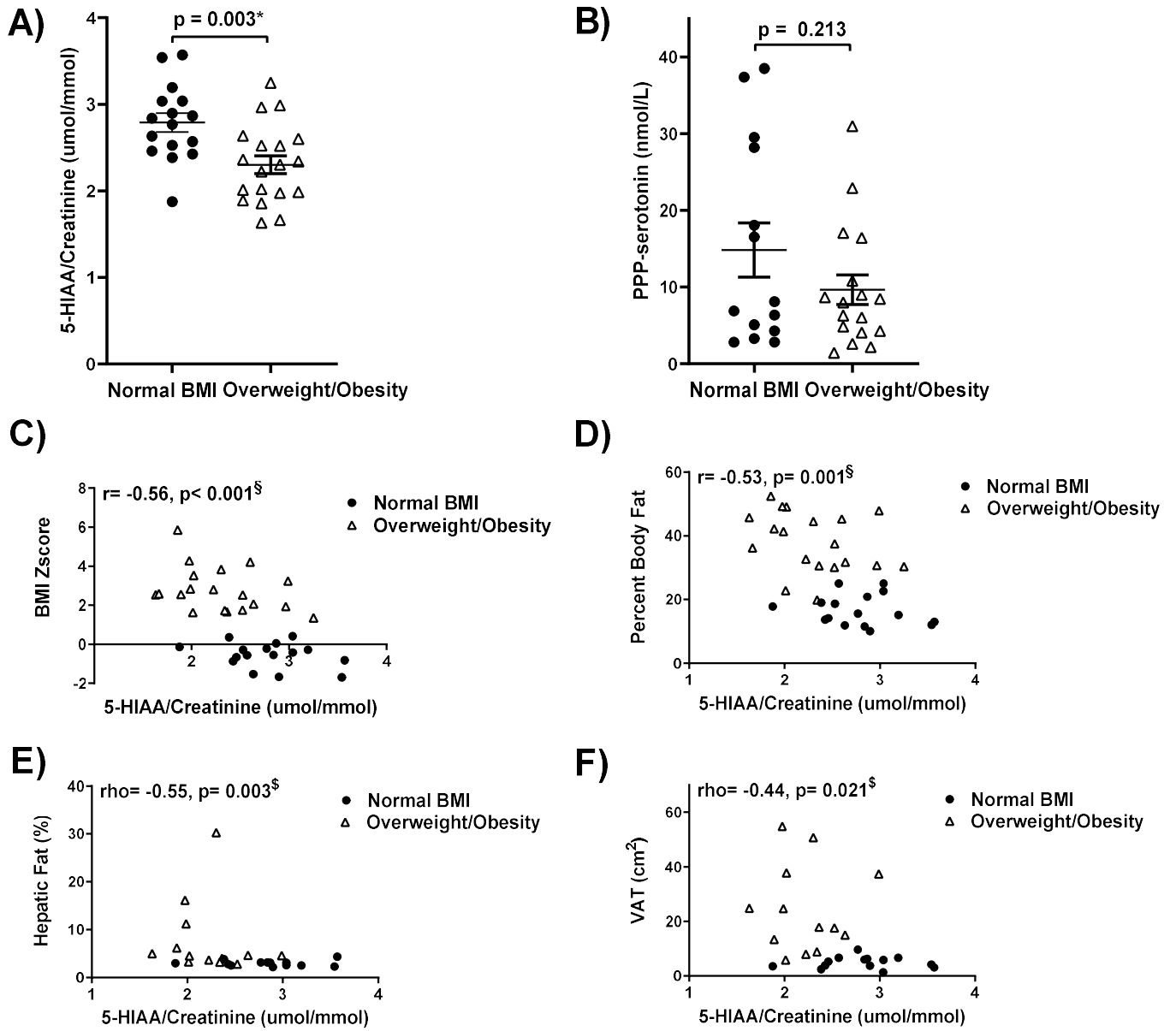


Figure 1: Urine 5-HIAA and PPP-serotonin between obesity groups and in relation to adiposity

Urine 5-HIAA/creatinine (**A**) and serotonin levels in PPP (**B**) between boys with normal BMI (black circles, n=16) and with overweight/obesity (white cones, n=19). Data are presented as the mean \pm standard errors of the mean.

The association of urine 5-HIAA/creatinine levels and BMI Z-score (**C**), total body fat (**D**), liver fat (**E**), and visceral adipose tissue area (**F**) in boys with normal BMI (black circles, n = 16) and with overweight/obesity (white cones, n= 19). * - $p < 0.05$ via Paired Student's t-test. § - $p < 0.05$ via Pearson's correlation. § - $p < 0.05$ via Spearman's correlation. 5-HIAA; 5-hydroxyindole acetic acid, PPP; platelet-poor plasma, VAT; visceral adipose tissue.

CHAPTER FIVE

DISCUSSION

Despite the increased interest in the therapeutic potential of BAT, the role of cold-stimulated BAT in regulating the metabolic health of adults and children is not fully understood. For example, although several preclinical studies have shown a protective role of BAT activity against NAFLD in rodents, there is a knowledge gap about whether the same relationship exists in humans. Additionally, there is a critical lack of knowledge about cold-stimulated BAT activity in children, its role in metabolic health, and factors that may impact BAT activity in this population i.e., the gut microbiota and serotonin. Thus, the purpose of this dissertation is to explore cold-stimulated BAT activity in adults and children and explore the gut microbiota and serotonin, as two potential impacting factors.

5.1 Exploring the association between cold-stimulated BAT activity and NAFLD

NAFLD is a common cause of chronic liver diseases and its contribution to liver-related deaths is increasing³³³. NAFLD trends are worsening globally and it is a major economic burden on health care systems³³⁴. Thus, there is a continuous need to navigate therapeutic avenues for NAFLD. Few studies have highlighted an association between the presence of BAT at ambient temperature and lower liver fat in humans^{193–195,212,213}. These studies did not investigate possible mechanisms that may explain the link between the two tissues. Also, most of these studies included retrospective examination of ¹⁸F-FDG PET-CT images that were done for clinical purposes (mostly follow-up for malignancies). As mentioned earlier, cold is one of the most powerful activators for BAT. However, to the best of our knowledge, the association between cold-stimulated BAT and NAFLD in adults has not been previously investigated. Therefore, chapter two of this dissertation aims to explore the relationship between BAT activity, after three hours of acute standardized mild cold exposure, and NAFLD in healthy adults. To the best of our knowledge, this is the first report to

show that individuals with NAFLD have lower cold-stimulated BAT activity, compared to those without NAFLD. Importantly, lower BAT activity is associated with higher hepatic fat independent of age, biological sex, total body fat, or visceral fat. This suggests that lower BAT activity is not just an association linked to obesity but may be an important contributing factor to the development of NAFLD. These findings are important as there are currently no approved pharmacotherapies for NAFLD²¹. This is despite the extensive efforts by the pharmaceutical industry in developing new agents which have shown promise in preclinical animal models and small clinical trials but have failed to reach primary endpoints of reduced fibrosis in stage 3 trials²¹. This suggests that combination therapies will likely be needed to treat NAFLD and our findings showing that BAT activity is reduced in people with NAFLD suggest that enhancing BAT activity may be beneficial.

There are many potential mechanisms linking BAT activity to NAFLD. One potential mechanism involves the gut microbiota which has been shown to have an established role in the development of NAFLD in rodents and humans and has been shown to regulate BAT activity in rodents. Therefore, we investigated the relationship between the gut microbiota, BAT activity, and NAFLD status. We did not identify characteristics of the gut microbiota related to BAT activity, nor evidence that BAT activity can be transmitted via fecal transplant from humans to germ-free mice. Thus, the mechanism by which higher BAT activity is linked to lower liver fat is still unclear.

Preclinical studies found that some BATokines (BAT secreted regulatory factors) target the liver and decrease hepatic steatosis like fibroblast growth factor-21 (FGF21), neuregulin 4 (NRG4), and IL-6³³⁵. Interestingly, it was recently reported that BAT transplantation in diabetic mice with fatty liver lowered their glycemia and reversed the hepatic pathological changes due to an increase in circulating BAT-derived miR-99a³³⁶. In future studies, it will be interesting to explore whether the

expression of these hormonal factors and miRNA are related to BAT activity and NAFLD status in our participants.

A strength of our study is that we had strict inclusion criteria like avoidance of any food, medications, supplements, or medical conditions that are known to impact either BAT activity or liver fat. However, this tightly controlled selection did not allow us to enroll older individuals or those with metabolic disorders. Although our study included a large sample size compared to other MRI studies that investigated BAT activity after cold exposure, it is hard to generalize our data to the larger population. Another strength of this study is that we assessed percent body fat, not BMI, as a measure of total adiposity since BMI is known to be an insensitive indicator of body fat³³⁷.

5.1.1 Limitations and future directions

Our study has some limitations. We use MRI to evaluate SCV BAT activity and liver fat. Liver biopsies are considered the gold standard diagnostic tool for NAFLD even though they can be adversely impacted by sampling location³³⁸. Therefore, to accurately measure hepatic fat, we segmented and analyzed the entire liver using MRI. The MRI scanner that we used had a limited bore size and weight limit (300 lbs), so we were not able to enroll participants if they did not meet the weight or the size limit of the scanner i.e., participants with morbid obesity. Also, we were not able to enroll participants who were not eligible to be inside the MRI scanner i.e., females with copper intrauterine devices and claustrophobic participants.

Another limitation is that we did not measure BAT activity by other methods like ¹⁸F-FDG PET-CT; the most used imaging modality to assess BAT activity. ¹⁸F-FDG PET-CT relies on the ability of BAT to uptake glucose after cold stimulation. However, and as mentioned earlier, lipolysis of the intracellular TGs is likely the main fuel source for BAT in response to acute cold stimulation¹¹³.

Glucose, but not FFAs, uptake in BAT was impaired in T2D patients⁶⁷ and in response to insulin resistance after prolonged fasting¹¹⁰. So, ¹⁸F-FDG PET-CT can not accurately evaluate BAT metabolism and thermogenesis especially in the context of insulin resistance and diabetes.

It is known that BAT mass and activity decline with age and that NAFLD affects mostly middle and older age groups³³⁹, thus enhancing BAT activity in these age groups could be beneficial. Cold is the most potent stimulus to BAT however, cold exposure is not comfortable for most people and may not be safe for older age groups³⁴⁰. Therefore, developing pharmacological agents that can increase BAT mass and activity are needed. Clinical trials considered using β 3-AR agonists such as Mirabegron to increase BAT activity and treat obesity^{341,342}. However, the daily doses of Mirabegron that are sufficient to increase BAT are much higher than the maximum clinically approved dosage and are associated with adverse cardiovascular stimulation^{81,200,343}. Recently, four weeks of treatment with Mirabegron, in women increased BAT activity, insulin sensitivity, and total bile acids, yet it did not change hepatic fat or stiffness²⁰⁰. Additionally, it was also recently reported that human brown adipocytes lack the expression of β 3-AR and that human BAT thermogenesis is likely to be mediated via β 2-AR³⁴⁴. Therefore, future work is still needed to develop pharmacological agents that can selectively stimulate human BAT activity with more tolerable systematic adverse effects.

5.2 Exploring cold-stimulated BAT activity in young boys

The increase in the prevalence of childhood obesity is alarming as it is associated with increased cardiometabolic morbidity and premature mortality in adulthood³⁴⁵. Additionally, children with obesity are at higher risk of mental health disorders like major depression and low self-esteem³⁴⁶.

As introduced earlier, evidence suggests that BAT activity may be lower in children with obesity however, to the best of our knowledge, there is no data available about the whole-body cold-

stimulated BAT activity in children. In chapter 3, we explored BAT activity via MRI in 8-10-year-old boys after one hour of whole-body cold exposure. We examined the differences in BAT activity between boys with and without overweight/obesity and those with normal BMI and we examined the association of cold-stimulated BAT activity with metabolic parameters. Our results showed that the SCV region in boys with overweight/obesity is less responsive to cold stimulation compared to those with normal BMI. These results suggest that BAT activity is reduced in young boys with overweight/obesity.

Another interesting observation from our study is that young boys have lower pre-cold SCV PDFF and lower percent changes in SCV PDFF in response to cold compared to adults, suggesting that BAT may be constitutively more active in young boys compared to adults. BAT activity is known to decline with obesity in adults however whether low BAT activity during childhood leads to adulthood obesity is not known. It was proposed that maximal chronic pharmacological activation of BAT in adults may lead to loss of ~5 kg body weight in the first year and 10 kg after 3 years⁸¹. Thus, consistent high BAT activity over childhood years may prevent the occurrence of obesity in adulthood by reducing weight gain, however longitudinal studies are needed to investigate this further.

Another strength of our study is the use of a standardized whole-body cold exposure protocol for one hour that was sufficient to induce a reduction in SCV PDFF. We adapted the one hour based on our previous findings in young adults in response to a similar cold exposure protocol that was done over three hours within the MRI scanner²⁵⁵. In that study, we followed the change in SCV PDFF in a time-course manner during cold exposure and demonstrated that the reduction in SCV PDFF starts as early as 10 minutes of cold exposure and stabilizes within 35 minutes after which no further decrease in SCV PDFF occurred²⁵⁵. It will be interesting to explore whether the same

kinetics occur in children. However, such a study will be challenging as it will require an extended stay for the children in the MRI scanner during cold exposure which will be associated with increased motion that may impact image quality.

5.2.1 Limitations and future directions

Previous studies have found that in boys, BAT volume assessed via ^{18}F -FDG PET-CT at ambient temperature, increases rapidly during puberty^{202,206}. One of the limitations of our study is that we did not use Tanner staging to assess puberty clinically. However, because the average age of puberty onset in boys is 11 years old³⁴⁷, it is unlikely we enrolled pubertal boys in this cohort. Additionally, the reported increase in BAT volume during puberty was evident mainly over the last two stages of puberty²⁰⁶, so it is unlikely that BAT activity was impacted with puberty in this cohort.

To the best of our knowledge, this is the first study to use MRI for imaging BAT after cold stimulation in children. However, we faced some challenges related to using MRI in young children. For example, due to the small size of the children compared to the adults and their tendency to move, we noticed a shift in the shoulder position in few participants between pre-and post-cold scans. Using a shoulder stabilizer/immobilizer³⁴⁸ i.e., vacuum bag or vacuum cushion was not available to use in this study but should be considered for future studies. For the analysis of the MRI images, we used the same protocol that we used for adults. This protocol does not involve registration/aligning of pre-cold to the post-cold images as this function does not work well in the software that we use. Registration is generally important to ensure capturing the same ROI between the pre-and post-cold images.

5.3 Exploring the relationship between BAT activity and circulating serotonin in children

We found that boys with obesity have lower cold-induced BAT activity than boys with normal BMI. As little is known about BAT activity in children, we wanted to explore potential factors that may impact BAT activity in this population. Given our previous observations in rodents²¹¹ and previous studies in adult humans^{237–239,329,349}, we wanted to explore the relationship between BAT activity and circulating free serotonin (serotonin in platelet-poor plasma (PPP) and 5-HIAA/Creatinine in the urine).

We found that, in contrast to studies in rodents, neither of the serotonin is related to SCV BAT activity in young boys. We also reported that boys with overweight/obesity have lower levels of urinary 5-HIAA/Creatinine (5-HIAA/Crt) compared to boys with normal BMI and that 5-HIAA/Crt is inversely related to total and visceral adiposity as well as liver fat. Also, PPP-serotonin is negatively related to total body fat but not to visceral or hepatic fat.

Given the potential challenges with measuring PPP-serotonin, we measured the serotonin metabolite 5-HIAA in the urine. We measured 5-HIAA in spot urine samples and corrected 5-HIAA to the urine levels of creatinine (5-HIAA/Crt) to control for variability in urine concentration³²⁷. We found that the urinary 5-HIAA/Crt ratio was moderately correlated with PPP-serotonin, yet only 5-HIAA/Crt was different between boys with overweight/obesity and boys with normal BMI. This might be explained by the larger variability in the PPP-serotonin (mean± SD: 11.9±10.2 and range: 35.7) compared to 5-HIAA/Crt levels (mean± SD: 2.5 ±0.51 and range: 1.9). Our findings of high interindividual variability in the level of PPP-serotonin are consistent with previous reports²²⁸. This high variability may be related²²⁸ to the collection of PPP which is known to be challenging and requires stringent preanalytical care i.e., during sample collection, the centrifugation process, etc., to avoid platelet contamination²²⁸. However, we used a robust

centrifugation protocol that allowed us to collect PPP without platelet contamination and we verified the absence of platelet contamination by assessing the platelet count on the same day of sample collection.

Another factor that may contribute to the variation in measures of circulating serotonin is the abundance of serotonin in food. An important strength in this study is that we asked our participants to avoid food that is known to impact circulating serotonin levels (banana, tomato, kiwi, walnut, avocado, pineapple, and plum) 24 hours before each study visit as previously recommended³⁵⁰. We also did not enroll participants who declared the use of any medications or supplements, or medical conditions that are known to impact either BAT activity or serotonin levels.

Our findings show that there is no association between circulating serotonin and cold-stimulated BAT could mean that serotonin is not critical for regulating BAT activity in humans or alternatively circulating serotonin levels are not critical. For example, a recent study has shown that while circulating serotonin levels are not different between women with and without NAFLD, the expression of the hepatic serotonin receptors is decreased³²⁹, and in studies in mice, this is sufficient to drive disease development³⁵¹. Another recent study has shown that in rodents, serotonin produced by mast cells is vital for inhibiting adipose tissue thermogenesis when mice are housed at thermoneutrality or fed an obesity-promoting high-fat diet³³². These results suggest a dissociation between the circulating levels of serotonin and its potential local effect on the liver and BAT. Further studies are needed on a larger population to explore this role potentially with liver and BAT biopsies if possible.

5.3.1 Limitations and future directions

One of the limitations of our study is that we did not measure 5-HIAA in 24-hour urine. Clinically, 24-hours urine collection is the most recommended and used urine collection method to measure 5-HIAA levels³⁵². However, 24-hour urine collection is troublesome and inconvenient^{352,353}. It also requires providing the participants with a special plastic container that has preservatives in it. The collected sample should be always refrigerated³⁵³. Therefore, some research groups explored whether spot urine 5-HIAA can replace 24-hours 5-HIAA measurements and found that spot urine 5-HIAA/Crt correlates well with 24-hours urine 5-HIAA ($r=0.863$) in 136 paired urine samples³⁵⁴.

Another limitation of this study is that it can not be generalized to prepubertal girls. Although it was reported that the detection of BAT via ¹⁸F-FDG PET-CT at ambient temperature was not different between girls and boys^{202,206,207} yet the change in SCV temperature, using IRT, after 5 minutes of hand cold exposure was higher in prepubertal girls than in boys²⁰⁸. On the other hand, no sex-related differences were found in the levels of whole blood serotonin neither in children³⁵⁵ nor in adults²³⁸. However, the association between whole blood serotonin and adiposity was reported in adult males and not in the females²³⁸. Therefore, further assessment of the association between circulating serotonin, BAT activity, and adiposity in girls is needed.

5.4 Overall limitations

A general limitation of using the chemical shift-based water-fat separation MRI technique for quantification of BAT is the lack of standardized protocols for BAT characteristics during the post imaging processing. For example, while we considered voxels with fat fractions (FF) ranging from 30-100% and with a T2* range of 2-25 milliseconds as BAT, other studies that explored BAT at ambient temperature in children using water-fat separation MRI did not use a T2* mask or used different FF thresholds i.e., 20-80%^{172,181,196}. Accordingly, there is no known cut-off for the SCV

FF that categorizes participants according to their BAT activity i.e., BAT positive vs BAT negative. Heterogeneity in the degree of reduction of SCV FF in response to cold was recently reported in adults i.e., voxels with high ambient FF show more FF reduction compared to voxels with low ambient FF within the same SCV region^{313,356}. Future studies are needed to investigate this in our cohort.

Another limitation of the water-fat separation MRI is the fat water swaps. Fat water swaps occur due to distortions in the magnetic field, which leads to failure of the fat suppression and subsequently, an interchange between the fat and the water signal i.e., fatty tissues visually look like skeletal muscles and vice versa^{357,358}. Even though the IDEAL-IQ MRI (a multi-point Dixon method) that we use in our studies is known to be more robust against the magnetic field heterogeneity compared 2-point Dixon method³⁵⁷⁻³⁵⁹, yet fat-water swaps occurred during the scan of some of our participants especially in those with lower body fat. The occurrence of fat-water swaps resulted in repeating the scans and thus prolonged the time the participants spent inside the MRI scanner.

5.5 Conclusion

In conclusion, the work presented in this dissertation has provided new knowledge about BAT activity in human adults and children. Our findings provide evidence that 1. Cold-stimulated BAT activity is reduced in adults with NAFLD. This suggests that designing therapies aimed at enhancing BAT activity in combination with medications aimed at modifying liver metabolism (e.g., lipogenesis inhibitors) may be beneficial for treating NAFLD. 2. Young boys with overweight/obesity have lower cold-stimulated BAT activity compared to boys with normal BMI. This suggests that strategies aimed at maintaining BAT activity in obese young children may be beneficial. 3. That BAT activity in adults and children is not dependent on the gut microbiota or

circulating serotonin, respectively suggesting that alternative mechanisms may be more important. The exploration of these mechanisms may provide new insights on the possibility of targeting BAT activity for the treatment of NAFLD and obesity in adults and children.

6.1 REFERENCES

1. WHO. Global status report on noncommunicable diseases 2014. *World Health* 176 (2014) doi:ISBN 9789241564854.
2. Twells, L., Janssen, I. & Kuk, J. Epidemiology of Adult Obesity. <https://obesitycanada.ca/guidelines/epidemiology/> (2020).
3. Noncommunicable diseases: Childhood overweight and obesity. <https://www.who.int/news-room/q-a-detail/noncommunicable-diseases-childhood-overweight-and-obesity>.
4. World Health Organization. Taking action on childhood obesity report. *World Heal. Organ.* 1–8 (2018).
5. Rao, D. P., Kropac, E., Do, M. T., Roberts, K. C. & Jayaraman, G. C. Childhood overweight and obesity trends in Canada. *Heal. Promot. chronic Dis. Prev. Canada Res. policy Pract.* **36**, 194–8 (2016).
6. World Obesity Federation. Atlas of Childhood Obesity. *World Obes. Fed.* **1**, 213 (2019).
7. Heymsfield, S. B. & Wadden, T. A. Mechanisms, Pathophysiology, and Management of Obesity. *N. Engl. J. Med.* **376**, 254–266 (2017).
8. Feingold, K. R. *Obesity and Dyslipidemia*. Endotext (MDText.com, Inc, 2000).
9. Bastien, M., Poirier, P., Lemieux, I. & Després, J.-P. Overview of Epidemiology and Contribution of Obesity to Cardiovascular Disease. *Prog. Cardiovasc. Dis.* **56**, 369–381 (2014).
10. Madala, M. C. *et al.* Obesity and age of first non-ST-segment elevation myocardial infarction. *J. Am. Coll. Cardiol.* **52**, 979–85 (2008).
11. Jood, K., Jern, C., Wilhelmsen, L. & Rosengren, A. Body Mass Index in Mid-Life Is Associated With a First Stroke in Men A Prospective Population Study Over 28 Years. *Stroke* **35**, 2764–2769 (2004).
12. Colditz, G. A., Willett, W. C., Rotnitzky, A. & Manson, J. E. Weight gain as a risk factor for clinical diabetes mellitus in women. *Ann. Intern. Med.* **122**, 481–486 (1995).
13. Kernan, W. N., Inzucchi, S. E., Sawan, C., Macko, R. F. & Furie, K. L. Obesity A Stubbornly Obvious Target for Stroke Prevention. *Stroke* **44**, 278–286 (2013).
14. Mandal, S. & Hart, N. Respiratory complications of obesity. *Clin. Med. (Northfield. Il)*. **12**, 75–78 (2012).
15. Wolin, K. Y., Carson, K. & Colditz, G. A. Obesity and cancer. *Oncologist* **15**, 556–65 (2010).
16. Sarwer, D. B. & Polonsky, H. M. The Psychosocial Burden of Obesity. *Endocrinol. Metab. Clin. North Am.* **45**, 677–688 (2016).

17. Hossain, P., Kavar, B. & El Nahas, M. Obesity and Diabetes in the Developing World — A Growing Challenge. *N. Engl. J. Med.* **356**, 213–215 (2007).
18. Abdullah, A., Peeters, A., de Courten, M. & Stoelwinder, J. The magnitude of association between overweight and obesity and the risk of diabetes: A meta-analysis of prospective cohort studies. *Diabetes Res. Clin. Pract.* **89**, 309–319 (2010).
19. Younossi, Z. M. *et al.* Global epidemiology of nonalcoholic fatty liver disease—Meta-analytic assessment of prevalence, incidence, and outcomes. *Hepatology* **64**, 73–84 (2016).
20. Di Martino, M., Koryukova, K., Bezzi, M. & Catalano, C. Imaging Features of Non-Alcoholic Fatty Liver Disease in Children and Adolescents. *Children* **4**, 73 (2017).
21. Romero, F. A., Jones, C. T., Xu, Y., Fenaux, M. & Halcomb, R. L. The Race to Bash NASH: Emerging Targets and Drug Development in a Complex Liver Disease. *J. Med. Chem.* **63**, 5031–5073 (2020).
22. Huang, D. Q., El-Serag, H. B. & Loomba, R. Global epidemiology of NAFLD-related HCC: trends, predictions, risk factors and prevention. *Nat. Rev. Gastroenterol. Hepatol.* **18**, 223–238 (2021).
23. Swain, M. G. *et al.* Burden of nonalcoholic fatty liver disease in Canada, 2019–2030: a modelling study. *C. Open* **8**, E429–E436 (2020).
24. Richard, A. J., White, U., Elks, C. M. & Stephens, J. M. *Adipose Tissue: Physiology to Metabolic Dysfunction.* *Endotext* (2000).
25. Verma, S. & Hussain, M. E. Obesity and diabetes: An update. *Diabetes Metab. Syndr. Clin. Res. Rev.* **11**, 73–79 (2017).
26. Cooke, A. A., Connaughton, R. M., Lyons, C. L., McMorrow, A. M. & Roche, H. M. Fatty acids and chronic low grade inflammation associated with obesity and the metabolic syndrome. *Eur. J. Pharmacol.* **785**, 207–214 (2016).
27. Donnelly, K. L. *et al.* Sources of fatty acids stored in liver and secreted via lipoproteins in patients with nonalcoholic fatty liver disease. *J. Clin. Invest.* **115**, 1343–1351 (2005).
28. Tilg, H., Adolph, T. E. & Moschen, A. R. Multiple Parallel Hits Hypothesis in Nonalcoholic Fatty Liver Disease: Revisited After a Decade. *Hepatology* **73**, 833–842 (2021).
29. Kure, T. *et al.* Nonalcoholic fatty liver disease is associated with both subcutaneous and visceral adiposity: A cross-sectional study. *Medicine (Baltimore)*. **98**, e17879 (2019).
30. Du Plessis, J. *et al.* Association of Adipose Tissue Inflammation with Histologic Severity of Nonalcoholic Fatty Liver Disease. *Gastroenterology* **149**, 635e14-648.e14 (2015).
31. Johnson, A. R., Justin Milner, J. & Makowski, L. The inflammation highway: metabolism accelerates inflammatory traffic in obesity. *Immunol. Rev.* **249**, 218–238 (2012).
32. Tilg, H. & Moschen, A. R. Evolution of inflammation in nonalcoholic fatty liver disease: The multiple parallel hits hypothesis. *Hepatology* **52**, 1836–1846 (2010).

33. Wong, V. W.-S. *et al.* Molecular Characterization of the Fecal Microbiota in Patients with Nonalcoholic Steatohepatitis – A Longitudinal Study. *PLoS One* **8**, e62885 (2013).
34. Hoyles, L. *et al.* Molecular phenomics and metagenomics of hepatic steatosis in non-diabetic obese women. *Nat. Med.* **24**, 1070–1080 (2018).
35. Boursier, J. *et al.* The severity of nonalcoholic fatty liver disease is associated with gut dysbiosis and shift in the metabolic function of the gut microbiota. *Hepatology* **63**, 764–75 (2016).
36. Wang, B. *et al.* Altered Fecal Microbiota Correlates with Liver Biochemistry in Nonobese Patients with Non-alcoholic Fatty Liver Disease. *Sci. Rep.* **6**, 32002 (2016).
37. Bastian, W. P., Hasan, I., Lesmana, C. R. A., Rinaldi, I. & Gani, R. A. Gut Microbiota Profiles in Nonalcoholic Fatty Liver Disease and Its Possible Impact on Disease Progression Evaluated with Transient Elastography: Lesson Learnt from 60 Cases. *Case Rep. Gastroenterol.* **13**, 125–133 (2019).
38. Caussy, C. *et al.* A gut microbiome signature for cirrhosis due to nonalcoholic fatty liver disease. *Nat. Commun.* **10**, 1406 (2019).
39. Da Silva, H. E. *et al.* Nonalcoholic fatty liver disease is associated with dysbiosis independent of body mass index and insulin resistance. *Sci. Rep.* **8**, 1466 (2018).
40. Raman, M. *et al.* Obese Humans With Nonalcoholic Fatty Liver Disease CONCLUSIONS : *YJCGH* **11**, 868-875.e3 (2013).
41. Hoyles, L. *et al.* hepatic steatosis in non-diabetic obese women. **24**, (2018).
42. Giorgio, V. *et al.* Intestinal permeability is increased in children with non-alcoholic fatty liver disease, and correlates with liver disease severity. *Dig. Liver Dis.* **46**, 556–560 (2014).
43. Miele, L. *et al.* Increased intestinal permeability and tight junction alterations in nonalcoholic fatty liver disease. *Hepatology* **49**, 1877–1887 (2009).
44. Volynets, V. *et al.* Nutrition, intestinal permeability, and blood ethanol levels are altered in patients with nonalcoholic fatty liver disease (NAFLD). *Dig. Dis. Sci.* **57**, 1932–41 (2012).
45. Safari, Z. & Gérard, P. The links between the gut microbiome and non - alcoholic fatty liver disease (NAFLD). *Cell. Mol. Life Sci.* **76**, 1541–1558 (2019).
46. Lonardo, A. *et al.* Nonalcoholic fatty liver disease: Evolving paradigms. *World J. Gastroenterol.* **23**, 6571–6592 (2017).
47. Ratziu, V. *et al.* Sampling variability of liver biopsy in nonalcoholic fatty liver disease. *Gastroenterology* **128**, 1898–1906 (2005).
48. Saadeh, S. *et al.* The utility of radiological imaging in nonalcoholic fatty liver disease. *Gastroenterology* **123**, 745–750 (2002).
49. Ballestri, S. *et al.* Ultrasonographic fatty liver indicator detects mild steatosis and

- correlates with metabolic/histological parameters in various liver diseases. *Metabolism*. **72**, 57–65 (2017).
50. Mottin, C. C. *et al.* The role of ultrasound in the diagnosis of hepatic steatosis in morbidly obese patients. *Obes. Surg.* **14**, 635–7 (2004).
 51. De Lédinghen, V. *et al.* Controlled attenuation parameter (CAP) for the diagnosis of steatosis: A prospective study of 5323 examinations. *J. Hepatol.* **60**, 1026–1031 (2014).
 52. Middleton, M. S. *et al.* Agreement Between Magnetic Resonance Imaging Proton Density Fat Fraction Measurements and Pathologist-Assigned Steatosis Grades of Liver Biopsies From Adults With Nonalcoholic Steatohepatitis. *Gastroenterology* **153**, 753–761 (2017).
 53. Z. Permutt*, T.-A. Le†, M. R. Peterson‡, E. Seki†, D. A. Brenner†, C. Sirlin§, and R. L. Correlation between liver histology and novel magnetic resonance imaging in adult patients with non-alcoholic fatty liver disease – MRI accurately quantifies hepatic steatosis in NAFLD. *Aliment Pharmacol Ther* **36**, 22–29 (2013).
 54. Di Martino, M. *et al.* Comparison of magnetic resonance spectroscopy, proton density fat fraction and histological analysis in the quantification of liver steatosis in children and adolescents. *World J. Gastroenterol.* **22**, 8812 (2016).
 55. Imajo, K. *et al.* Magnetic Resonance Imaging More Accurately Classifies Steatosis and Fibrosis in Patients with Nonalcoholic Fatty Liver Disease Than Transient Elastography. *Gastroenterology* **150**, 626-637.e7 (2016).
 56. Wong, V. W.-S. *et al.* Community-based lifestyle modification programme for non-alcoholic fatty liver disease: A randomized controlled trial. *J. Hepatol.* **59**, 536–542 (2013).
 57. Vilar-Gomez, E. *et al.* Weight Loss Through Lifestyle Modification Significantly Reduces Features of Nonalcoholic Steatohepatitis. *Gastroenterology* **149**, 367-378.e5 (2015).
 58. Albhaisi, S. & Sanyal, A. Recent advances in understanding and managing non-alcoholic fatty liver disease [version 1; referees: 2 approved]. *F1000Research* **7**, 1–11 (2018).
 59. Ong, F. J. *et al.* Recent advances in the detection of brown adipose tissue in adult humans: a review. *Clin. Sci. (Lond)*. **132**, 1039–1054 (2018).
 60. Virtanen, K. A. *et al.* Functional Brown Adipose Tissue in Healthy Adults. *N. Engl. J. Med.* **360**, 1518–1525 (2009).
 61. van Marken Lichtenbelt, W. D. *et al.* Cold-activated brown adipose tissue in healthy men. *N. Engl. J. Med.* **360**, 1500–8 (2009).
 62. Cypess, A. M. *et al.* Identification and Importance of Brown Adipose Tissue in Adult Humans. *N. Engl. J. Med.* **360**, 1509–1517 (2009).
 63. Saito, M. *et al.* High incidence of metabolically active brown adipose tissue in healthy adult humans: effects of cold exposure and adiposity. *Diabetes* **58**, 1526–31 (2009).
 64. Cinti, S. Transdifferentiation properties of adipocytes in the adipose organ. *Am. J. Physiol. Metab.* **297**, E977–E986 (2009).

65. Richard, D., Carpentier, A. C., Dore, G., Ouellet, V. & Picard, F. Determinants of brown adipocyte development and thermogenesis. *Int J Obes* **34 Suppl 2**, S59–S66 (2010).
66. Ouellet, V. *et al.* Brown adipose tissue oxidative metabolism contributes to energy expenditure during acute cold exposure in humans. *J. Clin. Invest.* **122**, 545–52 (2012).
67. Blondin, D. P. *et al.* Selective Impairment of Glucose but Not Fatty Acid or Oxidative Metabolism in Brown Adipose Tissue of Subjects With Type 2 Diabetes. *Diabetes* **64**, 2388–97 (2015).
68. u Din, M. *et al.* Human brown adipose tissue [15O]O₂ PET imaging in the presence and absence of cold stimulus. *Eur. J. Nucl. Med. Mol. Imaging* **43**, 1878–1886 (2016).
69. Cinti, S. The adipose organ: morphological perspectives of adipose tissues. *Proc. Nutr. Soc.* **60**, 319–28 (2001).
70. Giordano, A., Smorlesi, A., Frontini, A., Barbatelli, G. & Cinti, S. White, brown and pink adipocytes: The extraordinary plasticity of the adipose organ. *Eur. J. Endocrinol.* **170**, (2014).
71. Heaton, J. M. The distribution of brown adipose tissue in the human. *J. Anat.* **112**, 35–9 (1972).
72. Pfannenberg, C. *et al.* Impact of Age on the Relationships of Brown Adipose Tissue With Sex and Adiposity in Humans. *Diabetes* **59**, 1789–1793 (2010).
73. Yoneshiro, T. *et al.* Age-Related Decrease in Cold-Activated Brown Adipose Tissue and Accumulation of Body Fat in Healthy Humans. *Obesity* **19**, 1755–1760 (2011).
74. HULL, D. The Function of Brown Adipose Tissue in the Newborn. *Biochem. Soc. Trans.* **4**, 226–228 (1976).
75. Ouellet, V. *et al.* Outdoor temperature, age, sex, body mass index, and diabetic status determine the prevalence, mass, and glucose-uptake activity of 18F-FDG-detected BAT in humans. *J. Clin. Endocrinol. Metab.* **96**, 192–199 (2011).
76. Blondin, D. P. *et al.* A critical appraisal of brown adipose tissue metabolism in humans. *Clin. Lipidol.* **10**, 259–280 (2015).
77. Lee, P., Greenfield, J. R., Ho, K. K. Y. & Fulham, M. J. A critical appraisal of the prevalence and metabolic significance of brown adipose tissue in adult humans. *Am. J. Physiol. Endocrinol. Metab.* **299**, E601-6 (2010).
78. Cypess, A. M. *et al.* Cold but not sympathomimetics activates human brown adipose tissue in vivo. *Proc. Natl. Acad. Sci. U. S. A.* **109**, 10001–10005 (2012).
79. Carey, A. L. *et al.* Ephedrine activates brown adipose tissue in lean but not obese humans. *Diabetologia* **56**, 147–155 (2013).
80. Vosselman, M. J. *et al.* Systemic -Adrenergic Stimulation of Thermogenesis Is Not Accompanied by Brown Adipose Tissue Activity in Humans. *Diabetes* **61**, 3106–3113 (2012).

81. Cypess, A. M. *et al.* Activation of human brown adipose tissue by a β 3-adrenergic receptor agonist. *Cell Metab.* **21**, 33–38 (2015).
82. van der Lans, A. A. J. J. *et al.* Cold-activated brown adipose tissue in human adults: methodological issues. *AJP Regul. Integr. Comp. Physiol.* **307**, R103–R113 (2014).
83. Chen, K. Y. *et al.* Brown Adipose Reporting Criteria in Imaging Studies (BARCIST 1.0): Recommendations for Standardized FDG-PET/CT Experiments in Humans. *Cell Metabolism* vol. 24 210–222 (2016).
84. Robinson, L., Ojha, S., Symonds, M. E. & Budge, H. Body mass index as a determinant of brown adipose tissue function in healthy children. *J. Pediatr.* **164**, 318-322.e1 (2014).
85. Yoneshiro, T. *et al.* Tea catechin and caffeine activate brown adipose tissue and increase cold-induced thermogenic capacity in humans. *Am. J. Clin. Nutr.* **105**, 873–881 (2017).
86. Lee, P. *et al.* Temperature-Acclimated Brown Adipose Tissue Modulates Insulin Sensitivity in Humans. *Diabetes* **63**, 3686–3698 (2014).
87. Schopman, J. E. *et al.* 18F-fluorodeoxyglucose uptake in brown adipose tissue during insulin-induced hypoglycemia and mild cold exposure in non-diabetic adults. *Metabolism* **63**, 1280–1286 (2014).
88. Admiraal, W. M. *et al.* Combining 123I-Metaiodobenzylguanidine SPECT/CT and 18F-FDG PET/CT for the Assessment of Brown Adipose Tissue Activity in Humans During Cold Exposure. *J. Nucl. Med.* **54**, 208–212 (2013).
89. Lee, P. *et al.* Cold-activated brown adipose tissue is an independent predictor of higher bone mineral density in women. *Osteoporos. Int.* **24**, 1513–1518 (2013).
90. Vosselman, M. J. *et al.* Low brown adipose tissue activity in endurance-trained compared with lean sedentary men. *Int. J. Obes.* **39**, 1696–1702 (2015).
91. Vosselman, M. J. *et al.* Brown adipose tissue activity after a high-calorie meal in humans. *Am. J. Clin. Nutr.* **98**, 57–64 (2013).
92. Bahler, L. *et al.* Differences in Sympathetic Nervous Stimulation of Brown Adipose Tissue Between the Young and Old, and the Lean and Obese. *J. Nucl. Med.* **57**, 372–7 (2016).
93. Rachid, B. *et al.* Distinct regulation of hypothalamic and brown/beige adipose tissue activities in human obesity. *Int. J. Obes.* **39**, 1515–1522 (2015).
94. van der Lans, A. A. J. J., Vosselman, M. J., Hanssen, M. J. W., Brans, B. & van Marken Lichtenbelt, W. D. Supraclavicular skin temperature and BAT activity in lean healthy adults. *J. Physiol. Sci.* **66**, 77–83 (2016).
95. Schlögl, M. *et al.* Overfeeding over 24 hours does not activate brown adipose tissue in humans. *J. Clin. Endocrinol. Metab.* **98**, E1956-60 (2013).
96. Admiraal, W. M. *et al.* Cold-induced activity of brown adipose tissue in young lean men of South-Asian and European origin. *Diabetologia* **56**, 2231–2237 (2013).

97. Chen, K. Y. *et al.* Brown Fat Activation Mediates Cold-Induced Thermogenesis in Adult Humans in Response to a Mild Decrease in Ambient Temperature. *J. Clin. Endocrinol. Metab.* **98**, E1218–E1223 (2013).
98. Muzik, O. *et al.* ¹⁵O PET Measurement of Blood Flow and Oxygen Consumption in Cold-Activated Human Brown Fat. *J. Nucl. Med.* **54**, 523–531 (2013).
99. Muzik, O., Mangner, T. J. & Granneman, J. G. Assessment of Oxidative Metabolism in Brown Fat Using PET Imaging. *Front. Endocrinol. (Lausanne)*. **3**, 1–7 (2012).
100. Brooke, O. G., Harris, M. & Salvosa, C. B. The response of malnourished babies to cold. *J. Physiol.* **233**, 75–91 (1973).
101. Gifford, A., Towse, T. F., Walker, R. C., Avison, M. J. & Welch, E. B. Characterizing active and inactive brown adipose tissue in adult humans using PET-CT and MR imaging. *Am. J. Physiol. Metab.* **311**, E95–E104 (2016).
102. Lundström, E. *et al.* Magnetic resonance imaging cooling-reheating protocol indicates decreased fat fraction via lipid consumption in suspected brown adipose tissue. *PLoS One* **10**, 1–13 (2015).
103. Vrieze, A. *et al.* Fasting and Postprandial Activity of Brown Adipose Tissue in Healthy Men. *J. Nucl. Med.* **53**, 1407–1410 (2012).
104. Leitner, B. P. *et al.* Mapping of human brown adipose tissue in lean and obese young men. *Proc. Natl. Acad. Sci. U. S. A.* **114**, 8649–8654 (2017).
105. Blondin, D. P. *et al.* Dietary fatty acid metabolism of brown adipose tissue in cold-acclimated men. *Nat. Commun.* **8**, 14146 (2017).
106. Muzik, O., Mangner, T. J., Leonard, W. R., Kumar, A. & Granneman, J. G. Sympathetic Innervation of Cold-Activated Brown and White Fat in Lean Young Adults. *J. Nucl. Med.* **58**, 799–806 (2017).
107. Blondin, D. P. *et al.* Contributions of white and brown adipose tissues and skeletal muscles to acute cold-induced metabolic responses in healthy men. *J. Physiol.* **593**, 701–14 (2015).
108. Blondin, D. P. *et al.* Increased brown adipose tissue oxidative capacity in cold-acclimated humans. *J. Clin. Endocrinol. Metab.* **99**, 438–446 (2014).
109. van Rooijen, B. D. *et al.* Imaging cold-activated brown adipose tissue using dynamic T2*-weighted magnetic resonance imaging and 2-deoxy-2-[¹⁸F]fluoro-D-glucose positron emission tomography. *Invest. Radiol.* **48**, 708–14 (2013).
110. Hanssen, M. J. W. *et al.* Glucose uptake in human brown adipose tissue is impaired upon fasting-induced insulin resistance. *Diabetologia* **58**, 586–595 (2015).
111. Hanssen, M. J. W. *et al.* Serum FGF21 levels are associated with brown adipose tissue activity in humans. *Sci. Rep.* **5**, 10275 (2015).
112. Van Der Lans, A. A. J. J. *et al.* Cold acclimation recruits human brown fat and increases nonshivering thermogenesis. *J. Clin. Invest.* **123**, 3395–3403 (2013).

113. Blondin, D. P. *et al.* Inhibition of Intracellular Triglyceride Lipolysis Suppresses Cold-Induced Brown Adipose Tissue Metabolism and Increases Shivering in Humans. *Cell Metab.* **25**, 438–447 (2017).
114. Hanssen, M. J. W. *et al.* Short-term Cold Acclimation Recruits Brown Adipose Tissue in Obese Humans. *Diabetes* **65**, 1179–1189 (2016).
115. Hanssen, M. J. W. *et al.* Short-term cold acclimation improves insulin sensitivity in patients with type 2 diabetes mellitus. *Nat. Med.* **21**, 863–865 (2015).
116. Lynes, M. D. *et al.* The cold-induced lipokine 12,13-diHOME promotes fatty acid transport into brown adipose tissue. *Nat. Med.* **23**, 631–637 (2017).
117. Boon, M. R. *et al.* Supraclavicular skin temperature as a measure of 18F-FDG uptake by BAT in human subjects. *PLoS One* **9**, e98822 (2014).
118. Bakker, L. E. H. *et al.* Brown adipose tissue volume in healthy lean south Asian adults compared with white Caucasians: a prospective, case-controlled observational study. *lancet. Diabetes Endocrinol.* **2**, 210–7 (2014).
119. McCallister, A., Zhang, L., Burant, A., Katz, L. & Branca, R. T. A pilot study on the correlation between fat fraction values and glucose uptake values in supraclavicular fat by simultaneous PET/MRI. *Magn. Reson. Med.* **78**, 1922–1932 (2017).
120. U Din, M. *et al.* Human Brown Fat Radiodensity Indicates Underlying Tissue Composition and Systemic Metabolic Health. *J. Clin. Endocrinol. Metab.* **102**, 2258–2267 (2017).
121. Haq, T. *et al.* Optimizing the methodology for measuring supraclavicular skin temperature using infrared thermography; implications for measuring brown adipose tissue activity in humans. *Sci. Rep.* **7**, 11934 (2017).
122. Hu, H. H. *et al.* MRI detection of brown adipose tissue with low fat content in newborns with hypothermia. *Magn. Reson. Imaging* **32**, 107–17 (2014).
123. Deng, J. *et al.* MRI characterization of brown adipose tissue under thermal challenges in normal weight, overweight, and obese young men. *J. Magn. Reson. Imaging* **47**, 936–947 (2018).
124. Bredella, M. A., Fazeli, P. K., Lecka-Czernik, B., Rosen, C. J. & Klibanski, A. IGFBP-2 is a negative predictor of cold-induced brown fat and bone mineral density in young non-obese women. *Bone* **53**, 336–339 (2013).
125. Bredella, M. A. *et al.* Young Women with Cold-Activated Brown Adipose Tissue Have Higher Bone Mineral Density and Lower Pref-1 than Women without Brown Adipose Tissue: A Study in Women with Anorexia Nervosa, Women Recovered from Anorexia Nervosa, and Normal-Weight Women. *J. Clin. Endocrinol. Metab.* **97**, 584–590 (2012).
126. Salem, V. *et al.* Glucagon increases energy expenditure independently of brown adipose tissue activation in humans. *Diabetes, Obes. Metab.* **18**, 72–81 (2016).
127. Chondronikola, M. *et al.* Brown Adipose Tissue Improves Whole-Body Glucose

- Homeostasis and Insulin Sensitivity in Humans. *Diabetes* **63**, 4089–4099 (2014).
128. Chondronikola, M. *et al.* A percutaneous needle biopsy technique for sampling the supraclavicular brown adipose tissue depot of humans. *Int. J. Obes. (Lond)*. **39**, 1561–4 (2015).
 129. Flynn, A. *et al.* Contrast-Enhanced Ultrasound: A Novel Noninvasive, Nonionizing Method for the Detection of Brown Adipose Tissue in Humans. *J. Am. Soc. Echocardiogr.* **28**, 1247–54 (2015).
 130. Chen, Y. Y.-C. I. Y.-C. *et al.* Measurement of Human Brown Adipose Tissue Volume and Activity Using Anatomical MRI and Functional MRI. *J Nucl Med* **54**, 1584–1587 (2014).
 131. Stahl, V. *et al.* In vivo assessment of cold stimulation effects on the fat fraction of brown adipose tissue using DIXON MRI. *J. Magn. Reson. Imaging* **45**, 369–380 (2017).
 132. Vijgen, G. H. E. J. *et al.* Brown adipose tissue in morbidly obese subjects. *PLoS One* **6**, e17247 (2011).
 133. Vijgen, G. H. E. J. *et al.* Vagus Nerve Stimulation Increases Energy Expenditure: Relation to Brown Adipose Tissue Activity. *PLoS One* **8**, e77221 (2013).
 134. Vijgen, G. H. E. J. *et al.* Increase in brown adipose tissue activity after weight loss in morbidly obese subjects. *J. Clin. Endocrinol. Metab.* **97**, E1229-33 (2012).
 135. Lee, P. *et al.* Irisin and FGF21 Are Cold-Induced Endocrine Activators of Brown Fat Function in Humans. *Cell Metab.* **19**, 302–309 (2014).
 136. Holstila, M. *et al.* MR signal-fat-fraction analysis and T2* weighted imaging measure BAT reliably on humans without cold exposure. *Metabolism* **70**, 23–30 (2017).
 137. Chondronikola, M. *et al.* Brown Adipose Tissue Activation Is Linked to Distinct Systemic Effects on Lipid Metabolism in Humans. *Cell Metab.* **23**, 1200–1206 (2016).
 138. Koskensalo, K. *et al.* Human brown adipose tissue temperature and fat fraction are related to its metabolic activity. *J. Clin. Endocrinol. Metab.* **102**, 1200–1207 (2017).
 139. Hwang, J. J. *et al.* Imaging human brown adipose tissue under room temperature conditions with ¹¹C-MRB, a selective norepinephrine transporter PET ligand. *Metabolism* **64**, 747–755 (2015).
 140. Martinez-Tellez, B. *et al.* Differences between the most used equations in BAT-human studies to estimate parameters of skin temperature in young lean men. *Sci. Rep.* **7**, 10530 (2017).
 141. Orava, J. *et al.* Brown adipose tissue function is accompanied by cerebral activation in lean but not in obese humans. *J. Cereb. Blood Flow Metab.* **34**, 1018–1023 (2014).
 142. Yoneshiro, T. *et al.* Brown Adipose Tissue, Whole-Body Energy Expenditure, and Thermogenesis in Healthy Adult Men. *Obesity* **19**, 13–16 (2011).
 143. Matsushita, M. *et al.* Impact of brown adipose tissue on body fatness and glucose metabolism in healthy humans. *Int. J. Obes.* **38**, 812–817 (2014).

144. Yoneshiro, T. *et al.* Impact of UCP1 and β 3AR gene polymorphisms on age-related changes in brown adipose tissue and adiposity in humans. *Int. J. Obes.* **37**, 993–998 (2013).
145. Orava, J. *et al.* Blunted metabolic responses to cold and insulin stimulation in brown adipose tissue of obese humans. *Obesity* **21**, 2279–2287 (2013).
146. Symonds, M. E. *et al.* Thermal imaging to assess age-related changes of skin temperature within the supraclavicular region co-locating with brown adipose tissue in healthy children. *J. Pediatr.* **161**, 892–8 (2012).
147. El Hadi, H. *et al.* Infrared thermography for indirect assessment of activation of brown adipose tissue in lean and obese male subjects. *Physiol. Meas.* **37**, N118–N128 (2016).
148. Ang, Q. Y. *et al.* A new method of infrared thermography for quantification of brown adipose tissue activation in healthy adults (TACTICAL): a randomized trial. *J. Physiol. Sci.* **67**, 395–406 (2017).
149. Nirengi, S., Yoneshiro, T., Sugie, H., Saito, M. & Hamaoka, T. Human brown adipose tissue assessed by simple, noninvasive near-Infrared time-resolved spectroscopy. *Obesity* **23**, 973–980 (2015).
150. Yoneshiro, T. *et al.* Recruited brown adipose tissue as an antiobesity agent in humans. *J. Clin. Invest.* **123**, 3404–3408 (2013).
151. Raiko, J. *et al.* Brown adipose tissue triglyceride content is associated with decreased insulin sensitivity, independently of age and obesity. *Diabetes, Obes. Metab.* **17**, 516–519 (2015).
152. Orava, J. *et al.* Different metabolic responses of human brown adipose tissue to activation by cold and insulin. *Cell Metab.* **14**, 272–279 (2011).
153. Veicsteinas, A., Ferretti, G. & Rennie, D. W. Superficial shell insulation in resting and exercising men in cold water. *J. Appl. Physiol.* **52**, 1557–1564 (1982).
154. LeBlanc, J. SUBCUTANEOUS FAT AND SKIN TEMPERATURE. *Can. J. Biochem. Physiol.* **32**, 354–358 (1954).
155. Falk, B. *et al.* Physiological and cognitive responses to cold exposure in 11-12-year-old boys. *Am. J. Hum. Biol.* **9**, 39–49 (1997).
156. Ruth, M. Cold-Activated Brown Adipose Tissue in Healthy Men. *Yearb. Endocrinol.* **2010**, 115–117 (2010).
157. Saito, M. *et al.* High incidence of metabolically active brown adipose tissue in healthy adult humans: Effects of cold exposure and adiposity. *Diabetes* **58**, 1526–1531 (2009).
158. Nedergaard, J., Bengtsson, T. & Cannon, B. Unexpected evidence for active brown adipose tissue in adult humans. *Am. J. Physiol. Endocrinol. Metab.* **293**, 444–452 (2007).
159. Cheebsumon, P. *et al.* Measuring response to therapy using FDG PET: Semi-quantitative and full kinetic analysis. *Eur. J. Nucl. Med. Mol. Imaging* **38**, 832–842 (2011).

160. Muzi F.; Mankoff, D. A.; Doot, R. K.; Pierce, L. A.; Kurland, B. F.; Linden, H. M.; Kinahan, P. E., M. . O. Quantitative assessment of dynamic PET imaging data in cancer imaging. *Magn Reson Imaging* **30**, 1203–1215 (2012).
161. Lammertsma, A. A., Hoekstra, C. J., Giaccone, G. & Hoekstra, O. S. How should we analyse FDG PET studies for monitoring tumour response? *Eur. J. Nucl. Med. Mol. Imaging* **33**, 816–821 (2006).
162. Wangerin, K. A. *et al.* A virtual clinical trial comparing static versus dynamic PET imaging in measuring response to breast cancer therapy. *Phys. Med. Biol.* **62**, 3639–3655 (2017).
163. Croteau, E. *et al.* Image-derived input function in dynamic human PET/CT: Methodology and validation with ¹¹C-acetate and ¹⁸F- fluorothioheptadecanoic acid in muscle and ¹⁸F-fluorodeoxyglucose in brain. *Eur. J. Nucl. Med. Mol. Imaging* **37**, 1539–1550 (2010).
164. Din, M. U. *et al.* Human brown fat radiodensity indicates underlying tissue composition and systemic metabolic health. *J. Clin. Endocrinol. Metab.* **102**, 2258–2267 (2017).
165. Muzik, O., Mangner, T. J., Leonard, W. R., Kumar, A. & Granneman, J. G. Sympathetic Innervation of Cold-Activated Brown and White Fat in Lean Young Adults. *J. Nucl. Med.* **58**, 799–806 (2017).
166. Labbé, S. M. *et al.* In vivo measurement of energy substrate contribution to cold-induced brown adipose tissue thermogenesis. *FASEB J.* **29**, 2046–58 (2015).
167. Muzik, O., Mangner, T. J. & Granneman, J. G. Assessment of oxidative metabolism in brown fat using PET imaging. *Front. Endocrinol. (Lausanne)*. **3**, 1–7 (2012).
168. Jadvar, H. & Parker, J. A. *Clinical PET and PET/CT. Clinical PET and PET/CT* (Springer-Verlag, 2005). doi:10.1007/b138777.
169. Din, M., Raiko, J., Saari, T., Kudomi, N. & Tolvanen, T. Human brown adipose tissue [¹⁵O] O ₂ PET imaging in the presence and absence of cold stimulus. *Eur. J. Nucl. Med. Mol. Imaging* 1878–1886 (2016) doi:10.1007/s00259-016-3364-y.
170. Cypess, A. M., Haft, C. R., Laughlin, M. R. & Hu, H. H. Brown fat in humans: Consensus points and experimental guidelines. *Cell Metab.* **20**, 408–415 (2014).
171. Hu, H. H., Perkins, T. G., Chia, J. M. & Gilsanz, V. Characterization of human brown adipose tissue by chemical-shift water-fat MRI. *Am. J. Roentgenol.* **200**, 177–183 (2013).
172. Hu, H. H. *et al.* Comparison of brown and white adipose tissues in infants and children with chemical-shift-encoded water-fat MRI. *J. Magn. Reson. Imaging* **38**, 885–896 (2013).
173. Hu, H. H., Tovar, J. P., Pavlova, Z., Smith, M. L. & Gilsanz, V. Unequivocal identification of brown adipose tissue in a human infant. *J. Magn. Reson. Imaging* **35**, 938–942 (2012).
174. Reeder, S. B., Hu, H. H. & Sirlin, C. B. Proton density fat-fraction: A standardized mr-based biomarker of tissue fat concentration. *J. Magn. Reson. Imaging* **36**, 1011–1014

- (2012).
175. Franssens, B. T. *et al.* Reliability and agreement of adipose tissue fat fraction measurements with water-fat MRI in patients with manifest cardiovascular disease. *NMR Biomed.* **29**, 48–56 (2016).
 176. Franz, D. *et al.* Discrimination between brown and white adipose tissue using a 2-point dixon water-fat separation method in simultaneous pet/MRI. *J. Nucl. Med.* **56**, 1742–1747 (2015).
 177. Baba, S., Jacene, H. A., Engles, J. M., Honda, H. & Wahl, R. L. CT Hounsfield units of brown adipose tissue increase with activation: preclinical and clinical studies. *J. Nucl. Med.* **51**, 246–250 (2010).
 178. Hu, H. H. Magnetic resonance of brown adipose tissue: A review of current techniques. *Crit. Rev. Biomed. Eng.* **43**, 161–181 (2015).
 179. Lidell, M. E. *et al.* Evidence for two types of brown adipose tissue in humans. *Nat. Med.* **19**, 631–634 (2013).
 180. Reddy, N. L. *et al.* Identification of Brown Adipose Tissue Using MR Imaging in a Human Adult With Histological and Immunohistochemical Confirmation. *J. Clin. Endocrinol. Metab.* **99**, E117–E121 (2014).
 181. Rasmussen, J. M. *et al.* Brown Adipose Tissue Quantification in Human Neonates Using Water-Fat Separated MRI. *PLoS One* **8**, e77907 (2013).
 182. Deng, J. *et al.* MRI characterization of brown adipose tissue in obese and normal-weight children. *Pediatr. Radiol.* **45**, 1682–1689 (2015).
 183. Franssens, B. T., Hoogduin, H., Leiner, T., van der Graaf, Y. & Visseren, F. L. J. Relation between brown adipose tissue and measures of obesity and metabolic dysfunction in patients with cardiovascular disease. *J. Magn. Reson. Imaging* **46**, 497–504 (2017).
 184. Wu, J. *et al.* Beige adipocytes are a distinct type of thermogenic fat cell in mouse and human. *Cell* **150**, 366–376 (2012).
 185. Chavhan, G. B., Babyn, P. S., Thomas, B., Shroff, M. M. & Haacke, E. M. Principles, techniques, and applications of T2*-based MR imaging and its special applications. *Radiographics* **29**, 1433–1449 (2009).
 186. Gossuin, Y., Muller, R. N. & Gillis, P. Relaxation induced by ferritin: A better understanding for an improved MRI iron quantification. *NMR in Biomedicine* vol. 17 427–432 (2004).
 187. Bammer, R. Basic principles of diffusion-weighted imaging. *Eur. J. Radiol.* **45**, 169–184 (2003).
 188. Law, W. P. & McGill, G. Identification of brown adipose tissue in an adult human using parametric data reconstructed from a 2-point Dixon magnetic resonance imaging sequence acquired simultaneously with FDG PET. *J. Clin. Transl. Endocrinol. Case Reports* **2**, 27–29 (2016).

189. Gariani, K. *et al.* Hybrid PET/MRI as a tool to detect brown adipose tissue: Proof of principle. *Obes. Res. Clin. Pract.* **9**, 613–617 (2015).
190. Rossato, M., Cecchin, D. & Vettor, R. Brown adipose tissue localization using 18F-FDG PET/MRI in adult. *Endocrine* **54**, 562–563 (2016).
191. Johannesen, H. H. *et al.* Identification and characterization of human brown adipose tissue (BAT) content and metabolism in adults using [18F]-FDG PET/MR – a pilot study. *EJNMMI Phys.* **1**, A68 (2014).
192. Wang, Q. *et al.* Brown adipose tissue activation is inversely related to central obesity and metabolic parameters in adult human. *PLoS One* **10**, 1–13 (2015).
193. Brendle, C. *et al.* Correlation of Brown Adipose Tissue with Other Body Fat Compartments and Patient Characteristics. *Acad. Radiol.* **25**, 102–110 (2018).
194. Green, A. L. *et al.* Brown adipose tissue detected by PET/CT imaging is associated with less central obesity. *Nucl. Med. Commun.* **38**, 629–635 (2017).
195. Franz, D. *et al.* Association of proton density fat fraction in adipose tissue with imaging-based and anthropometric obesity markers in adults. *Int. J. Obes.* **42**, 175–182 (2018).
196. Tint, M. T. *et al.* Brown adipose tissue, adiposity and metabolic profile in preschool children. *J. Clin. Endocrinol. Metab.* (2021) doi:10.1210/clinem/dgab447.
197. Entringer, S. *et al.* Association between supraclavicular brown adipose tissue composition at birth and adiposity gain from birth to 6 months of age. *Pediatr. Res.* **82**, 1017–1021 (2017).
198. Rodovalho, S. *et al.* Impairment of body mass reduction-associated activation of brown/beige adipose tissue in patients with type 2 diabetes mellitus. *Int. J. Obes.* **41**, 1662–1668 (2017).
199. Becher, T. *et al.* Brown adipose tissue is associated with cardiometabolic health. *Nat. Med.* **27**, 58–65 (2021).
200. O'Mara, A. E. *et al.* Chronic mirabegron treatment increases human brown fat, HDL cholesterol, and insulin sensitivity. *J. Clin. Invest.* **130**, 2209–2219 (2020).
201. Richard, M. A., Pallubinsky, H. & Blondin, D. P. Functional characterization of human brown adipose tissue metabolism. *Biochem. J.* **477**, 1261–1286 (2020).
202. Drubach, L. A. *et al.* Pediatric brown adipose tissue: Detection, epidemiology, and differences from adults. *J. Pediatr.* **159**, 939–944 (2011).
203. Senn, J. R. *et al.* Outdoor temperature influences cold induced thermogenesis in humans. *Front. Physiol.* **9**, 1–9 (2018).
204. Au-Yong, I. T. H., Thorn, N., Ganatra, R., Perkins, A. C. & Symonds, M. E. Brown adipose tissue and seasonal variation in humans. *Diabetes* **58**, 2583–2587 (2009).
205. Fletcher, L. A. *et al.* Sexual Dimorphisms in Adult Human Brown Adipose Tissue. *Obesity (Silver Spring)*. **28**, 241–246 (2020).

206. Gilsanz, V. *et al.* Changes in Brown Adipose Tissue in Boys and Girls during Childhood and Puberty. *J. Pediatr.* **160**, 604-609.e1 (2012).
207. Gilsanz, V., Chung, S. A., Jackson, H., Dorey, F. J. & Hu, H. H. Functional brown adipose tissue is related to muscle volume in children and adolescents. *J. Pediatr.* **158**, 722–6 (2011).
208. Malpique, R. *et al.* Brown adipose tissue in prepubertal children: associations with sex, birthweight, and metabolic profile. *Int. J. Obes.* **43**, 384–391 (2019).
209. Poekes, L. *et al.* Defective adaptive thermogenesis contributes to metabolic syndrome and liver steatosis in obese mice. *Clin. Sci.* **131**, 285–296 (2017).
210. Poekes, L., Gillard, J., Farrell, G. C., Horsmans, Y. & Leclercq, I. A. Activation of brown adipose tissue enhances the efficacy of caloric restriction for treatment of nonalcoholic steatohepatitis. *Lab. Investig.* **99**, 4–16 (2019).
211. Crane, J. D. *et al.* Inhibiting peripheral serotonin synthesis reduces obesity and metabolic dysfunction by promoting brown adipose tissue thermogenesis. *Nat. Med.* **21**, 166–72 (2015).
212. Yilmaz, Y. *et al.* Association between the presence of brown adipose tissue and non-alcoholic fatty liver disease in adult humans. *Aliment. Pharmacol. Ther.* **34**, 318–323 (2011).
213. Ozguven, S., Ones, T., Yilmaz, Y., Turoglu, H. T. & Imeryuz, N. The role of active brown adipose tissue in human metabolism. *Eur. J. Nucl. Med. Mol. Imaging* **43**, 355–361 (2016).
214. Blondin, D. P. & Carpentier, A. C. The role of BAT in cardiometabolic disorders and aging. *Best Pract. Res. Clin. Endocrinol. Metab.* **30**, 497–513 (2016).
215. Suárez-Zamorano, N. *et al.* Microbiota depletion promotes browning of white adipose tissue and reduces obesity. *Nat. Med.* **21**, 1497–1501 (2015).
216. Li, G. *et al.* Intermittent Fasting Promotes White Adipose Browning and Decreases Obesity by Shaping the Gut Microbiota. *Cell Metab.* **26**, 672-685.e4 (2017).
217. Ziętak, M. *et al.* Altered Microbiota Contributes to Reduced Diet-Induced Obesity upon Cold Exposure. *Cell Metab.* **23**, 1216–1223 (2016).
218. Worthmann, A. *et al.* Cold-induced conversion of cholesterol to bile acids in mice shapes the gut microbiome and promotes adaptive thermogenesis. *Nat. Med.* **23**, 839–849 (2017).
219. Li, B. *et al.* Microbiota Depletion Impairs Thermogenesis of Brown Adipose Tissue and Browning of White Adipose Tissue. *Cell Rep.* **26**, 2720-2737.e5 (2019).
220. Palego, L., Betti, L., Rossi, A. & Giannaccini, G. Tryptophan Biochemistry: Structural, Nutritional, Metabolic, and Medical Aspects in Humans. *J. Amino Acids* **2016**, 1–13 (2016).
221. Namkung, J., Kim, H. & Park, S. Peripheral Serotonin: a New Player in Systemic Energy Homeostasis. *Mol. Cells* **38**, 1023–1028 (2015).

222. Martin, A. M. *et al.* The diverse metabolic roles of peripheral serotonin. *Endocrinology* **158**, 1049–1063 (2017).
223. Bertrand, R. L. *et al.* A Western diet increases serotonin availability in rat small intestine. *Endocrinology* **152**, 36–47 (2011).
224. Martin, A. M. *et al.* Regional differences in nutrient-induced secretion of gut serotonin. *Physiol. Rep.* **5**, 1–12 (2017).
225. Reigstad, C. S. *et al.* Gut microbes promote colonic serotonin production through an effect of short-chain fatty acids on enterochromaffin cells. *FASEB J.* **29**, 1395–1403 (2015).
226. Martin, A. M. *et al.* The gut microbiome regulates host glucose homeostasis via peripheral serotonin. *Proc. Natl. Acad. Sci.* **116**, 19802–19804 (2019).
227. Mercado, C. P. & Kilic, F. Molecular Mechanisms of SERT in Platelets: Regulation of Plasma Serotonin Levels. *Mol. Interv.* **10**, 231–241 (2010).
228. Brand, T. & Anderson, G. M. The Measurement of Platelet-Poor Plasma Serotonin: A Systematic Review of Prior Reports and Recommendations for Improved Analysis. *Clin. Chem.* **57**, 1376–1386 (2011).
229. Yubero-Lahoz, S. *et al.* Determination of free serotonin and its metabolite 5-HIAA in blood human samples with consideration to pre-analytical factors. *Biomed. Chromatogr.* **28**, 1641–1646 (2014).
230. Zuetenhorst, J. M. *et al.* Daily Cyclic Changes in the Urinary Excretion of 5-Hydroxyindoleacetic Acid in Patients with Carcinoid Tumors. *Clin. Chem.* **50**, 1634–1639 (2004).
231. Jones, A. W. & Helander, A. Disclosing recent drinking after alcohol has been cleared from the body. *J. Anal. Toxicol.* **20**, 141–2 (1996).
232. Compan, V. *et al.* Serotonin signaling in eating disorders. *Wiley Interdiscip. Rev. Membr. Transp. Signal.* **1**, 715–729 (2012).
233. Young, R. L. *et al.* Augmented capacity for peripheral serotonin release in human obesity. *Int. J. Obes. (Lond).* **42**, 1880–1889 (2018).
234. Takahashi, T. *et al.* Sarpogrelate hydrochloride, a serotonin_{2A} receptor antagonist, reduces albuminuria in diabetic patients with early-stage diabetic nephropathy. *Diabetes Res. Clin. Pract.* **58**, 123–129 (2002).
235. Fukui, M. *et al.* High plasma 5-hydroxyindole-3-acetic acid concentrations in subjects with metabolic syndrome. *Diabetes Care* **35**, 163–167 (2012).
236. Afarideh, M. *et al.* Association Of Peripheral 5-Hydroxyindole-3-Acetic Acid, A Serotonin Derivative, with Metabolic Syndrome and Low-Grade Inflammation. *Endocr. Pract.* **21**, 711–718 (2015).
237. Mödder, U. I. *et al.* Relation of serum serotonin levels to bone density and structural parameters in women. *J. Bone Miner. Res.* **25**, 415–422 (2010).

238. Hodge, S., Bunting, B. P., Carr, E., Strain, J. J. & Stewart-Knox, B. J. Obesity, whole blood serotonin and sex differences in healthy volunteers. *Obes. Facts* **5**, 399–407 (2012).
239. Ojeda-Rodríguez, A. *et al.* Reduced serotonin levels after a lifestyle intervention in obese children: association with glucose and anthropometric measurements. *Nutr. Hosp.* **35**, 279–285 (2018).
240. P.G., B., J., B., M., M., T.L., O. & S.A., C. Pathogenesis of type 2 diabetes in obese adolescents: Metabolites of serotonin and mitochondrial function in 24-hour urine samples. *Endocr. Rev.* **38**, 24–25 (2017).
241. Bonacina, M. *et al.* 18F-FDG PET/CT brown fat detection: Differences between adult and pediatric population in a 12 year experience. *Rev. Esp. Med. Nucl. Imagen Mol.* **38**, 224–228 (2019).
242. Gilsanz, V. *et al.* The depiction of brown adipose tissue is related to disease status in pediatric patients with lymphoma. *Am. J. Roentgenol.* **198**, 909–913 (2012).
243. Zukotynski, K. A. *et al.* Seasonal variation in the effect of constant ambient temperature of 24 degrees C in reducing FDG uptake by brown adipose tissue in children. *Eur. J. Nucl. Med. Mol. Imaging* **37**, 1854–60 (2010).
244. Hu, H. H., Chung, S. A., Nayak, K. S., Jackson, H. A. & Gilsanz, V. Differential Computed Tomographic Attenuation of Metabolically Active and Inactive Adipose Tissues. *J. Comput. Assist. Tomogr.* **35**, 65–71 (2011).
245. Zukotynski, K. A. *et al.* Constant ambient temperature of 24°C significantly reduces FDG uptake by brown adipose tissue in children scanned during the winter. *Eur. J. Nucl. Med. Mol. Imaging* **36**, 602–606 (2009).
246. Kim, S., Krynyckyi, B. R., Machac, J. & Kim, C. K. Temporal relation between temperature change and FDG uptake in brown adipose tissue. *Eur. J. Nucl. Med. Mol. Imaging* **35**, 984–989 (2008).
247. Gelfand, M. J., O’Hara, S. M., Curtwright, L. A. & MacLean, J. R. Pre-medication to block [18F]FDG uptake in the brown adipose tissue of pediatric and adolescent patients. *Pediatr. Radiol.* **35**, 984–990 (2005).
248. Truong, M. T. *et al.* Focal FDG Uptake in Mediastinal Brown Fat Mimicking Malignancy: A Potential Pitfall Resolved on PET/CT. *Am. J. Roentgenol.* **183**, 1127–1132 (2004).
249. Gilsanz, V., Hu, H. H. & Kajimura, S. Relevance of brown adipose tissue in infancy and adolescence. *Pediatr. Res.* **73**, 3–9 (2013).
250. Hu, H. H. & Gilsanz, V. Developments in the imaging of brown adipose tissue and its associations with muscle, puberty, and health in children. *Front. Endocrinol. (Lausanne)*. **2**, 33 (2011).
251. Law, J. M. *et al.* Reduced brown adipose tissue-associated skin temperature following cold stimulation in children and adolescents with type 1 diabetes. *Pediatr. Diabetes* **22**, 407–416 (2021).

252. Law, J. M. *et al.* Brown Adipose Tissue Response to Cold Stimulation Is Reduced in Girls With Autoimmune Hypothyroidism. *J. Endocr. Soc.* **3**, 2411–2426 (2019).
253. Cannon, B. & Nedergaard, J. Brown adipose tissue: function and physiological significance. *Physiol. Rev.* **84**, 277–359 (2004).
254. Gatidis, S. *et al.* Is it possible to detect activated brown adipose tissue in humans using single-time-point infrared thermography under thermoneutral conditions? Impact of BMI and subcutaneous adipose tissue thickness. *PLoS One* **11**, (2016).
255. Oreskovich, S. M. *et al.* MRI Reveals Human Brown Adipose Tissue Is Rapidly Activated in Response to Cold. *J. Endocr. Soc.* **3**, 2374–2384 (2019).
256. Andersson, J. *et al.* MRI estimates of brown adipose tissue in children - Associations to adiposity, osteocalcin, and thigh muscle volume. *Magn. Reson. Imaging* **58**, 135–142 (2019).
257. Hui, S. C. N. *et al.* Quantification of brown and white adipose tissue based on Gaussian mixture model using water–fat and T2* MRI in adolescents. *J. Magn. Reson. Imaging* **46**, 758–768 (2017).
258. Lundström, E. *et al.* Brown adipose tissue estimated with the magnetic resonance imaging fat fraction is associated with glucose metabolism in adolescents. *Pediatr. Obes.* **14**, e12531 (2019).
259. Younossi, Z. *et al.* Global burden of NAFLD and NASH: trends, predictions, risk factors and prevention. *Nat. Rev. Gastroenterol. Hepatol.* **15**, 11–20 (2018).
260. Samuel, V. T. & Shulman, G. I. Nonalcoholic Fatty Liver Disease as a Nexus of Metabolic and Hepatic Diseases. *Cell Metab.* **27**, 22–41 (2018).
261. Loomba, R. *et al.* Gut Microbiome-Based Metagenomic Signature for Non-invasive Detection of Advanced Fibrosis in Human Nonalcoholic Fatty Liver Disease. *Cell Metab.* **25**, 1054-1062.e5 (2017).
262. Liu, X. *et al.* Brown Adipose Tissue Transplantation Reverses Obesity in Ob/Ob Mice. *Endocrinology* **156**, 2461–2469 (2015).
263. Liu, X. *et al.* Brown adipose tissue transplantation improves whole-body energy metabolism. *Cell Res.* **23**, 851–854 (2013).
264. van den Beukel, J. C. *et al.* Cold Exposure Partially Corrects Disturbances in Lipid Metabolism in a Male Mouse Model of Glucocorticoid Excess. *Endocrinology* **156**, 4115–4128 (2015).
265. Shapira, S. N. & Seale, P. Transcriptional Control of Brown and Beige Fat Development and Function. *Obesity* **27**, 13–21 (2019).
266. Sponton, C. H. & Kajimura, S. Multifaceted roles of beige fat in energy homeostasis beyond UCP1. *Endocrinology* vol. 159 2545–2553 (2018).
267. Chevalier, C. *et al.* Gut Microbiota Orchestrates Energy Homeostasis during Cold. *Cell* **163**, 1360–1374 (2015).

268. Wang, D. *et al.* LSD1 mediates microbial metabolite butyrate-induced thermogenesis in brown and white adipose tissue. *Metabolism* **102**, 154011 (2020).
269. Carpentier, A. C. *et al.* Brown Adipose Tissue Energy Metabolism in Humans. *Front. Endocrinol. (Lausanne)*. **9**, 447 (2018).
270. Loh, R. K. C., Kingwell, B. A. & Carey, A. L. Human brown adipose tissue as a target for obesity management; beyond cold-induced thermogenesis. *Obes. Rev.* **18**, 1227–1242 (2017).
271. American Diabetes Association. 2. Classification and Diagnosis of Diabetes: Standards of Medical Care in Diabetes—2018. *Diabetes Care* **41**, S13–S27 (2018).
272. Haman, F. & Blondin, D. P. Shivering thermogenesis in humans: Origin, contribution and metabolic requirement. *Temp. (Austin, Tex.)* **4**, 217–226 (2017).
273. Szczepaniak, L. S. *et al.* Magnetic resonance spectroscopy to measure hepatic triglyceride content: prevalence of hepatic steatosis in the general population. *Am. J. Physiol. Metab.* **288**, E462–E468 (2005).
274. Bartelt, A. *et al.* Brown adipose tissue activity controls triglyceride clearance. *Nat. Med.* **17**, 200–205 (2011).
275. Simcox, J. *et al.* Global Analysis of Plasma Lipids Identifies Liver-Derived Acylcarnitines as a Fuel Source for Brown Fat Thermogenesis. *Cell Metab.* **26**, 509–522.e6 (2017).
276. Yun, Y. *et al.* Fecal and blood microbiota profiles and presence of nonalcoholic fatty liver disease in obese versus lean subjects. *PLoS One* **14**, e0213692 (2019).
277. Jiang, W. *et al.* Dysbiosis gut microbiota associated with inflammation and impaired mucosal immune function in intestine of humans with non-alcoholic fatty liver disease. *Sci. Rep.* **5**, 8096 (2015).
278. Foley, K. P. *et al.* Long term but not short term exposure to obesity related microbiota promotes host insulin resistance. *Nat. Commun.* **9**, 4681 (2018).
279. Crane, J. D., Mottillo, E. P., Farncombe, T. H., Morrison, K. M. & Steinberg, G. R. A standardized infrared imaging technique that specifically detects UCP1-mediated thermogenesis in vivo. *Mol. Metab.* **3**, 490–494 (2014).
280. Deschasaux, M. *et al.* Depicting the composition of gut microbiota in a population with varied ethnic origins but shared geography. *Nat. Med.* **24**, 1526–1531 (2018).
281. Nahon, K. J. *et al.* The effect of mirabegron on energy expenditure and brown adipose tissue in healthy lean South <scp>Asian and Europid</scp> men. *Diabetes, Obes. Metab.* **22**, 2032–2044 (2020).
282. Healey, G. R., Murphy, R., Brough, L., Butts, C. A. & Coad, J. Interindividual variability in gut microbiota and host response to dietary interventions. *Nutr. Rev.* **75**, 1059–1080 (2017).
283. Haman, F., Legault, S. R., Rakobowchuk, M., Ducharme, M. B. & Weber, J.-M. Effects of carbohydrate availability on sustained shivering II. Relating muscle recruitment to fuel

- selection. *J. Appl. Physiol.* **96**, 41–49 (2004).
284. Caussy, C., Reeder, S. B., Sirlin, C. B. & Loomba, R. Noninvasive, Quantitative Assessment of Liver Fat by MRI-PDFF as an Endpoint in NASH Trials. *Hepatology* **68**, 763–772 (2018).
 285. Hu, H. H., Perkins, T. G., Chia, J. M. & Gilsanz, V. Characterization of human brown adipose tissue by chemical-shift water-fat MRI. *AJR. Am. J. Roentgenol.* **200**, 177–83 (2013).
 286. Demerath, E. W. *et al.* Approximation of total visceral adipose tissue with a single magnetic resonance image. *Am. J. Clin. Nutr.* **85**, 362–368 (2007).
 287. Friedewald, W. T., Levy, R. I. & Fredrickson, D. S. Estimation of the Concentration of Low-Density Lipoprotein Cholesterol in Plasma, Without Use of the Preparative Ultracentrifuge. *Clin. Chem.* **18**, 499–502 (1972).
 288. Whelan, F. J. *et al.* The loss of topography in the microbial communities of the upper respiratory tract in the elderly. *Ann. Am. Thorac. Soc.* **11**, 513–21 (2014).
 289. De Palma, G. *et al.* Microbiota and host determinants of behavioural phenotype in maternally separated mice. *Nat. Commun.* **6**, 7735 (2015).
 290. Gohir, W. *et al.* Pregnancy-related changes in the maternal gut microbiota are dependent upon the mother’s periconceptual diet. *Gut Microbes* **6**, 310–20 (2015).
 291. Stearns, J. C. *et al.* Culture and molecular-based profiles show shifts in bacterial communities of the upper respiratory tract that occur with age. *ISME J.* **9**, 1246–59 (2015).
 292. Yusta, B. *et al.* GLP-1R Agonists Modulate Enteric Immune Responses Through the Intestinal Intraepithelial Lymphocyte GLP-1R. *Diabetes* **64**, 2537–2549 (2015).
 293. Bartram, A. K., Lynch, M. D. J., Stearns, J. C., Moreno-Hagelsieb, G. & Neufeld, J. D. Generation of Multimillion-Sequence 16S rRNA Gene Libraries from Complex Microbial Communities by Assembling Paired-End Illumina Reads. *Appl. Environ. Microbiol.* **77**, 3846–3852 (2011).
 294. Callahan, B. J., McMurdie, P. J. & Holmes, S. P. Exact sequence variants should replace operational taxonomic units in marker-gene data analysis. *ISME J.* **11**, 2639–2643 (2017).
 295. Martin, M. Cutadapt removes adapter sequences from high-throughput sequencing reads. *EMBnet.journal* **17**, 10–12 (2011).
 296. McMurdie, P. J. & Holmes, S. phyloseq: An R Package for Reproducible Interactive Analysis and Graphics of Microbiome Census Data. *PLoS One* **8**, e61217 (2013).
 297. Wickham, H. ggplot2 by Hadley Wickham. *Media* vol. 35 211 (2009).
 298. Conway, J. R., Lex, A. & Gehlenborg, N. UpSetR: an R package for the visualization of intersecting sets and their properties. *Bioinformatics* **33**, 2938–2940 (2017).
 299. Denou, E. *et al.* Defective NOD2 peptidoglycan sensing promotes diet-induced

- inflammation, dysbiosis, and insulin resistance. *EMBO Mol. Med.* **7**, 259–74 (2015).
300. Harris, R. J. *A Primer of Multivariate Statistics. A Primer of Multivariate Statistics* (Academic Press, 2001). doi:10.4324/9781410600455.
 301. Barbara G. Tabachnick & Linda S. Fidell. *Using Multivariate Statistics*. (Allyn and Bacon/Pearson Education, 2007).
 302. Philip Dixon. VEGAN, a package of R functions for community ecology. *J. Veg. Sci.* **14**, 927–930 (2003).
 303. Love, M. I., Huber, W. & Anders, S. Moderated estimation of fold change and dispersion for RNA-seq data with DESeq2. *Genome Biol.* **15**, 550 (2014).
 304. Costa-Silva, J., Domingues, D. & Lopes, F. M. RNA-Seq differential expression analysis: An extended review and a software tool. *PLoS One* **12**, e0190152 (2017).
 305. World Health Organization. *Final report of the Commission on ending childhood obesity*. (2016) doi:10.1016/j.xphs.2016.04.033.
 306. Greydanus, D. E. *et al.* Pediatric obesity: Current concepts. *Disease-a-Month* **64**, 98–156 (2018).
 307. Speiser, P. W. *et al.* Consensus statement: Childhood obesity. *J. Clin. Endocrinol. Metab.* **90**, 1871–1887 (2005).
 308. Gurnani, M., Birken, C. & Hamilton, J. Childhood Obesity: Causes, Consequences, and Management. *Pediatr. Clin. North Am.* **62**, 821–840 (2015).
 309. Kumar, S. & Kelly, A. S. Review of Childhood Obesity: From Epidemiology, Etiology, and Comorbidities to Clinical Assessment and Treatment. *Mayo Clin. Proc.* **92**, 251–265 (2017).
 310. Desjardins, E. M. & Steinberg, G. R. Emerging Role of AMPK in Brown and Beige Adipose Tissue (BAT): Implications for Obesity, Insulin Resistance, and Type 2 Diabetes. *Curr. Diab. Rep.* **18**, 80 (2018).
 311. Parysow, O. *et al.* Low-Dose Oral Propranolol Could Reduce Brown Adipose Tissue F-18 FDG Uptake in Patients Undergoing PET Scans. **32**, 351–357 (2007).
 312. Lichtenbelt, W. D. V. M. *et al.* Cold-Activated Brown Adipose Tissue in Healthy Men. *N. Engl. J. Med.* **360**, 1500–1508 (2016).
 313. Abreu-Vieira, G. *et al.* Human Brown Adipose Tissue Estimated With Magnetic Resonance Imaging Undergoes Changes in Composition After Cold Exposure: An in vivo MRI Study in Healthy Volunteers. *Front. Endocrinol. (Lausanne)*. **10**, 1–15 (2020).
 314. Alexander Iwen, K. *et al.* Cold-induced brown adipose tissue activity alters plasma fatty acids and improves glucose metabolism in men. *J. Clin. Endocrinol. Metab.* **102**, 4226–4234 (2017).
 315. Soundarajan, M. *et al.* Activated brown adipose tissue and its relationship to adiposity and metabolic markers: an exploratory study. *Adipocyte* **9**, 87–95 (2020).

316. Shao, X. *et al.* The role of active brown adipose tissue (aBAT) in lipid metabolism in healthy Chinese adults. *Lipids Health Dis.* **15**, 138 (2016).
317. Lidell, M. E. Brown adipose tissue in human infants. in *Handbook of Experimental Pharmacology* vol. 251 107–123 (2019).
318. Chen, H., Sullivan, G. & Quon, M. J. Assessing the predictive accuracy of QUICKI as a surrogate index for insulin sensitivity using a calibration model. *Diabetes* **54**, 1914–1925 (2005).
319. International Organization for Standardization. *ISO 10551:1995*. (1995).
320. Kasza, I., Hernando, D., Roldán-Alzate, A., Alexander, C. M. & Reeder, S. B. Thermogenic profiling using magnetic resonance imaging of dermal and other adipose tissues. *JCI insight* **1**, e87146 (2016).
321. Puhakka, K., Anttonen, H., Niskanen, J. & Ryhänen, P. Calculation of mean skin temperature and changes in body heat content during paediatric anaesthesia. *Br. J. Anaesth.* **72**, 548–553 (1994).
322. Blitman, N. M. *et al.* Feasibility of using single-slice MDCT to evaluate visceral abdominal fat in an urban pediatric population. *Am. J. Roentgenol.* **197**, 482–487 (2011).
323. Jonnakuty, C. & Gragnoli, C. What do we know about serotonin? *J. Cell. Physiol.* **217**, 301–6 (2008).
324. Miller, A. G., Brown, H., Degg, T., Allen, K. & Keevil, B. G. Measurement of plasma 5-hydroxyindole acetic acid by liquid chromatography tandem mass spectrometry- Comparison with HPLC methodology. *J. Chromatogr. B Anal. Technol. Biomed. Life Sci.* **878**, 695–699 (2010).
325. Apak, S. *et al.* Spot urine 5-hydroxyindoleacetic acid levels in the early diagnosis of acute appendicitis. *J. Pediatr. Surg.* **40**, 1436–9 (2005).
326. Bosak Versic, A., Glavan, N., Bukvic, N., Tomasic, Z. & Nikolic, H. Does elevated urinary 5-hydroxyindole acetic acid level predict acute appendicitis in children? *Emerg. Med. J.* **33**, 848–852 (2016).
327. Bolandparvaz, S. *et al.* Urinary 5-hydroxy indole acetic acid as a test for early diagnosis of acute appendicitis. *Clin. Biochem.* **37**, 985–9 (2004).
328. Visentin, V. *et al.* Alteration of Amine Oxidase Activity in the Adipose Tissue of Obese Subjects. *Obes. Res.* **12**, 547–555 (2004).
329. Binetti, J. *et al.* Deregulated serotonin pathway in women with morbid obesity and nafld. *Life* **10**, 1–17 (2020).
330. McBride, P. A. *et al.* Effects of diagnosis, race, and puberty on platelet serotonin levels in autism and mental retardation. *J. Am. Acad. Child Adolesc. Psychiatry* **37**, 767–76 (1998).
331. Oh, C.-M. *et al.* Regulation of systemic energy homeostasis by serotonin in adipose tissues. *Nat. Commun.* **6**, 6794 (2015).

332. Yabut, J. M. *et al.* Genetic deletion of mast cell serotonin synthesis prevents the development of obesity and insulin resistance. *Nat. Commun.* **11**, 1–11 (2020).
333. Paik, J. M., Golabi, P., Younossi, Y., Mishra, A. & Younossi, Z. M. Changes in the Global Burden of Chronic Liver Diseases From 2012 to 2017: The Growing Impact of NAFLD. *Hepatology* **72**, 1605–1616 (2020).
334. Younossi, Z. M. *et al.* The economic and clinical burden of nonalcoholic fatty liver disease in the United States and Europe. *Hepatology* **64**, 1577–1586 (2016).
335. Gavaldà-Navarro, A., Villarroya, J., Cereijo, R., Giralt, M. & Villarroya, F. The endocrine role of brown adipose tissue: An update on actors and actions. *Rev. Endocr. Metab. Disord.* (2021) doi:10.1007/s11154-021-09640-6.
336. Li, P. *et al.* Transplantation of brown adipose tissue up-regulates miR-99a to ameliorate liver metabolic disorders in diabetic mice by targeting NOX4. *Adipocyte* **9**, 57–67 (2020).
337. Nuttall, F. Q. Body mass index: Obesity, BMI, and health: A critical review. *Nutr. Today* **50**, 117–128 (2015).
338. Décarie, P.-O. *et al.* Fatty liver deposition and sparing: a pictorial review. *Insights Imaging* **2**, 533–538 (2011).
339. Allen, A. M. *et al.* Nonalcoholic fatty liver disease incidence and impact on metabolic burden and death: A 20 year-community study. *Hepatology* **67**, 1726–1736 (2018).
340. Guergova, S. & Dufour, A. Thermal sensitivity in the elderly: a review. *Ageing Res. Rev.* **10**, 80–92 (2011).
341. Redman, L. M. *et al.* Lack of an Effect of a Novel β 3-Adrenoceptor Agonist, TAK-677, on Energy Metabolism in Obese Individuals: A Double-Blind, Placebo-Controlled Randomized Study. *J. Clin. Endocrinol. Metab.* **92**, 527–531 (2007).
342. Larsen, T. M. *et al.* Effect of a 28-d treatment with L-796568, a novel β 3-adrenergic receptor agonist, on energy expenditure and body composition in obese men. *Am. J. Clin. Nutr.* **76**, 780–788 (2002).
343. Baskin, A. S. *et al.* Regulation of human adipose tissue activation, gallbladder size, and bile acid metabolism by a β 3-adrenergic receptor agonist. *Diabetes* **67**, 2113–2125 (2018).
344. Blondin, D. P. *et al.* Human Brown Adipocyte Thermogenesis Is Driven by β 2-AR Stimulation. *Cell Metab.* **32**, 287–300.e7 (2020).
345. Horesh, A., Tsur, A. M., Bardugo, A. & Twig, G. Adolescent and Childhood Obesity and Excess Morbidity and Mortality in Young Adulthood—a Systematic Review. *Curr. Obes. Rep.* (2021) doi:10.1007/s13679-021-00439-9.
346. Sanderson, K., Patton, G. C., McKercher, C., Dwyer, T. & Venn, A. J. Overweight and obesity in childhood and risk of mental disorder: A 20-year cohort study. *Aust. N. Z. J. Psychiatry* **45**, 384–392 (2011).
347. Stages of puberty: what happens to boys and girls. No Title. <https://www.nhs.uk/live->

well/sexual-health/stages-of-puberty-what-happens-to-boys-and-girls/.

348. Mathur, A. M., Neil, J. J., McKinstry, R. C. & Inder, T. E. Transport, monitoring, and successful brain MR imaging in unsedated neonates. *Pediatr. Radiol.* **38**, 260–264 (2008).
349. Adaway, J. E. *et al.* Serum and plasma 5-hydroxyindoleacetic acid as an alternative to 24-h urine 5-hydroxyindoleacetic acid measurement. *Ann. Clin. Biochem.* **53**, 554–560 (2016).
350. Tohmola, N. *et al.* Transient elevation of serum 5-HIAA by dietary serotonin and distribution of 5-HIAA in serum protein fractions. *Ann. Clin. Biochem.* **52**, 428–33 (2015).
351. Choi, W. *et al.* Serotonin signals through a gut-liver axis to regulate hepatic steatosis. *Nat. Commun.* **9**, 1–9 (2018).
352. Burks, M. L. & Bao, S. the 24-Hour Urinary 5-Hiaa: a Simple Test With a Common Pitfall. *AACE Clin. Case Reports* **2**, EP15794.CR (2015).
353. Deacon, A. C. The measurement of 5-hydroxyindoleacetic acid in urine. *Ann. Clin. Biochem.* **31**, 215–232 (1994).
354. Calanchini, M. *et al.* Measurement of urinary 5-HIAA: Correlation between spot versus 24-h urine collection. *Endocr. Connect.* **8**, 1082–1088 (2019).
355. Hughes, C. W., Petty, F., Sheikha, S. & Kramer, G. L. Whole-blood serotonin in children and adolescents with mood and behavior disorders. *Psychiatry Res.* **65**, 79–95 (1996).
356. Coolbaugh, C. L., Damon, B. M., Bush, E. C., Welch, E. B. & Towse, T. F. Cold exposure induces dynamic, heterogeneous alterations in human brown adipose tissue lipid content. *Sci. Rep.* **9**, 13600 (2019).
357. Chiang, I. C., Lu, C. H., Chung, W. S., Huang, Y. F. & Hsieh, T. J. Fat-Water Swaps in Iterative Decomposition of Water and Fat With Echo Asymmetry and Least-Squares Estimation Magnetic Resonance Imaging for Postinstrumentation Spine. *J. Comput. Assist. Tomogr.* **44**, 977–983 (2020).
358. Hernando, D., Kellman, P., Haldar, J. P. & Liang, Z. P. Robust water/fat separation in the presence of large field inhomogeneities using a graph cut algorithm. *Magn. Reson. Med.* **63**, 79–90 (2010).
359. Kirchgesner, T., Acid, S., Perlepe, V., Lecouvet, F. & Vande Berg, B. Two-point Dixon fat-water swapping artifact: lesion mimicker at musculoskeletal T2-weighted MRI. *Skeletal Radiol.* **49**, 2081–2086 (2020).